ADIPOR1 AND LKB1 ARE DOWNREGULATED IN RCC

ADIPONECTIN RECEPTOR 1 AND LIVER KINASE B1 ARE DOWNREGULATED IN RENAL CELL CARCINOMA

By LAURA K. BEATTY, B.Sc. (HONS.)

A Thesis

Submitted to the School of Graduate Studies

in Partial Fulfilment of the Requirements

for the Degree

Master of Science

McMaster University

MASTER OF SCIENCE (2011) McMaster University

(Medical Science) Hamilton, Ontario

TITLE: Adiponectin Receptor 1 and Liver Kinase B1 are downregulated in renal cell carcinoma

AUTHOR: Laura K. Beatty, B.Sc. (Hons.) (McMaster University)

SUPERVISORS: Jehonathan Pinthus, PhD, MD.

Richard C. Austin, PhD.

NUMBER OF PAGES: xiii, 147

ABSTRACT

Obesity is the latest epidemic of the 21st century. Indeed, numerous studies have associated obesity with an increased risk of developing several health conditions, including cancer. Moreover, modest increases in body mass index increase the risk of developing cancer, especially cancer of the kidney. Although the mechanism mediating this increased risk is unknown, the plasma level of adiponectin is known to be inversely correlated with body weight and risk of developing kidney cancer. This suggests that a reduction in adiponectin, due to obesity, may promote the development of kidney cancer.

Tumour suppression via adiponectin is believed to be mediated through adiponectin receptor-1 (AdipoR1), which activates 5'-AMP activated-protein kinase (AMPK) by liver kinase-B1 (LKB1) and suppresses pathways upregulated in cancer by inhibiting the mammalian target of rapamycin (mTOR). Consistent with the anti-tumourigenic properties of this pathway, several cancers display reduced AdipoR1 and LKB1 expression and/or increased mTOR activity. In this study we identified reduced AdipoR1 and LKB1 protein expression in 8/10 patients' renal cell carcinomas (RCC) and quantified the reduction in LKB1, on tissue microarrays containing 201 RCC patients, to be significant.

To generate an *in vitro* model of our observations in human RCC tumours, a knockdown of AdipoR1 or LKB1 was performed in CRL-1932 cells and, the effect of the knockdown on tumourigenesis was examined. Targeted knockdown of LKB1 in shLKB1 cells was accompanied by a reduction in AdipoR1, and recapitulated our observations in RCC tumours. These shLKB1 cells were unable to execute established events of adiponectin-AMPK signalling and, presented increased proliferation and invasion abilities *in vitro* and tumour growth *in vivo*. Collectively, these results suggest that a reduced plasma level of adiponectin coupled with a downregulation of AdipoR1 and LKB1 expression, disrupts the tumour-suppressive adiponectin-AMPK signalling pathway, and rationalizes the association of obesity with the development of RCC.

ACKNOWLEDGEMENTS

Several people have assisted me throughout this research project and I am grateful to everyone for their guidance and support. First and foremost I would like to thank my supervisors Dr. Jehonathan Pinthus and Dr. Richard Austin for their immense knowledge and assistance. I feel very fortunate to have had not one, but two extraordinary supervisors all the way through my graduate studies and I will always value their unending enthusiasm for research and outstanding leadership. I would also like to thank my committee member Dr. Gregory Steinberg for his exceptional expertise, constructive criticisms and encouragement in the, occasionally confusing, field of adiponectin and AMPK.

I am grateful to all members of my supervisors' research groups. Juravinski Cancer Centre Translational Uro-Oncology Research Group members, Dr. Jian-Ping Lu, Dr. Shengjun Qiao, Daniel Gallino and especially Dr. Helga Duivenvoorden for their endless assistance and support. St. Joseph's Healthcare Hamilton Centre for Kidney Research (HCKR) members, Dr. Sarka Lhotak, Dr. Sudesh Sood, Dr. Jeffrey Dickhout, and Dr. Edward Lynn for their technical knowledge and guidance, Brianne Hill for her continual motivation and support and future doctors Liz Crane, Adrian Rybak, Sana Bassari and Ali Al-Hashimi for their friendship and ultimately, love of sushi. I feel honoured to have worked in such an amazing environment with a talented group of researchers and friends over the past two and a half years.

I will always be grateful to my parents, Doug and Mary-Anne Beatty, and sister Karen, for their love, support and interest in my studies at McMaster University over the past seven years. Finally, I would like to thank my friends for their words of encouragement, patience and believing in me. Without my supervisors, peers, family and friends, this research project would not be what it is today.

TABLE OF CONTENTS

ABSTRACT iii

ACKNOWLEDGEMENTS v

LIST OF TABLES ix

LIST OF FIGURES x

LIST OF *ABBREVIATIONS* xii

1.0 INTRODUCTION

1.1 *Obesity and adiponectin* 2

1.2 *Adiponectin receptors, binding partners and signalling pathways* 5

1.3 *Adiponectin, AdipoR1 and LKB1 in cancer* 13

2.0 RATIONALE 22

3.0 HYPOTHESIS 23

4.0 OBJECTIVES

4.1 *Objective 1* 24

4.2 *Objective 2* 25

5.0 EXPERIMENTAL PROCEDURES

5.1 *Cell lines and culture conditions* 26

5.2 *Animals and handling* 27

5.3 *Human tissue collection and preparation* 27

5.4 *RNA extraction, quantification, synthesis and analysis* ….....31

5.5 *shRNA and viral plasmids, retroviral and lentiviral particle infections* ...36

5.6 *Bacterial transformation and DNA purification* 42

5.7 *Protein lysis, preparation and Western blot analysis* 45

5.8 *Adiponectin and treatments* 49

5.9 *Proliferation, invasion, tumour growth, VEGF and adiponectin assays* ..51

5.10 *Human tissue and mouse xenograft staining* 58

5.11 *Tissue Microarray staining, scanning and analysis* 62

6.0 RESULTS

6.1.1 *AdipoR1 and LKB1 transcript levels are dysregulated in patient RCC* 64

6.1.2 *AdipoR1 and LKB1 protein expression is reduced in patient RCC* 69

6.1.3 *AdipoR1 and LKB1 staining is reduced in patient RCC* 75

6.2.1 *CRL-1932 is the in vitro cell model of human RCC*.....84

6.2.2 *AdipoR1 and LKB1 knockdown in shVAdipoR1 and shLKB1 cell lines* 87

6.2.3 *AdipoR1 and LKB1 transcript and protein levels in shVAdipoR1 and shLKB1 cell lines* 90

6.2.4 *Adiponectin signalling is disrupted with AdipoR1 and LKB1 knockdown* 94

6.2.5 *AdipoR1 and LKB1 knockdown increases RCC tumourigenic potential* 97

7.0 FUTURE DIRECTIONS 110

8.0 DISCUSSION 115

9.0 REFERENCES 132

LIST OF TABLES

Table 1 | Primer sequences used for quantitative real time PCR 35

Table 2 | Short hairpin target sequences 37

Table 3 | Primary antibodies used in Western blot analysis 48

Table 4 | Secondary antibodies used in Western blot analysis 49

Table 5 | Primary antibodies used for immunohistochemical staining 61

Table 6 | Secondary antibodies used for immunohistochemical staining 61

LIST OF FIGURES

Figure 1 | *AdipoR1* transcript level is increased in patient RCC tumours 65

Figure 2 | *AdipoR2* transcript level is increased in patient RCC tumours 66

Figure 3 | *LKB1* transcript level is reduced in patient RCC tumours 67

Figure 4 | *VEGFA* transcript level confirmed patient tumour and normal tissues 68

Figure 5 | AdipoR1 protein expression is reduced in patient RCC tumours 70

Figure 6 | AdipoR1 and LKB1 protein expression is reduced in patient RCC tumours 71

Figure 7 | CAIX expression distinguished RCC tumour from normal tissue 74

Figure 8 | AdipoR1 expression is slightly reduced in histological sections of patient RCC tumours 77

Figure 9 | LKB1 expression is reduced in histological sections of patient RCC tumours 79

Figure 10 | TMA confirms LKB1 reduction in 201 patient RCC tumours 81

Figure 11 | p-ACC staining in histological sections of patient RCC tumour and normal tissue was not conclusive 83

Figure 12 | CRL-1932 and CRL-1933 cell lines express AdipoR1 and AdipoR2 85

Figure 13 | Adiponectin activates AMPKα and inhibits mTOR in CRL-1932 cells 86

Figure 14 | Retroviral infection knockdown of AdipoR1 in shVAdipoR1 cells 89

Figure 15 | Lentiviral particle infection knockdown of LKB1 in shLKB1 cells 90

Figure 16 | *AdipoR1* and *LKB1* transcript levels are reduced with AdipoR1 and LKB1 knockdown 92

Figure 17 | AdipoR1 protein expression is reduced with LKB1 knockdown, LKB1 protein expression is not reduced with AdipoR1 knockdown 93

Figure 18 | Adiponectin-mediated phosphorylation of AMPKα and ACC is disrupted with LKB1 knockdown 95

Figure 19 | LKB1 knockdown increases VEGF secretion and disrupts adiponectin-mediated inhibition of VEGF secretion 97

Figure 20 | LKB1 knockdown in shLKB1 cells remains stable over 15 days 98

Figure 21 | LKB1 knockdown increases cell proliferation 100

Figure 22 | LKB1 knockdown increases cell migration and invasion 101

Figure 23 | LKB1 knockdown increases xenograft size and proliferation ….....102

Figure 24 | shLKB1 xenografts retain LKB1 knockdown 105

Figure 25 | LKB1 knockdown xenografts did not significantly affect serum VEGF and adiponectin levels 108

Figure 26 | Adiponectin treatment stimulates activation of CK2β and CDC37 111

Figure 27 | CK2 inhibition reduces adiponectin-mediated activation of AMPKα, CDC37 and LKB1 protein expression 113

LIST OF ABBREVIATIONS

Acrp30	Adipocyte complement-related protein of 30kDa
AdipoR1	Adiponectin receptor 1
AdipoR2	Adiponectin receptor 2
AMP	Adenosine monophosphate
ATP	Adenosine triphosphate
AMPK	5'-AMP activated protein kinase
APPL1	Adaptor protein containing PH domain, PTB domain and Leucine zipper motif
ATCC	American type culture collection
BMI	Body mass index
CaMKKβ	Calmodulin-dependent protein kinase kinase-beta
CBS	Cystathionine beta synthase
CDC37	Cell division cycle protein 37
CK2	Casein kinase II
CMV	Cytomegalovirus
CT	Critical threshold
DMEM	Dulbecco's Modified Eagle Medium
DMSO	Dimethyl Sulfoxide
E. Coli	Escherichia Coli
FBS	Fetal bovine serum

FDA	Food and Drug Administration
GBP28	Gelatin-binding protein-28
GFP	Green fluorescent protein
GPI	Glycosylphosphatidylinositol
HRP	Horse radish peroxidise
HSP90	Heat shock protein 90
LKB1	Liver kinase B1
mTOR	Mammalian target of rapamycin
NADPH	Nictoinamide adenine dinucleotide phosphate
NGS	Normal goat serum
PBS	Phosphate buffered saline
PPARα	Peroxisome proliferator-activated receptor alpha
qRT-PCR	Quantitative real time polymerase chain reaction
RACK1	Receptor for activated protein kinase C1
RCC	Renal cell carcinoma
RFP	Red Fluorescent Protein
shRNA	Short hairpin RNA
STK11	Serine threonine kinase 11
STRAD	STE20-related adaptor
TBB	4,5,6,7-Tetrabromobenzotriazole
VEGF	Vascular endothelial growth factor
YFP	Yellow fluorescent protein

INTRODUCTION

It is well known that the prevalence of obesity is rising in developed countries, with obesity becoming one of the leading health concerns (Bjursell *et al.*, 2007). In fact, the *World Health Organization* has labelled obesity as the new epidemic of the 21st century and estimates that by the year 2015, more than 2.3 billion adults worldwide will be overweight with a **b**ody **m**ass **i**ndex (BMI) of 25.0 kg/m^2 – 29.9 kg/m^2, and 700 million will be obese (BMI: ≥ 30 kg/m^2) (Rojas *et al.*, 2010). In 2009 the *Public Health Agency of Canada* approximated that 25% of Canadian adults are obese, compared to 23% in 2004 and 14% in 1978. This rising incidence of obesity has profound implications on the health of Canadians because numerous epidemiological studies have associated obesity with the onset of a variety of health conditions including type 2 diabetes, cardiovascular disease, hypertension, and cancer (Bjursell *et al.*, 2007) (Cammisotto *et al.*, 2008). Indeed, the *World Cancer Research Fund* agrees strongly with research findings associating body fatness with an increased risk of developing oesophageal adenocarcinoma, and cancers of the pancreas, colorectum, postmenopausal breast, endometrium and kidney (Renehan *et al.*, 2008). Regrettably, the exact mechanism(s) linking excess weight to an increased risk of developing these cancers is not fully understood, however, three hormonal systems are among the most studied candidates.

1.1 *Obesity and adiponectin*

Originally regarded solely as an energy storage site, the importance of adipose tissue as an endocrine organ has become quite evident by the identification of numerous secreted factors, collectively known as adipokines, which regulate energy balance, lipid and glucose metabolism as well as vascular and blood pressure (Vettor *et al.*, 2005) (Trujillo *et al.*, 2006) (Bjursell *et al.*, 2007). One of these adipokines is adiponectin, a hormone initially believed to be secreted solely by adipocytes, but, recently it was also identified to be secreted by myoblasts, cardiomyocytes and hepatocytes (Bonnard *et al.*, 2008). Clinical trials involving obese patients and healthy controls revealed that, in contrast to other adipokines (Mistry *et al.*, 2006), adiponectin levels in the serum are inversely correlated with body weight (Gavrila *et al.*, 2003). From those clinical trials, it was determined that adiponectin circulates in the plasma of healthy individuals at a concentration of approximately 10 μg/mL and in obese patients at approximately 2 μg/mL (Arita *et al.*, 1999) (Mao *et al.*, 2006). Although the exact mechanism(s) governing this reduction in adiponectin remains unknown, it likely depends on adiponectin expression in and secretion from adipocytes, as well as adiponectin turnover rate in the blood (Mao *et al.*, 2006). Another possible explanation could come from the findings of Furukawa *et al.* (2004), who demonstrated that obesity induces an increase in oxidative stress in accumulated fat, by means of increased **n**icotinamide **a**denine **d**inucleotide **p**hosp**h**ate (NADPH) oxidase and decreased antioxidant enzyme activities, and leads to the dysregulated production of a variety of adipokines, including adiponectin.

Adiponectin concentrations are higher in women than in men, even when matched for BMI, and this gender-related difference is suggested to relate to the diversity between peripheral and visceral adipose tissues (Schalkwijk *et al.*, 2006). Indeed, peripheral and visceral adipose tissues differ considerably from the histological, physiological and metabolic point of view. As well, visceral, but not peripheral, adipose accumulation is a known risk factor to developing the metabolic syndrome and type 2 diabetes (Martinez-Agustin *et al.*, 2010). Peripheral fat is the predominant storage site in women, compared to visceral fat in men, and these differences could explain the higher plasma adiponectin concentration in women (Schalkwijk *et al.*, 2006). Analysis of the gene expression profile of peripheral and visceral adipose tissues revealed that 20% of all genes in peripheral adipose tissue encode secretory proteins whereas this frequency rises to 30% in visceral adipose tissue (Matsuzawa *et al.*, 2010). Encoding a greater number of secretory proteins is biologically significant considering secretory proteins are predominately bioactive molecules that interact in signalling pathways. Thus, the potential to interfere with molecular signalling pathways, through the disruption of secretory proteins by excessive weight gain, is greater in visceral adipose tissue and, accordingly, in men (Matsuzawa *et al.*, 2010). In addition, co-culturing cells isolated from peripheral adipose tissue, which secrete high levels of adiponectin, with cells isolated from visceral adipose tissue, which secrete low levels of adiponectin, resulted in the drastic reduction of adiponectin secretion from peripheral adipose cells (Matsuzawa *et al.*, 2010). Although, as previously mentioned, the exact mechanism governing the reduction of adiponectin levels is not

known, it is feasible that inhibiting factors for adiponectin synthesis or secretion are secreted from visceral adipose tissue (Matsuzawa *et al.*, 2010).

Remarkably, adiponectin was initially identified by four independent research groups, and therefore is cited in the literature under an assortment of names, including **a**dipocyte **c**omplement-**r**elated **p**rotein of **30** kDa (Acrp30), apM1 protein, adipoQ and **g**elatin-**b**inding **p**rotein-**28** (GBP28). The identification of adiponectin as the most abundant transcript in adipose tissue and as one of the most abundant proteins in human serum, by the four research groups, was achieved through the screening of multiple cDNA libraries (Maeda *et al.*, 1996) (Fruebis *et al.*, 2001). Adiponectin was later isolated from human serum as both a full-length and cleaved globular fragment, which were demonstrated to configure into a variety of species with differing molecular weights including trimers, hexamers and high molecular weight isoforms (Fruebis *et al.*, 2001) (Kobayashi *et al.*, 2004). Unfortunately, to date, little is known about the significance of the various isoforms of adiponectin or about the events that lead to the generation of the biologically active ligand (Pajvanti *et al.*, 2003). Following its identification and isolation, the adiponectin gene was sequenced and predicted to contain four structural domains: an N-terminal signal peptide, a short hypervariable region, a collagen domain and a C-terminal globular domain (Mao *et al.*, 2006).

The adiponectin gene has been mapped to human chromosome 3q27, which is a diabetes-susceptibility locus (Mao *et al.*, 2006). Indeed, targeted deletion of the

adiponectin gene in mice, which were subsequently fed a high sucrose or high fat diet, led to a marked elevation of plasma glucose and insulin levels, as well as insulin resistance and obesity (Nedvidkova *et al.*, 2005). Moreover, the reintroduction of adiponectin into these mice improved insulin resistance, and consequently supported a role for adiponectin in the prevention of insulin resistance (Matsuzawa *et al.*, 2010). Similarly, in humans, clinical trials have correlated reduced serum concentrations of adiponectin with insulin resistance, obesity and type 2 diabetes (Mao *et al.*, 2006). Collectively, these findings implicate adiponectin as a regulator of energy homeostasis. Due to the fact that serum contains thousands of proteins and that many proteins in serum form large complexes to regulate their biological activity (Wang *et al*., 2006), identifying adiponectin's interaction partners would provide valuable information with regards to its regulation.

1.2 ***Adiponectin receptors, binding partners and signalling pathways***

Adiponectin primarily signals through two receptors on the plasma membrane; **adipo**nectin **r**eceptor **1** (AdipoR1), located on human chromosome 1 (q32.1), and **adipo**nectin **r**eceptor **2** (AdipoR2), located on human chromosome 12 (p13.3) (Crimmins *et al.*, 2007). These two receptors were independently discovered by the Kadowaki *et al.* and Dong *et al.* research groups through the screening of a cDNA library with globular and full-length adiponectin, respectively (Yamauchi *et al.*, 2007). Although both AdipoR1 and AdipoR2 are seven transmembrane spanning receptors with a predicted

intracellular N-terminal signalling moiety and extracellular C-terminal ligand binding domain, AdipoR1 only shares a 66.7% homology with AdipoR2 (Kadowaki *et al.*, 2003) (Yamauchi *et al.*, 2003). Expression of **y**ellow **f**luorescent **p**rotein (YFP) fusion proteins of AdipoR1 or AdipoR2 in cells, confirmed that the receptors localize to the plasma membrane with the predicted intracellular N-terminus and extracellular C-terminus orientation (Deckert *et al.*, 2006). Although adiponectin receptors are ubiquitously expressed in human tissues, AdipoR1 is preferentially expressed in skeletal muscle, while AdipoR2 is most abundantly expressed in the liver (Mistry *et al.*, 2006). A third receptor that was identified to bind adiponectin is the co-receptor T-cadherin, which is often referred to in literature as CDH13, cadherin 13, or H-cadherin (Hug *et al.*, 2004). This co-receptor is a **g**lycosyl**p**hosphatidyl**i**nositol (GPI)-anchored extracellular protein that functions in transmitting adiponectin signals, and suggestively regulates metabolism (Mao *et al.*, 2006) (Takeuchi *et al.*, 2007).

The majority of studies performed on the adiponectin receptors have focused on AdipoR1 and AdipoR2 function in the metabolic syndrome, and specifically, in muscle, adipose and liver cells (Mao *et al.*, 2006). Briefly, in 2005 Kadowaki *et al.* demonstrated that the muscle and adipose tissues of insulin-resistant ob/ob mice have decreased *AdipoR1* and *AdipoR2* mRNA levels, which suggestively reduces adiponectin sensitivity and leads to insulin resistance. The same insulin-resistant ob/ob mice also presented a significantly lower mRNA level of *AdipoR1* in the pancreas and liver when compared to healthy weight control mice (Wade *et al.*, 2009). Similarly to the insulin-resistant ob/ob

mouse strain presenting lower levels of *AdipoR1*, the targeted knockout of AdipoR1 in mice led to insulin resistance (Yamauchi *et al.*, 2007) (Bjursell *et al.*, 2007). As well, considering *AdipoR1* and *AdipoR2* mRNA transcript levels normally increase following adiponectin treatment, the finding that the *AdipoR1* transcript level increase in skeletal muscle cells derived from lean patients and not in the cells isolated from obese and type 2 diabetic patients, suggests that adiponectin signalling is disrupted in obesity and type 2 diabetes (McAinch *et al.*, 2006). Taking the results of these research studies together, it is likely that the adiponectin receptors, but in particular AdipoR1, have an important role in regulating whole-body homeostasis and energy metabolism. Only recently has the function of adiponectin receptors, inferred from the identification of receptor binding partners, begun to be explored outside of the metabolic syndrome, which has greatly increased understanding of the receptors.

There is a growing of body evidence that supports a unique regulatory role for each adiponectin receptor to selectively regulate a distinct aspect of adiponectin signalling (Charlton *et al.*, 2010). Reasons for this specificity may be explained by the differential affinity of the receptors towards the various isoforms of adiponectin as well as by the distinct downstream targets. Indeed, AdipoR1 possess an increased affinity for the globular form of adiponectin, while AdipoR2 binds both globular and full-length adiponectin with an intermediate affinity (Hug *et al.*, 2004) (Bjursell *et al.*, 2007). Adiponectin treatment is tightly linked to the activation of 5'-**AMP** activated protein **k**inase (AMPK) by means of AdipoR1, whereas adiponectin stimulates the nuclear

transcription factor, **p**eroxisome **p**roliferator-**a**ctivated **r**eceptor **α** (PPARα) and increases expression of PPARα target genes via AdipoR2 (Yamauchi *et al.*, 2002) (Kadowaki *et al.*, 2005). This diversity in activating different downstream signalling targets of adiponectin could be explained by the differences in AdipoR1 and AdipoR2 binding partners.

Unlike protein kinase receptors, the adiponectin receptors have no detectable tyrosine phosphorylation upon adiponectin activation, thus adiponectin may trigger a conformational change of the receptors, which in turn recruits binding proteins and subsequently activates downstream signalling molecules (Mao *et al.*, 2006). To date, four adiponectin receptor binding partners have been identified using either the yeast two-hybrid or co-immunoprecipitation approach: **(1)** Screening of a cDNA library with the intracellular N-terminal portion of AdipoR1 revealed that the C-terminus of **A**daptor protein containing **P**H domain, **P**TB domain and **L**eucine zipper motif (APPL1) interacts with the intracellular domain of both AdipoR1 and AdipoR2 (Mao *et al*., 2006). APPL1 is a protein with multiple functional domains, and its association with the adiponectin receptors on the plasma membrane is greatly enhanced following adiponectin treatment. Due to its various binding domains and increased association with the receptors after adiponectin activation, APPL1 likely functions as an adaptor protein to positively mediate adiponectin signalling to downstream targets (Deepa *et al.*, 2008). Interestingly, an APPL1 isoform, named APPL2, was recently discovered to possess a 54% identity with APPL1 and was demonstrated to negatively regulate AdipoR1 signalling by both competing with APPL1 for binding to AdipoR1 and forming a heterodimer with APPL1

to inhibit the APPL1 positive signalling influence on AdipoR1 (Deepa *et al.*, 2008) (Buechler *et al.*, 2010). Interestingly, the *APPL1* gene is mapped to human chromosome 3p14.3-21.1 and mutations of this region have been correlated with the development of various types of cancer, suggesting a role for adiponectin in tumourigenesis (Mao *et al.*, 2006). **(2)** The yeast two-hybrid screen of a liver cDNA library with full-length AdipoR1 determined that the **r**eceptor for **ac**tivated protein **k**inase **C1** (RACK1) binds an intracellular portion of AdipoR1, however the function and significance of this interaction is largely unknown (Xu *et al.*, 2009). **(3)** Co-immunoprecipitation with full-length AdipoR1 revealed that ERp46, an endoplasmic reticulum- and plasma-resident chaperone protein, binds to amino acids 1-70 in the intracellular region of AdipoR1 (Charlton *et al.*, 2010). Attempts to co-immunoprecipitate ERp46 and full-length AdipoR2 were unsuccessful, though the discovery that amino acids 1-70 in AdipoR1 are not present in AdipoR2 justifies this lack of binding (Charlton *et al.*, 2010). Knockdown of ERp46 increased AdipoR1 levels at the plasma membrane, suggesting ERp46 negatively regulates AdipoR1 abundance and, possibly, signalling (Charlton *et al.*, 2010). **(4)** Screening of a testis cDNA library with a peptide sequence identical to an intracellular portion of AdipoR1 identified that the regulatory subunit of **c**asein **k**inase **II** (CK2), CK2β, binds to amino acids 113-132 in the intracellular domain of AdipoR1. CK2 exists as a holoenzyme with catalytic α or α' and regulatory β subunits, and is an important signaling molecule involved in the regulation of an assortment of cellular processes including proliferation, apoptosis and differentiation (Miyata *et al.*, 2008) (Buechler *et al.*, 2010). Levels of CK2 are consistently elevated in cancer cells when compared to

normal cells of the same type, suggesting a role for CK2, and its binding partner AdipoR1, in tumourigenesis (Ahmad *et al.*, 2008). Interestingly, the 113-132 amino acid sequence in AdipoR1 that binds CK2β is conserved in AdipoR2, yet numerous attempts by Heiker *et al.* (2009) to co-immunoprecipitate AdipoR2 and CK2β were not successful.

CK2 is the only known kinase that phosphorylates and activates the co-chaperone **c**ell **d**ivision **c**ycle protein **37** (CDC37) on its serine 13 residue, an event essential for the stable interaction of CDC37 with **h**eat **s**hock **p**rotein **90** (HSP90) (Miyata *et al*., 2004). HSP90 is a molecular chaperone that supports the functionality of a wide variety of signal transducing proteins by maintaining their correct conformation (Miyata *et al.*, 1997). Specifically, association of phosphorylated CDC37 with HSP90 protects cytoplasmic **l**iver **k**inase **B1** (LKB1), formerly known as **s**erine **t**hreonine **k**inase **11** (STK11), from proteasomal-mediated degradation by binding the kinase domain of LKB1 without impacting its catalytic activity (Boudeau *et al*., 2003) (Nony *et al*., 2003). This interaction was confirmed by treating cells with geldanamycin, an HSP90 inhibitor that interferes with the ATP/ADP binding pocket of HSP90 and causes the dissociation of HSP90 from its client proteins. Geldanamycin disrupted the CDC37-HSP90-LKB1 complex and promoted the degradation of LKB1 by the proteasome (Nony *et al.*, 2003). Interestingly, a cell line isolated from a testicular tumour was found to have a mutation in the catalytic domain of LKB1 where CDC37-HSP90 bind. This mutation to LKB1 impaired the formation of the CDC37-HSP90-LKB1 complex and reduced the half-life of the mutated LKB1 from two hours to 30 minutes (Nony *et al.*, 2003). Taken together, these studies

suggest that these proteins interact through the hypothetical signalling cascade, AdipoR1-CK2β-CDC37-HSP90-LKB1.

LKB1 is an upstream serine/threonine kinase for the 14 members of the AMPK family of proteins, though, the major downstream target of LKB1 is AMPK (Marignani *et al.*, 2005). The large range of different targets of LKB1 enables it to impact an assortment of cellular processes including cell cycle arrest, p53-mediated apoptosis, Wnt signalling, cell polarity, TGF-β signalling, ras-induced cell transformation and energy metabolism (Just, 2011) (Shorning *et al.*, 2011). Activity of LKB1 results from an allosteric modification induced by the pseudo-kinase **STE**20-**r**elated **ad**aptor (STRAD), which adopts a conformation similar to an active kinase and associates with LKB1 as one of its substrates, and the scaffolding protein MO25, which stabilizes the activation loop of LKB1 (Hawley *et al.*, 2003) (Marignani *et al.*, 2005). LKB1 is believed to be constitutively active in cells, however, it is the condition of low cellular energy that induces a conformational change in the structure of AMPK and permits LKB1 to phosphorylate and activate AMPK (Alessi *et al.*, 2006). AMPK is a heterotrimeric protein comprised of regulatory β and γ, and catalytic α subunits, that functions to maintain the cellular energy balance, measured through the AMP:ATP ratio (Michell *et al.*, 1996). Metabolic stress increases cellular AMP levels and activates AMPK to increase ATP production and decrease energy consumption through the regulation of an array of signalling pathways including glycolysis, glucose uptake, lipid oxidation, fatty acid synthesis, cholesterol synthesis and gluconeogenesis (Hawley *et al.*, 2003). Specifically,

AMPK is activated by AMP, which binds to the four **c**ystathionine **b**eta **s**ynthase (CBS) domains in the γ subunit, and causes the activation of the catalytic α subunit on the threonine 172 residue by one of three upstream kinases: LKB1, **ca**l**m**odulin-dependent protein **k**inase **k**inase-**β** (CaMKKβ) or TAK1 (Hawley *et al.*, 1996) (Viollet *et al.*, 2010). CaMMKβ appears to play a minor role in the adiponectin-mediated activation of AMPK, when compared to LKB1 (Buechler *et al.*, 2010). Indeed, studies in LKB1 tissue-specific knockout mice revealed that LKB1 mediates AMPK activation in the majority of tissues, while CaMKKβ activates AMPK in some hypothalamic neurons, T cells and endothelial cells (Shackelford *et al.*, 2009).

Adiponectin treatment has been established to induce the phosphorylation of AMPKα on threonine 172 in a variety of cell types, and accordingly, adiponectin-knockout mice have reduced expression of AMPK (Martinez-Agustin *et al.*, 2010) Thus, the ability of adiponectin to mediate the activation of AMPK is clear, however the mechanism by which adiponectin signals through the plasma membrane to AMPK is not clear (Mao *et al.*, 2006). Interestingly, targeted disruption of AdipoR1 in cells abrogates the adiponectin-mediated activation of AMPK (Yamauchi *et al.*, 2007). Moreover, adenoviral-mediated restoration of AdipoR1 to these cells and subsequent adiponectin treatment results in a significant increase in phosphorylated AMPKα levels (Yamauchi *et al.*, 2007). Taken together, these results suggest a critical role for AdipoR1 in the adiponectin-mediated activation of AMPK. As well, skeletal muscle cells derived from obese and type 2 diabetic patients with low adiponectin levels, cannot activate AMPK in

response to adiponectin treatment, indicating that disrupted adiponectin-AMPK signalling may have profound effects in human disease (McAinch *et al.*, 2006).

1.3 ***Adiponectin, AdipoR1 and LKB1 in cancer***

Although the exact mechanism by which obesity contributes to an increased risk of developing various health conditions is not known, recent clinical trials have identified body weight as an important risk factor in the development of a variety of cancers (Renehan *et al.*, 2008). Morbidly obese patients, with a BMI larger than 40 kg/m^2, have a greater rate of death caused by cancer, 52% higher in men and 62% higher in women, compared to individuals with normal weight individuals (Calle *et al.*, 2003). In particular, an increased BMI was significantly associated with higher rates of death due to cancer of the esophagus, colon, rectum, liver, gallbladder, pancreas and kidney (Calle *et al.*, 2003). In the case of kidney cancer, 75% of which develops as **r**enal **c**ell **c**arcinoma (RCC), clinical studies have consistently shown obesity to be a significant risk factor (Chow *et al.*, 1999). Briefly, a study by Chow *et al.* (2000) demonstrated a higher BMI increased the long-term risk of developing RCC in a cohort of 759 men. As well, another study by Calle *et al.* (2003) identified a BMI in both men and women between 18.5 kg/m^2 – 24.9 kg/m^2, 25.0 kg/m^2 – 29.9 kg/m^2, 30.0 kg/m^2 – 34.9 kg/m^2, and 35.0 kg/m^2 – 39.9 kg/m^2 to have a 1.00, 1.18, 1.36 and 1.70 relative risk of developing RCC, respectively. Due to the association of obesity with an increased risk of developing cancer and the association of

obesity with reduced adiponectin levels, it is plausible that adiponectin has a role in preventing tumourigenesis.

Indeed, recent studies suggest that adiponectin might act as a preventive agent (Pfeiler *et al.*, 2010). An *in vitro* study on six gastric cancer cell lines determined that adiponectin potently inhibits proliferation of the cells and induces apoptosis (Ishikawa *et al.*, 2007). Furthermore, down regulation of AdipoR1 and AdipoR2 in these six cancer cell lines abrogates the growth inhibitory effects of adiponectin (Ishikawa *et al.*, 2007). Similarly to the adiponectin-mediated growth inhibition in the gastric cancer cell lines, adiponectin suppresses the proliferation of three colon cancer cell lines at the G1/S cell cycle boundary and concurrently increases expression of activated AMPK (Kim *et al.*, 2010). Moreover, knockdown of adiponectin receptors in these three colon cancer cell lines reverses the growth suppressive effects of adiponectin (Kim *et al.*, 2010). Another study on the MCF-7 breast cancer cell line demonstrated that adiponectin treatment reduces the growth of the cancer cells (Dieudonne *et al.*, 2006). Likewise, adiponectin treatment of the MCF-10A breast cancer cell line inhibits the growth of the cells to approximately 30% in relation to untreated MCF-10A cells (Treeck *et al.*, 2008). Examination of adiponectin and breast cancer *in vivo* determined that women with high adiponectin levels have a 65% reduced risk of developing breast cancer compared to age-matched cancer-free women (Korner *et al.*, 2007). Another clinical study associated low adiponectin levels in patients with breast cancer with a more aggressive tumour phenotype, defined as having a larger tumour size, a greater lymph node positivity and higher histological grade,

when compared to breast tumours in patients with high adiponectin levels (Takahata *et al.*, 2007).

The association between high adiponectin levels and reduced cancer risk is not exclusive to breast cancer. In fact, clinical trials have directly correlated reduced adiponectin levels with an increased incidence of developing a variety of malignancies, including breast, colon, endometrial, prostate and kidney (Chou *et al.*, 2010). Specifically with kidney cancer, a study by Spyridopoulos *et al*. (2007) concluded that serum adiponectin levels are significantly and inversely associated with the risk of developing RCC, which persists after adjustment for BMI. Specifically, overweight and obese patients have a 1.5 to 3.0 higher risk for developing RCC when compared to subjects of normal weight (Spyridopoulos *et al.*, 2007). Horiguchi *et al.* (2008) also confirmed that the serum level of adiponectin is decreased in patients with metastatic RCC compared to patients with non-metastatic RCC. As well, a recent study with RCC patients determined an association between low levels of adiponectin and an increased risk of developing a larger and more aggressive tumour, as well as having an increased likelihood of metastasis (Pinthus *et al.*, 2008). Specifically, a significantly lower plasma adiponectin level is observed in RCC tumours larger than 4cm when compared to tumours smaller than 4cm (Pinthus *et al.*, 2008). Significantly lower plasma adiponectin levels are also observed in RCC patients with metastatic disease, compared to RCC patients without metastatic disease (Pinthus *et al.*, 2008). These anti-proliferative effects of adiponectin on a variety of cancers further suggest that adiponectin may inhibit cellular processes

involved in tumourigenesis, and reduction in adiponectin and/or adiponectin receptors would disrupt this inhibition.

Yamauchi *et al.* (2007) demonstrated that the tumour-suppressive effects of adiponectin are mediated to a greater extent through AdipoR1 than AdipoR2 because the signalling pathways involved in anti-tumour effects require AMPK, which is activated through AdipoR1. Therefore, AdipoR1 expression is a critical factor in mediating tumour-suppressive effects by adiponectin. In agreement with this view, mRNA levels of *AdipoR1* were found to be lower in the gastric tumour tissue of 67 patients when compared to the matched normal surrounding tissue (Otani *et al.*, 2010). Immunohistochemical staining for AdipoR1 in prostate tumour tissue and prostate tissue from normal controls determined that 29% of prostate tumour samples express AdipoR1 compared to 62% of normal tissue samples (Michalakis *et al.*, 2007). As well, approximately 50% of RCC patients with metastatic disease present a lower expression of AdipoR1 in the tumour tissue compared to normal surrounding kidney tissue (Pinthus *et al.*, 2008). Taken together these studies suggest a critical role for AdipoR1 in mediating the tumour-suppressive effects of adiponectin in a variety of cancers.

Adiponectin-mediated tumour suppression likely involves the activation of AMPK and its inhibition of the **m**ammalian **t**arget **o**f **r**apamycin (mTOR). Downregulation of this pathway results in the loss of AMPK-mediated inhibition of mTOR and thus the constitutive activation of mTOR. Hyperactive mTOR is associated with a wide variety of

cancers (Van Veelen *et al.*, 2011). Specifically, hyperactive mTOR has been established to be present in a variety of RCC cell lines and patient tumours (Robb *et al.*, 2007). In fact, immunohistochemical staining of a renal tissue microarray containing RCC tumour tissue from 29 patients and normal renal tissue from 17 patients revealed that the majority of RCC tumours possess increased mTOR activity levels, inferred through p-mTORser2448 levels (Robb *et al.*, 2007). Hence, inhibition of mTOR in RCC has been suggested as an effective treatment option (Woodard *et al.*, 2010). Indeed, the mTOR inhibitors temsirolimus and everolimus were approved by the **F**ood and **D**rug **A**dministration (FDA) in May 2007 and March 2009, respectively, for the treatment of advanced RCC (Van Veelen *et al.*, 2011). As well, treatment of RCC with the mTOR inhibitor rapamycin for 22 months results in regression of RCC tumour size in the first nine months of therapy and stabilizes RCC tumour growth during the subsequent 13 months of therapy (Pressey *et al*., 2010). Another clinical study using the mTOR inhibitor CCI-779 involving patients with advanced RCC demonstrates an objective response rate of 7%, including one complete and seven partial responses (Robb *et al.*, 2007).

LKB1 is essential for the effective inhibition of mTOR by the majority of mTOR inhibitors (Sanchez-Cespedes *et al.*, 2002). In line with the hyperactivation of mTOR in a variety of cancers, inactivating mutations of LKB1 have been observed in a variety of tumours (Sanchez-Cespedes, 2011). Approximately 33% of sporadic lung adenocarcinomas display somatic mutations in the LKB1 gene, while the frequency of LKB1 mutations is lower in breast tumours, ovarian carcinomas, pancreatic

adenocarcinomas and biliary adenocarcinomas (Marignani *et al.*, 2005). Sequencing of LKB1 in a variety of tumours identified numerous somatic mutations in the catalytic domain of LKB1, all of which predicted a truncated and non-functional protein (Sanchez-Cespedes *et al.*, 2002). Hypermethylation of the LKB1 promoter, resulting in the transcriptional silencing of the LKB1 gene, has also been identified in the lung tumour tissue of patients, suggesting an additional method to inactivate LKB1 (Sanchez-Cespedes *et al.*, 2002). As well, the absence of LKB1 in the HeLa cervical cancer cell line was determined to be the result of the biallelic inactivation of LKB1 attributed to promoter hypermethylation rather than mutation (Shorning *et al.*, 2011). Thus, the previously mentioned low frequency of LKB1 mutation in various types of cancer, may not reflect the actual expression of LKB1 because of epigenetic silencing events, including promoter hypermethylation, that are undetected in sequencing (Shorning *et al.*, 2011). Analysis of human pancreatic tumour tissue supports this suggestion because only a small number of mutations to LKB1 were reported in pancreatic tumours (Van Veelen *et al.*, 2011), however in a study by Morton *et al.* (2010), approximately 20% of the pancreatic tumours examined presented a downregulation of LKB1 protein expression when compared to matched normal ductal epithelium.

Germline mutation to the LKB1 gene on human chromosome 19p13.3 is the predominant cause of Peutz-Jeghers syndrome, which contrasts the somatic mutations to LKB1 in tumours (Hemminki *et al.*, 1998). Peutz-Jeghers syndrome is an autosomal dominant genetic disease characterized by the development of multiple benign

gastrointestinal hamartomatous polyps, the presence of abnormal melanin pigmentation and an increased risk of developing cancer (Hemminki *et al.*, 1998). In fact, patients with Peutz-Jeghers syndrome have an 84-fold increased risk of developing colon cancer, a 213-fold increased risk of developing gastric cancers and a 520-fold increased risk of developing cancers of the small intestinal, when compared to patients without Peutz-Jeghers syndrome (Marignani *et al.*, 2005). The molecular mechanism that underlies Peutz-Jeghers syndrome and its associated malignancies is not fully understood. Attempts to study the loss of LKB1 function, through the use of LKB1 knockout mice, were not successful because $LKB1^{-/-}$ mice are not viable (Ylikorkala *et al.*, 2001). Analysis of $LKB1^{-/-}$ embryos at embryonic day 9.25 revealed significant vascular defects and an increased expression of **v**ascular **e**ndothelial **g**rowth **f**actor (VEGF) in the mesenchyme, heart and yolk sac (Ylikorkala *et al.*, 2001). As well, mouse embryonic fibroblasts isolated from $LKB1^{-/-}$ mice present reduced AMPK activation (Marcus *et al.*, 2010). Interestingly, heterozygous $LKB1^{+/-}$ mice are viable and show similarity to the Peutz-Jeghers syndrome phenotype, defined by the development of benign intestinal polyps and an increased risk of developing a range of cancers later in life (Sanchez-Cespedes *et al.*, 2007).

Reintroduction of LKB1 into human cancer cell lines with reduced LKB1 expression resulted in growth suppression due to a G1 cell cycle arrest (Tiainen *et al.*, 2002), which was also observed with the overexpression of LKB1 in the LKB1-deficient HeLa cancer cell line (Boudeau *et al.*, 2003). As well, overexpression of LKB1 in a melanoma cell line

induces the expression of the $p21^{WAF1/CIP1}$ inhibitor of cyclin-dependent kinases, which could explain the ability of LKB1 to induce a G1 cell cycle arrest (Boudeau *et al.*, 2003). Karuman *et al.* (2001) demonstrated LKB1 physically associates with p53 to regulate p53-dependent apoptosis pathways, which was supported by a microarray analysis of A549 human lung adenocarcinoma cells treated with LKB1 that demonstrated an induction of p53 response genes (Boudeau *et al.*, 2003).

Regretfully, the incidence of **r**enal **c**ell **c**arcinoma (RCC) appears to be steadily rising, for which the reason is not understood (Chow *et al.*, 1999). Although improvements in diagnosis may contribute to the rising incidence, the frequency of both late-stage RCC and mortality from RCC have also been increasing, implying that other factors are contributing to the increase in incidence (Setiawen *et al.*, 2007). RCC is a highly aggressive cancer for which treatment options are limited (Woodard *et al.*, 2010). What is more, surgical removal of RCC may be curative if the disease is confined, however approximately 30% of RCC will metastasize, and be resistant to chemotherapy and radiation (Chow *et al.*, 1999). Although the roles of adiponectin, AdipoR1 and LKB1 as molecular inhibitors of tumourigenesis have been examined in several types of cancers, limited research has been conducted on RCC. Thus, clarifying the expression and significance of adiponectin, AdipoR1 and LKB1 in RCC would provide fresh insight into the link between two prevailing health problems in the Western world: obesity, in which adiponectin levels are low, and cancer, in which adiponectin, AdipoR1 and LKB1 levels are low. Knowledge that will be gained from this study will likely provide new drug

targets for the development of innovative pharmacological strategies to decrease the development and progression of RCC.

RATIONALE

Previous studies have examined adiponectin, AdipoR1 and LKB1 expression in several malignancies in an attempt to explain their role in inhibiting tumourigenesis. Indeed, reduced levels of adiponectin associate strongly with an increased risk of developing RCC, however, the expression of AdipoR1 and LKB1 in RCC is not conclusive. AdipoR1 mediates the tumour-suppressive adiponectin-AMPK signalling pathway and LKB1 is an established tumour suppressor that activates the AMPK-mediated inhibition of mTOR. Thus, coupling the established reduction of adiponectin in RCC with a dysregulation in AdipoR1 and/or LKB1 expression would provide fresh insight into the mechanism underlying the association of obesity and RCC development.

HYPOTHESIS

AdipoR1, the receptor which mediates adiponectin-AMPK tumour suppression, and LKB1, the upstream kinase of AMPK, are downregulated in RCC. Thus, dysregulation of AdipoR1 and LKB1 leads to an increased tumourigenic potential of human RCC cells, and coupled with the reduction in plasma level of adiponectin, contributes to the development of RCC.

OBJECTIVES

The following two objectives are proposed to test the hypothesis that LKB1 and AdipoR1 are downregulated in RCC, and that the dysregulation leads to an increased tumourigenic potential of human RCC cells.

Objective 1

Identify dysregulations in AdipoR1 and LKB1 transcript and protein expression levels in RCC patient tumours

4.1.1 Measure *AdipoR1*, *LKB1* and *VEGFA* transcript levels in patients' RCC tumour tissue and compare to the transcript levels in the matched normal surrounding parenchyma

4.1.2 Confirm that any dysregulation to the transcript level in RCC tumours translates to a dysregulation of protein expression

4.1.3 Visualize any dysregulations to protein expression levels in RCC tumours by immunohistochemical staining of patient tumour and matched normal tissues

Objective 2

Demonstrate that downregulated AdipoR1 and LKB1 expression in RCC disturbs the tumour-suppressive adiponectin-AMPK signalling pathway and increases RCC cells' tumourigenic potential

4.2.1 Rationalize the CRL-1932 human RCC cell line as an *in vitro* model for human RCC by confirming the presence and functionality of adiponectin receptors

4.2.2 Generate stable CRL-1932 AdipoR1 and LKB1 knockdown cell lines

4.2.3 Investigate the impact of AdipoR1 and LKB1 knockdown on LKB1 and AdipoR1 transcript and protein expression, respectively

4.2.4 Demonstrate the importance of AdipoR1 and LKB1 in adiponectin-AMPK signalling by examining established signalling events in AdipoR1 and LKB1 knockdown cell lines

4.2.5 Examine the impact of AdipoR1 and LKB1 knockdown on RCC tumourigenicity by examining the hallmarks of tumour progression

EXPERIMENTAL PROCEDURES

5.1 Cell lines and culture conditions

Bacterial cell line. *E. Coli* DH5α (*Invitrogen*, Burlington ON, Catalogue Number 18265-017) was transformed with various plasmids (reference ***Bacterial transformation***), amplified at 37ºC in LB broth (20 g/L) (*Sigma-Aldrich*, Oakville ON, Catalogue Number L3022) and on LB agar (35 g/L) (*Sigma-Aldrich*, Catalogue Number L2897) supplemented with 100 μg/mL ampicillin (*EMD Millipore*, Burlington MA, Catalogue Number CA80055-786), 50 μg/mL kanamycin (*EMD Millipore*, Catalogue Number CA80502-840) or 25 μg/mL chloramphenicol (*Sigma-Aldrich*, Catalogue Number C7795) and purified (reference ***DNA purification***).

Mammalian cell lines. The CRL-1932 and CRL-1933 human RCC kidney cell lines (*ATCC*, Burlington ON, Catalogue Numbers 786-O and 769-P) were originally isolated from the clear cell renal adenocarcinoma of a 58-year old male and 63-year old female, respectively. Cells were cultured in GIBCO® RPMI-1640 medium (*Invitrogen*, Catalogue Number 22400) supplemented with 10% FBS (*Sigma-Aldrich*, Catalogue Number F1051) and 100μg/mL penicillin and streptomycin (*Invitrogen,* Catalogue Number 15070). The 293T cell line (*ATCC*, Catalogue Number CRL-11268) is a derivative of the HEK293 human embryonic kidney cell line, which includes a temperature sensitive SV40 T-antigen, that was used to produce high titres of infectious retrovirus (reference ***shRNA***

and viral plasmid infection). 293T cells were grown in GIBCO® DMEM medium (*Invitrogen*, Catalogue Number 11965-092) supplemented with 10% FBS and 100 µg/mL penicillin and streptomycin. All cells were propagated at 37ºC in 5% CO_2 and in a humidified atmosphere containing 21% O_2.

5.2 **Animals and handling**

Nude mice. *In vivo* studies were performed using 20 male BALB/c Nu/Nu (homozygous) immunodeficient mice (*Charles River*, Sherbrooke QC, Strain Number 194) that were received at four weeks of age. Mice were left to acclimatize in the animal facility for one week before being injected (reference ***Tumour growth assay***) at five weeks of age. The *Animal Research Ethics Board* at McMaster University approved all experimental procedures.

5.3 **Human tissue collection and preparation**

Human tissue collection. A sample of tumour tissue and normal surrounding parenchyma was taken from the extracted kidney of patients diagnosed with RCC that underwent a radical nephrectomy surgery at *St. Joseph's Healthcare Hamilton* (Hamilton ON) in accordance with hospital ethics standards. Immediately upon removal, the tissue was

inserted into a 2mL Nalgene Cryogenic Vial (*Thermo Fisher Scientific*, Whitby ON, Catalogue Number 5000-0020) and flash frozen in liquid nitrogen until it was homogenized (reference ***Tissue homogenization for pilot study's AdipoR1 protein analysis*** and ***Tissue homogenization for AdipoR1, AdipoR2, LKB1 and VEGFA RNA analysis and LKB1 protein analysis***) or prepared for immunohistochemical staining (reference ***Immunohistochemical staining of human kidney tissue and mouse xenografts***).

Tissue homogenization for pilot study's AdipoR1 protein analysis. Kidney tissue was removed from storage in liquid nitrogen and ground to a fine powder with a mortar and pestle (*VWR*, Mississauga ON, Catalogue Number 89038-144). Throughout the homogenization a small volume of liquid nitrogen was added to the tissue to maintain a cold temperature. The ground tissue was transferred into a 1.5 mL microcentrifuge tube (*Dia-Med*, Mississauga ON, Catalogue Number SPE155-N) and kept on ice. Immediately prior to lysis, 1 mM PMSF, 2 µg/mL Leupeptin and 10 µg/mL Aprotinin was added to the stock lysis buffer (50 mM Tris pH7.4, 150 mM NaCl, 5 mM EDTA, 1% Triton X100, 10% Glycerol, 100 µM Na_3UO_4, 1 mM p-glycerophosphate and 1 mM NaF) and 100 µL of the buffer was transferred into each microcentrifuge tube containing ground kidney tissue. The contents of the microcentrifuge tube were mixed thoroughly and left on ice for 30 min to lyse the cells. Samples were centrifuged at 13,000 g for 5min at 4ºC and the supernatant was transferred to a chilled 1.5 mL microcentrifuge tube. The protein concentration was calculated (reference ***DC protein assay***) and standardized to 4 µg/mL

using 4X SDS lysis buffer. Then, 1/20 volume of 1M DTT (*Fisher BioReagents*, Whitby ON, Catalogue Number BP172-5) and 1/5 volume of 0.05% bromophenol blue (*Bio-Rad*, Mississauga ON, Catalogue Number 161-0404) was added to each sample and the samples were stored at -80ºC until analysis by western blot (reference ***Western blot analysis***).

Tissue homogenization for AdipoR1, AdipoR2, LKB1 and VEGFA RNA analysis and LKB1 protein analysis. Kidney tissue was removed from storage in liquid nitrogen and separated into both total protein and total RNA using the Ambion PARIS^{TM} Kit (*Applied Biosystems*, Burlington ON, Catalogue Number AM1921). Briefly, each sample of kidney tissue was cut to weigh approximately 75 mg, inserted into a 1.5 mL microcentrifuge tube and placed on ice. Then, 600 µL of ice-cold Cell Disruption Buffer was added to the microcentrifuge tube and an OMNI TH_Q digital tissue homogenizer (*VWR,* Catalogue Number 12-200-1) was applied at medium intensity for 10 sec intervals until the tissue was ground. Debris including connective tissue was removed from the tissue lysate by centrifuging the sample at 14,000 g for 10 min at 4ºC. Then, 400 µL of the supernatant was transferred into a clean microcentrifuge tube labelled "protein", which remained on ice for 10min to complete cell disruption. The protein concentration was calculated (reference ***DC protein assay***) and standardized to 4 µg/mL using 4X SDS lysis buffer. Then, 1/20 volume of 1M DTT and 1/5 volume of 0.05% bromophenol blue was added to each sample and the samples were stored at -80ºC until analysis by western blot (reference ***Western blot analysis***). The remaining 200 µL of supernatant was transferred

into a microcentrifuge tube labelled "RNA" and an equal volume (200 µL) of 2X Lysis/Binding Solution at room temperature was added to the microcentrifuge tube. Then, 200 µL of 100% ethanol was added and the microcentrifuge tube was inverted five times to mix the solution thoroughly. To reduce the viscosity of the solution and prevent clogging of the Filter Cartridge, the solution was passed through a 1 mL syringe (*Becton Dickinson*, Mississauga ON, Catalogue Number 309659) attached to a $20G1^{1/2}$ needle (*Becton Dickinson*, Catalogue Number 305176) ten times. The 600 µL solution was applied to a Filter Cartridge assembled in a Collection Tube and the unit was centrifuged at 14,000 g at 4ºC for 30 sec. The flowthrough was discarded. Then the Filter Cartridge was washed with 700 µL of Wash Solution 1 at room temperature, 500 µL of Wash Solution 2/3 at room temperature and again with 500 µL of Wash Solution 2/3 at room temperature through successive centrifugations at 14,000 g for 30 sec at 4ºC. Following the final wash, the Filter Cartridge and Collection Tube unit was centrifuged at 14,000g for 1 min at 4ºC to remove traces of Wash Solution 2/3. The Filter Cartridge was moved into a new Collection Tube and 40 µL of 95ºC Elution Buffer was applied to the center of the filter. The unit was centrifuged at 14,000 g for 1 min at 4ºC and then the 40 µL flowthrough was reapplied to the center of the filter and the unit was centrifuged at 14,000 g for 1 min at 4Cº to concentrate the RNA. The amount of RNA was determined (reference ***RNA quantification***), synthesized into cDNA (reference ***cDNA synthesis***) and stored at -80ºC until it was analyzed by qRT-PCR (reference ***Quantitative real time PCR***).

5.4 **RNA extraction, quantification, synthesis and analysis**

RNA extraction from mammalian cell lines. Total RNA was extracted from the CRL-1932, shLKB1, shCONTROL, shVAdipoR1 and shVControl cell lines using the RNeasy® Mini kit (*Qiagen*, Mississauga ON, Catalogue Number 74104). Approximately $2.0x10^5$ cells were washed thoroughly with GIBCO® **P**hosphate **B**uffered **S**aline (PBS) (*Invitrogen*, Catalogue Number 10010-023) and 600 µL of Buffer RLT was applied to the 100 mm plate (*Corning*, Corning NY, Catalogue Number 430167). Cells were lifted off the tissue culture plate using a Cell Scraper (*BD*, Mississauga ON, Catalogue Number 353086) and transferred to a 1.5 mL microcentrifuge tube. The tube was vortexed to remove clumps of cells and each lysate was passed through a $20G1^{½}$ needle attached to a 1mL syringe, five times. An equal volume of 70% ethanol was added into the microcentrifuge tube and the solution was mixed thoroughly by pipetting. An RNeasy Mini Spin Column was inserted into a 2 mL Collection Tube and 700 µL of the lysate was placed into the Spin Column. The Spin Column was centrifuged for 15 sec at 8,000 g and the flowthrough was discarded. All remaining lysate was applied to the Spin Column and the unit was centrifuged for 15 sec at 8,000 g. Then, 700 µL of Buffer RW1 was applied to the Spin Column, the unit was centrifuged for 15 sec at 8,000 g and the flowthrough was discarded. Then, 500 µL of Buffer RPE was applied to the Spin Column and the unit was centrifuged for 15 sec at 8,000 g, twice. The Spin Column was moved into a new 2 mL Collection Tube and the unit was centrifuged for 1 min at full speed. The Spin Column was moved into a new 1.5 mL Collection Tube, 30 µL of *GIBCO®*

UltraPure™ Distilled Water (*Invitrogen*, Catalogue Number 10977-015) was applied to the Spin Column and the unit was centrifuged for 1 min at 8,000 g to elute the RNA. The concentration of RNA was measured (reference ***RNA quantification***) and the sample was stored at -80ºC until synthesis into cDNA (reference ***cDNA synthesis***) and analysis by **q**uantitative **r**eal **t**ime **p**olymerase **c**hain **r**eaction (qRT-PCR) (reference ***Quantitative real time PCR***).

RNA quantification. The concentration of RNA was measured by absorbance on a NanoVue Plus Spectrophotometer (*General Electric Healthcare*, Piscataway NJ, Catalogue Number 28-9569-65) at 260 nm and was determined as the average of two independent trials using 2 µL of sample.

cDNA synthesis. RNA was transcribed into cDNA using the SuperScript VILO™ cDNA Synthesis Kit (*Invitrogen*, Catalogue Number 11754-010). Briefly, 2.5 µg of RNA was added to a 0.2 µL PCR tube (*Dia-Med*, Catalogue Number 3240-00) containing 4 µL of 5X VILO™ Reaction Mix (which included random primers, $MgCl_2$ and dNTPs) and 2µL of 10X SuperScript Enzyme Mix (which included SuperScript III reverse transcriptase and RNaseOUT™ Recombinant Ribonuclease Inhibitor). The solution was brought to a final volume of 20 µL with UltraPure™ Distilled Water and was gently mixed. The PCR tube was incubated at 25ºC for 10 min, 42ºC for 1 h and 85ºC for 5 min. The cDNA product was diluted 1:4 in UltraPure™ Distilled Water and stored at -80ºC until it was analyzed by qRT-PCR (reference ***Quantitative real time PCR***).

Quantitative real time PCR (qRT-PCR). RNA samples were analyzed for *AdipoR1*, *AdipoR2*, *LKB1*, *VEGFA*, *β-Actin* and *18S* induction using established primer sequences (**Table 1**). Primers were ordered from *Integrated DNA Technologies* (Hamilton ON) as de-salted and at a synthesis scale of 0.025 µmol. The primers were suspended in a volume of UltraPure™ Distilled Water specified by the *Applied Biosystems* 'Calculator for Suspension of Dry Single-Stranded Oligonucleotides' (http://www4.appliedbiosystems.com/techlib/append/oligo_dilution.html) to achieve both a 100 µM stock and a 10 µM working concentration, and were stored at -20ºC. For each target gene, 12.5 µL of Power SYBR Green PCR Master Mix (*Applied Biosystems*, Catalogue Number 4367659), 9.5 µL of UltraPure™ Distilled Water, 0.5 µL of 10 µM forward target gene primer, 0.5 µL of 10 µM reverse target gene primer and 2.0 µL of diluted cDNA were assembled as a mixture in a 1.5 mL microcentrifuge tube that was placed on ice. In triplicate the 25 µL mixture was added into a single well of a MicroAmp Optical 96-Well Reaction Plate (*Applied Biosystems*, Catalogue Number N8010560) and a MicroAmp Optical 8-Cap Strip (*Applied Biosystems*, Catalogue Number 4323032) was applied to each column of the 96-well plate. The plate was centrifuged at 3,500 g for 1 min at 4ºC to remove bubbles and loaded into a 7500 Real Time PCR System (*Applied Biosystems*, Catalogue Number 4351105). Target gene analysis was performed using the manufacturer's 7500 System SDS Software, Sequence Detection Software, Version 1.2.2 with SYBR programmed as the *Detector* and ROX as the *Passive Reference*. Fluorescence emission data was collected during the second step of the third stage of the program: (Stage 1) 50ºC for 2 min, (Stage 2) 95ºC for 10 min, (Stage 3) 95ºC for 15 sec and 60ºC for 1 min (40 cycles),

with an added Dissociation Stage of 95ºC for 15 sec, 60ºC for 1 min and 95ºC for 15 sec to monitor primer dimer formation. *AdipoR1*, *AdipoR2*, *LKB1* and *VEGFA* gene expression was determined using the average of the triplicate **c**ritical **t**hreshold (C_T) values in the $2^{-\Delta CT}$ equation relative to the expression of housekeeping genes', *β-Actin* and *18S*.

Table 1 | **Primer sequences used for quantitative real time PCR** to target *AdipoR1*, *AdipoR2*, *LKB1*, *VEGFA*, *β-Actin* and *18S* genes.

TARGET	SPECIES	REFERENCE	(FORWARD/REVERSE) PRIMER SEQUENCE
AdipoR1	Human	McAinch et *al*, 2006	(Forward) 5'-CGC CAT GGA GAA GAT GGA A-3'
	Human	McAinch et *al*, 2006	(Reverse) 5'-TCA TAT GGG ATG ACC CTC CAA-3'
AdipoR2	Human	McAinch et *al*, 2006	(Forward) 5'-GGA TCC CCG AAC GCT TTT T-3'
	Human	McAinch et *al*, 2006	(Reverse) 5'-TGA GAC ACC ATG GAA GTG AAC AA-3'
LKB1	Human	Harvard PrimerBank ID: 4507271a1	(Forward) 5'-GAG CTG ATG TCG GTG GGT ATG-3'
	Human	Harvard PrimerBank ID: 4507271a1	(Reverse) 5'-CAC CTT GCC GTA AGA GCC T-3'
VEGFA	Human	Thijssen et *al*, 2004	(Forward) 5'-AAG GAG GAG GGC AGA ATC AT-3'
	Human	Thijssen et *al*, 2004	(Reverse) 5'-CCA GGC CCT CGT CAT TG-3'
β-Actin	Human	Sloan et *al*, 2009	(Forward) 5'-CCC TGA AGT ACC CCA TCG AG-3'
	Human	Sloan et *al*, 2009	(Reverse) 5'-CAG ATT TTC TCC ATG TCG TCC C-3'
18S	Human	Wei et *al*,2003	(Forward) 5'-GTA ACC CGT TGA ACC CCA TT-3'
	Human	Wei et *al*, 2003	(Reverse) 5'-CCA TCC AAT CGG TAG TAG CG-3'

5.5 **shRNA and viral plasmids, retroviral and lentiviral particle infections**

shRNA plasmids. The shRNA-mediated knockdown of AdipoR1 and AdipoR2 was facilitated by two HuSH^{TM} pGFP-V-RS plasmids (shVAdipoR1 and shVAdipoR2) (*OriGene*, Rockville MD, Catalogue Number TG306815 and TG306814), each containing a 29 nucleotide target sequence to the protein of interest (**Table 2**), puromycin and kanamycin resistant cassettes as well as a CMV-promoter driven GFP tag. Similarly, shRNA-mediated knockdown of LKB1 was performed with a HuSH^{TM} pRFP-C-RS plasmid (shVLKB1) (*OriGene*, Catalogue Number TF320541) containing a 29 nucleotide target sequence to LKB1 (**Table 2**), puromycin and chloramphenicol resistance cassettes as well as a CMV-promoter driven RFP tag. A non-effective scrambled shRNA target sequence plasmid (shVControl) (*OriGene*, Catalogue Number TR30015) served as the negative control for the knockdown of AdipoR1, AdipoR2 and LKB1. All knockdown experiments were performed in CRL-1932 cells in combination with viral plasmids (reference ***Viral plasmids***) using a retroviral infection method (reference ***shRNA and viral plasmid infection***).

Table 2 | **Short hairpin target sequences** for the retroviral-mediated knockdown of AdipoR1, AdipoR2 and LKB1.

TARGET	SPECIES	shRNA PLASMID	(TUBE ID) shRNA TARGET SEQUENCE
AdipoR1	Human Mouse	shVAdipoR1	(GI327255) 5′-CTGGTTCTTCCTCATGGCTGTGATGTACA-3′
AdipoR2	Human Mouse	shVAdipoR2	(GI327252) 5′-ATGTGACATCTGGTTTCACTCTCATCAGC-3′
LKB1	Human	shVLKB1	(FI379380) 5′-AGAAGACTGCGCTCGGCCGTGTTCATACT-3′

Viral plasmids. The shRNA plasmid specific to AdipoR1 (shVAdipoR1), AdipoR2 (shVAdipoR2), LKB1 (shVLKB1) or scrambled (shVControl) was cotransfected with the *env*-expressing plasmid, pVPack-VSV-G (*Agilent Technologies*, Mississauga ON, Catalogue Number 217567), containing an ampicillin resistance cassette and the *gag-pol*-expressing plasmid, pVPack-GP (*Agilent Technologies*, Catalogue Number 217566), containing an ampicillin resistance cassette to generate a recombinant retrovirus specific to the knockdown of AdipoR1, AdipoR2 or LKB1.

shRNA and viral plasmid infection. Production of recombinant retrovirus specific to the knockdown of AdipoR1, AdipoR2 or LKB1 was performed according to the *Agilent Technologies* protocol. Briefly, 293T cells were seeded to 4.0×10^5 cells/100 mm plate and grown in 10 mL of DMEM media supplemented with 10% FBS for 24 h. Following the

incubation, shRNA and viral plasmids were prepared for calcium phosphate-based transfection in a sterile 1.5 mL microcentrifuge tube by combining 10 µg of pVPack-VSV-G, 10 µg of pVPack-GP, 10 µg of the respective shRNA plasmid (shVAdipoR1, shVAdipoR2 or shVLKB1) and dH_2O to a final volume of 450 µL. Then, 50 µL of 2.5 M $CaCl_2$ (*Fisher Chemical*, Whitby ON, Catalogue Number C79-500) was added to the 1.5 mL microcentrifuge tube and the solution was mixed thoroughly. Then, 500 µL of 2xHBSS was placed in a *Falcon* 14 mL polystyrene round-bottom tube (*VWR*, Catalogue Number 352057) and 500 µL of the prepared DNA was added drop-wise into the 2xHBSS. The 14 mL tube was immediately vortexed at medium speed for 30 sec and the mixture was incubated at room temperature for 20 min. Then, the mixture was added to the 100 mm plate of 293T cells in a drop-wise manner and the cells were incubated for 10 h. Following the incubation, GFP and RFP expression was examined under an Axiovert 200M inverted fluorescent microscope (*Carl Zeiss*, Toronto ON, Catalogue Number 1275-232) to estimate the efficiency of transfection. In the case of successful transfection, the 10 mL of media was carefully aspirated and 10 mL of fresh DMEM supplemented with 10% FBS was added to the 293T cells for a 48 h incubation. Approximately 24 h prior to infection, CRL-1932 cells were seeded to $4.0x10^5$ cells/100 mm plate in 10 mL of RPM1-1640 media supplemented with 10% FBS. On the day of infection, the 10 mL of media from the 100 mm plate of 293T cells was filtered through a 30 mL syringe (*BD*, Catalogue Number 309650) attached to an Acrodisc® 25 mm syringe filter with a *Pall Corporation* 0.45 µm Supor® membrane (*VWR*, Catalogue Number PN4614) and into a sterile 50 mL Nalgene® oak ridge centrifuge tube (*Thermo Fisher Scientific*, Catalogue

Number 3119-0050). The tube was centrifuged at 50,000 g for 1.5 h at 4ºC to pellet the recombinant virus, and the supernatant was aspirated. The virus was resuspended in 1 mL of RPMI-1640 supplemented with 10% FBS and 1 µL of 10 mg/mL Polybrene® (*Santa Cruz Biotechnology*, Santa Cruz CA, Catalogue Number sc-134220). The 1 mL was carefully added to the 100 mm plate of CRL-1932 cells without any RPMI-1640 media covering the cells. The infection was incubated for 2 h, during which at 20 min intervals the 100 mm plate was carefully rotated for 1 min to disperse the virus. Following the incubation, 9 mL of RPMI-1640 media supplemented with 10% FBS and 9 µL of 10 mg/mL Polybrene® was added to the infected CRL-1932 cells and incubated overnight. The media was aspirated and 10 mL of RPMI-1640 media supplemented with 10% FBS was added for 48 h. Infected CRL-1932 cells were selected with 1 µg/mL puromycin dihydrochloride (puromycin) (*Santa Cruz Biotechnology*, Catalogue Number sc-10871) in RPMI-1640 media supplemented with 10% FBS for approximately two weeks, during which the selection media was replaced every two days. Total cell lysates of the infected CRL-1932 cells were prepared to confirm the effective knockdown of the target genes. Briefly, CRL-1932 cells were lysed (reference ***Cell lysate collection***), the protein concentration was calculated (reference ***DC protein assay***) and standardized to 4 µg/mL using 4X SDS lysis buffer. Then, 1/20 volume of 1 M DTT and 1/5 volume of 0.05% bromophenol blue was added to each sample and the samples were stored at -80ºC until analysis by western blot (reference ***Western blot analysis***). Following selection the infected cells were trypsinized and centrifuged in a 50 mL polypropylene tube (*BD*, Catalogue Number 352070) at 1,000 g for 10 min at 4ºC. The pellet was resuspended in 1

mL of RPMI-1640 with 10% FBS and 5% DMSO (*Sigma-Aldrich*, Catalogue Number D8418) that was filtered through a 5 mL syringe (*BD*, Catalogue Number 309603) attached to an *Acrodisc*® 25 mm Syringe Filter with a *Pall Corporation* 0.2 μm Supor® Membrane (*VWR*, Catalogue Number PN4612). The mixture was aliquoted into 2mL *Nalgene*® Cryogenic Vials (*Thermo Fisher Scientific*, Catalogue Number 5000-0020) and stored in liquid nitrogen.

Lentiviral particles. Knockdown of LKB1 in CRL-1932 cells was also facilitated by infection with human LKB1 shRNA Lentiviral Particles (shLKB1) (*Santa Cruz Biotechnology*, Catalogue Number sc-35816-V) (reference ***Lentiviral particle infection***). The Lentiviral Particles contained three target-specific constructs, each with a 19-25 nucleotide shRNA designed to knockdown LKB1 gene expression. Control shRNA Lentiviral Particles (shCONTROL) (*Santa Cruz Biotechnology*, Catalogue Number sc-108080) with a scrambled shRNA sequence not specific to the degradation of any known cellular mRNA were used as a negative control reference for assessing LKB1 knockdown.

Lentiviral particle infection. CRL-1932 cells were seeded at 4.0×10^4 cells/well in a *Falcon* Multiwell™ 12-well tissue culture plate (*VWR*, Catalogue Number 353043) with 1 mL of RPMI-1640 media supplemented with 10% FBS, and were incubated for 24 h. Following incubation, the media was aspirated and the cells were washed thoroughly with 2 mL PBS. Both LKB1 shRNA Lentiviral Particles (shLKB1) and negative control

shRNA Lentiviral Particles (shCONTROL) were thawed on ice, after which 25 µL of each was added per well of CRL-1932 cells along with 1mL of RPMI-1640 media with 10% FBS and 0.5 µL of 10 mg/mL Polybrene®. Following a 24 h incubation, the media was aspirated and replaced with 1mL of fresh RPMI-1640 media with 10% FBS for an additional 48 h incubation. The shLKB1 and shCONTROL cells were selected with 1 µg/mL puromycin in RPMI-1640 media with 10% FBS for two weeks, with fresh selection media added every two days. A total cell lysate of shLKB1 and shCONTROL cells was prepared to confirm the effective knockdown of LKB1 expression. Briefly, cells were lysed (reference ***Cell lysate collection***), the protein concentration was calculated (reference ***DC protein assay***) and standardized to 4 µg/mL using 4X SDS lysis buffer. Then, 1/20 volume of 1 M DTT and 1/5 volume of 0.05% bromophenol blue was added to each sample and the samples were stored at -80ºC until analysis by western blot (reference ***Western blot analysis***). Following selection, shLKB1 and shCONTROL cells were trypsinized and centrifuged in a 50 mL polypropylene tube (*BD*, Catalogue Number 352070) at 1,000 g for 10 min at 4ºC. The pellet was resuspended in 1mL of RPMI-1640 with 10% FBS and 5% DMSO that was filtered through a 5 mL syringe attached to an *Acrodisc*® 25 mm Syringe Filter with a *Pall Corporation* 0.2µm Supor® Membrane. The mixture was aliquoted into 2 mL *Nalgene*® Cryogenic Vials and stored in liquid nitrogen.

5.6 **Bacterial transformation and DNA purification**

Bacterial transformation. All shRNA plasmids (reference ***shRNA plasmids***) and viral plasmids (reference ***Viral plasmids***) were amplified through transformation into *E. Coli* DH5α and subsequent purification (reference ***DNA purification***). Briefly, *E. Coli* DH5α was removed from -80ºC storage and immediately placed on ice to thaw. A 1.5 mL microcentrifuge tube was placed on ice for each plasmid being transformed in addition to two microcentrifuge tubes for the negative controls, 'DH5α-deficient' and 'plasmid-deficient', and one microcentrifuge tube for the positive control, 'pUC19' (*Invitrogen*, Catalogue Number 54395). Then, 50 µL of DH5α bacteria was transferred into each microcentrifuge tube (excluding the DH5α-deficient control) along with 2 µL of the respective plasmid (excluding the plasmid-negative control). The solutions were mixed gently by pipetting and placed on ice for 20 min. Bacteria were heat shocked in a 42ºC water bath for 45 sec and immediately returned to ice for 2 min. Then, 450 µL of SOC Medium (*Invitrogen*, Catalogue Number 15544-034) at room temperature was applied into each microcentrifuge tube and the tubes were placed in a MaxQ 5000 incubating floor shaker (*Thermo Fisher Scientific*, Catalogue Number EW-51708-00) for 1 h at 37ºC. During the incubation four LB agar plates containing 100 µg/mL ampicillin (pVPack-VSV-G and pVPack-GP), or 50 µg/mL kanamycin (shVAdipoR1 and shVAdipoR2), or 25 µg/mL chloramphenicol (shVLKB1 and shVControl) were warmed to 37ºC. Following the incubation, each 450 µL solution was spread uniformly across one respective LB agar plate and the plates were incubated overnight (approximately 16 h) in

a TempCon® Incubator Oven (*Baxter Healthcare*, Mississauga ON, Catalogue Number J1450-4) at 37ºC. Individual bacterial colonies were picked from the LB agar plates and inoculated in a sterile 250 mL flask (*VWR*, Catalogue Number 89000-362) with 30 mL of LB broth containing the appropriate antibiotic. The flask was incubated overnight (approximately 16h) in a MaxQ 5000 incubating floor shaker at 37ºC. Following incubation, a stock of each plasmid was generated by mixing 750 µL of the transformed bacteria (from the 30mL culture) with 750 µL of 30% glycerol (*Caledon Laboratories*, Georgetown ON, Catalogue Number 5350-1) and was stored at -20°C. The remaining bacteria were used for purification of the plasmid (reference ***DNA purification***).

DNA purification. Plasmids were purified using the EndoFree® Plasmid Maxi Kit (*Qiagen*, Catalogue Number 12362) following the manufacturer's protocol from the remaining culture of transformed bacteria (reference ***Bacterial transformation***) or from inoculating 5 µL of a glycerol stock of transformed bacteria into 30 mL of LB broth containing the respective antibiotic and incubating overnight (approximately 16 h) in the MaxQ 5000 incubating floor shaker at 37°C. Briefly, 30 mL of bacteria were transferred into a 50 mL polypropylene tube and were pelleted by centrifugation at 7,000 g for 15 min at 4°C. The supernatant was aspirated and the pelleted bacteria were homogenously resuspended in 10 mL of ice-cold Buffer P1. Then, 10 mL of Buffer P2 at room temperature was applied to the bacteria, the polypropylene tube was vigorously inverted six times and the mixture was incubated at room temperature for 5 min to lyse the bacteria. Following the incubation, 10 mL of ice-cold Buffer P3 was added to the

polypropylene tube and again the polypropylene tube was vigorously inverted six times. The lysate was moved into a QIAfilter™ Maxi Cartridge, incubated at room temperature for 10 min and then gently expelled from the cartridge using the Plunger into a clean 50 mL polypropylene tube. Then, 2.5 mL of Buffer ER was applied to the lysate and the polypropylene tube was inverted ten times and incubated on ice for 30 min. A QIAGEN-tip 500 was equilibrated by gravity flow with 10 mL of Buffer QBT, after which the lysate was placed into the tip and allowed to pass through using gravity flow. The QIAGEN-tip 500 was washed twice with 30 mL of Buffer QC before the plasmid DNA was eluted with 15 mL of Buffer QN. DNA was precipitated by adding 10.5 mL of isopropanol (*Caledon Laboratories*, Catalogue Number 8600-1) at room temperature into a sterile 50 mL *Nalgene*® oak ridge tube with the eluted DNA and centrifuged for 30 min at 11,000 g at 4ºC. The supernatant was aspirated and the DNA pellet was washed with 5 mL of 70% ethanol and centrifuged at 11,000 g for 10 min at 4ºC. Again, the supernatant was aspirated, and the pellet was air-dried for 10 min before being resuspended in 500 µL of dH_2O. Concentration of DNA was measured (reference ***DNA quantification***) and samples were stored at -20°C until use (reference ***shRNA and viral plasmid infection***).

DNA quantification. DNA concentration was measured by absorbance on a NanoVue Plus Spectrophotometer at 260 nm and was determined as the average of two independent trials using 2 µL of sample.

5.7 **Protein lysis, preparation and Western blot analysis**

Cell lysate collection. CRL-1932, shVControl, shVAdipoR1, shVAdipoR2, shVLKB1, shCONTROL, shLKB1 and 293T cells were washed twice with chilled PBS before the respective amount (100 µL in 6-well plate and 800 µL in 100 mm plate) of 4X SDS lysis buffer was applied to the cell culture vessel. Using a sterile cell scraper, cells were lifted from the cell culture vessel and transferred to a chilled 1.5 mL microcentrifuge tube. The lysate was homogenized with a 20G1$^{1/2}$ needle attached to a 1 mL syringe and stored at -80ºC until use.

DC protein assay. Protein concentration of the cell lysates was measured using the Bio-Rad DC Protein Assay. Briefly, the 5 mg/mL Bio-Rad Protein Assay Standard II (*Bio-Rad*, Catalogue Number 500-0007) was prepared as a serial dilution (5 mg/mL, 2.5 mg/mL, 1.3 mg/mL, 0.6 mg/mL, 0.3 mg/mL and 0.2 mg/mL) in 4X SDS lysis buffer. The six standard concentrations were mixed thoroughly and 5 µL of each standard was transferred, in duplicate, into a sterile 96-well microtiter plate (*VWR*, Catalogue Number 353072) along with 5 µL of each sample, in duplicate. Then, 20 µL of Reagent S (*Bio-Rad*, Catalogue Number 500-0115) was added to 1 mL of Reagent A (*Bio-Rad*, Catalogue Number 500-0113) in a 1.5 mL microcentrifuge tube and the solution was mixed thoroughly. Then, 25 µL of the mixture was added to every well of the 96-well microtiter plate followed by 200 µL of Reagent B (*Bio-Rad*, Catalogue Number 500-0114). The 96-well microtiter plate was gently agitated to mix the reagents and any bubbles that formed

in the wells were removed. The microtiter plate was shielded from light with aluminum foil for 15 min, the absorbance was read with a SPECTRAmax Plus 384 spectrophotometer (*Molecular Devices*, Sunnyvale CA) at 750 nm and analyzed with the *Molecular Devices* SoftMax Pro 5.2 software. The protein concentration of the sample, in mg/mL, was calculated from the standard curve and standardized to 4 µg/mL using 4X SDS lysis buffer.

***Western blot analysis*.** After collecting protein, measuring the concentration and standardizing samples to 4 µg/mL, the samples were boiled for 5 min and centrifuged at maximum speed for 5 sec. Then, samples were loaded into a 10% separating and 4% stacking gel along with 7 µL of Precision Plus Protein™ Standard (*Bio-Rad*, Catalogue Number 161-0374). The gel was run at 180 V and 400 mA in 1X SDS running buffer (0.025 M Tris, 0.192 M glycine and 0.1% SDS) for approximately 1 h or until the dye front reached the bottom. Then, the gel was removed from the running apparatus and placed onto a Trans-Blot® Transfer Medium Nitrocellulose Membrane (*Bio-Rad*, Catalogue Number 162-0094) with two sheets of Mini blot size Extra Thick Blot Paper (*Bio-Rad*, Catalogue Number 1703966) saturated in BSN transfer buffer (48 mM Tris, 39 mM glycine, 10% SDS and 20% methanol) surrounding the gel and membrane. The transfer was performed in a Trans-Blot® SD Semi-Dry Transfer Cell (*Bio-Rad*, Catalogue Number 170-3940) set at 15 V and 300 mA for 25 min. The membrane was blocked in TBST (10 mM Tris pH 7.5, 150mM NaCl, 0.005% Tween 20) with 5% milk for 2 h at room temperature with shaking and then washed with TBST three times. Primary

antibodies were prepared in TBST containing 1% milk at the respective dilution (see ***Antibodies for Western blot analysis***) and were incubated with the membrane overnight at 4ºC with shaking. The membrane was washed with TBST five times for 5 min on a shaking platform and then was incubated with the respective HRP-conjugated secondary antibody at a dilution of 1:200 in 1% milk in TBST for 1 h at room temperature with shaking. The membrane was again washed five times for 5 min with TBST, incubated with 2 mL of GE Healthcare ECL™ Western Blotting Detection Reagents (*VWR*, Catalogue Number RPN2106) and developed on GE Healthcare High Performance Chemiluminescence Film (*VWR*, Catalogue Number 28906838). The detection of multiple antibodies on a single membrane was performed without stripping the membrane, where each protein of interest was detected using the abovementioned procedure of blocking, incubating with primary antibody, incubating with secondary antibody and detecting.

***Antibodies for Western blot analysis*.** Primary antibodies used to examine the proteins of interest in Western blot analysis are detailed in **Table 3** and the HRP-conjugated secondary antibodies are listed in **Table 4**.

Table 3 | **Primary antibodies used in Western blot analysis** of the proteins of interest in human kidney tissue and mammalian cell lysates.

PROTEIN	ANTI-	DILUTION	MANUFACTURER (CATALOGUE NUMBER)
Actin	Mouse	1:2,000	*Sigma-Aldrich* (A3853)
pACCser79	Rabbit	1:1,000	*Cell Signaling* (3661S)
AdipoR1	Rabbit	1:500	*ABBIOTEC* (250476)
AdipoR2	Rabbit	1:500	*ABBIOTEC* (250477)
AMPKα	Rabbit	1:1,000	*Cell Signaling* (2532)
pAMPKαthr172	Rabbit	1:1,000	*Cell Signaling* (2535)
CAIX	Rabbit	1:1,000	*Cell Signaling* (5649)
CDC37	Rabbit	1:1,000	*Cell Signaling* (4222S)
pCDC37ser13	Rabbit	1:1,000	*Lab Supply Mall* (8-61797)
CK2β	Rabbit	1:1,000	*Novus Biologics* (NB100-92160)
pCK2βser209	Rabbit	1:1,000	*MBL* (AT-7083)
pCK2βser209	Rabbit	1:1,000	*GenWay Biotech* (18-272-195824)
GAPDH	Rabbit	1:1,000	*Cell Signaling* (2118)
LKB1	Rabbit	1:1,000	*Cell Signaling* (3050S)
mTOR	Rabbit	1:1,000	*Cell Signaling* (2983)
pmTORser2448	Rabbit	1:1,000	*Rockland* (600-401-422)

Table 4 | **Secondary antibodies used in Western blot analysis** of human kidney tissue and mammalian cell lysates.

ANTI-(PRIMARY)	DILUTION	MANUFACTURER (CATALOGUE NUMBER)
Mouse	1:200	*Dako* (K4000)
Rabbit	1:200	*Dako* (K4002)

Densitometric analysis. The intensity of Western blot bands were quantified by densitometric analysis using the public domain Java image-processing program, *ImageJ* Version 1.44 (http://rsbweb.nih.gov/ij/). Values were analyzed and graphed using *Microsoft Excel* software.

5.8 **Adiponectin and treatments**

Adiponectin. Full length human adiponectin (*BioVendor Laboratory Medicine Inc.*, Candler NC, Catalogue Number RD172023100) consisted of adiponectin purified from HEK293 cells stably transfected with a pchAd-F plasmid encoding a FLAG epitope-tagged human adiponectin. The manufacturer confirmed the biological activity of purified adiponectin with an *in vitro* gluconeogenesis assay to demonstrate adiponectin's ability to

inhibit glucose production. Working solutions of adiponectin were prepared by reconstituting 100 µg into 2 mL of sterile PBS to generate a 50 µg/mL stock. The stock was sterile-filtered with a 3 mL syringe (*BD*, Catalogue Number 309585) attached to an *Acrodisc*® 13 mm Syringe Filter with a *Pall Corporation* 0.2 µm Supor® Membrane (*VWR*, Catalogue Number PN 4602), divided into 50 µL aliquots and stored at -20°C. Adiponectin (0 ngmL, 30 ng/mL, 60 ng/mL, 90 ng/mL and 120 ng/mL) was added to *GIBCO*® OPTI-MEM® Reduced Serum Medium (*Invitrogen*, Catalogue Number 51985) on CRL-1932, shCONTROL or shLKB1 cells for the appropriate amount of time and then cell lysates were collected (reference ***Cell lysate collection***). The protein concentration was determined (reference ***DC protein assay***) and standardized to 4 µg/mL using 4X SDS lysis buffer. Then, 1/20 volume of 1 M DTT and 1/5 volume of 0.05% bromophenol blue was added to each sample and the samples were stored at -80ºC until analysis by western blot (reference ***Western blot analysis***).

4,5,6,7-Tetrabromobenzotriazole (TBB). TBB (*Sigma-Aldrich*, Catalogue Number T0826) is an ATP-site directed kinase inhibitor of the protein CK2 that was applied to the OPTI-MEM® media of cells for 1 h in various concentrations (0 µM, 1 µM, 10 µM, 50 µM and 100 µM).

5.9 **Proliferation, invasion, tumour growth, VEGF and adiponectin assays**

Proliferation assay. The rate of proliferation of shCONTROL and shLKB1 cell lines was determined by cell counting. Briefly, both shCONTROL and shLKB1 cells were seeded at $1.0x10^4$ cells/well in a 6-well plate in 2 mL of RPMI-1640 supplemented with 10% FBS and 2 µg/mL puromycin. A total of six 6-well plates were seeded per cell line in order to assess proliferation over six days (at time points of 24 h, 48 h, 72 h, 96 h, 120 h and 144 h), and the cells were incubated at 37ºC. Following the respective incubation time, the triplicate wells were observed under an Axiovert 200M inverted fluorescent microscope and quantified using a Trypan Blue test of cell viability. Briefly, cells were washed once with PBS and trypsinized with 500 µL per well. The 500 µL was transferred into a 1.5 mL microcentrifuge tube and combined with 500 µL of Trypan Blue Stain 0.4% (*GIBCO*®, Catalogue Number 0682). Then, 10 µL of the solution was applied to a hemacytometer (*Fisher Scientific*, Catalogue Number 0267110) and the number of viable (unstained) cells was counted in five primary squares and multiplied by $4x10^3$ to yield the total number of cells. The average was taken for the triplicate wells and the values were plotted in *Microsoft Excel* software to generate a proliferation curve.

Invasion assay. The invasive and migratory potential of shCONTROL and shLKB1 cells was assessed using the *BD* BioCoat™ Matrigel™ Invasion Chamber Kit. Briefly, six 24-well insert Invasion Chambers (*BD*, Catalogue Number 354480) were removed from -20ºC storage and brought to room temperature, and six 24-well insert Control Chambers

(*BD*, Catalogue Number 354578) not containing Matrigel™ were removed from 4ºC storage and brought to room temperature. The six Invasion Chambers and six Control Chambers were inserted into one sterile 24-well plate (*BD*, Catalogue Number 353504) and 500 µL of warm (37ºC) RPMI-1640 media without FBS, penicillin and streptomycin was applied into the Chambers and the wells. The 24-well plate was incubated for 2 h at 37ºC in order to rehydrate the Matrigel™. Following incubation, media was aspirated and $2.5x10^4$ cells of each cell line were applied into three Invasion Chambers and three Control Chambers. RPMI-1640 media without FBS, penicillin or streptomycin was applied into each Chamber to bring the total volume to 500 µL, while 750 µL of RPMI-1640 media supplemented with 10% FBS was applied into each well to serve as the chemoattractant. Chambers were incubated inside the wells for 22 h at 37ºC. Following incubation, the non-invading (or non-migrating) cells were removed from the Chambers by scrubbing the insert twice with an *Alliance*® Cotton Tip Swab (*VWR*, Catalogue Number 211-806) moistened with RPMI-1640 media. Chambers were immediately placed in 750 µL of 2% Formaldehyde (*Caledon Laboratories*, Catalogue Number 5300-4-25) for 10 min and then moved into 750 µL of Crystal Violet (*Sigma-Aldrich*, Catalogue Number C3886) for 10 min. The Chambers were rinsed in dH_2O three times to destain and left to dry at room temperature for 2 h. A *Schreiber*® *Instrumente* scalpel (*VWR*, Catalogue Number 0483) was applied to the bottom of the Chamber to extract the membrane, which was then mounted onto a microscope slide (*VWR*, Catalogue Number 48323-185) with Immunon™ PermaFluor Mountant (*Thermo Fisher Scientific*, Catalogue Number 434990). The slides were allowed to dry for 1 h before five 40x objective field of

view images (top left, top right, center, bottom left and bottom right) were taken for each membrane with an Axiovert 200M inverted fluorescent microscope. The average number of cells in the five images and across the triplicate membranes for each chamber type and cell line was determined. Then, for each cell line, the average number of invaded cells in the Invasion Chamber was divided by the average number of migrated cells in the Control Chamber to determine the percentage of invasion, and the values were graphed using *Microsoft Excel* software.

Tumour growth assay. The tumourigenicity of shCONTROL and shLKB1 cells was assessed by injecting the cells subcutaneously into 10 BALB/c Nu/Nu mice and monitoring tumour growth (reference ***Animals and handling***). Briefly, shCONTROL and shLKB1 cells were propagated in T75 tissue culture flasks (*Starstedt*, Montreal QC, Catalogue Number 83.1813.002) and on the day of injection were washed twice with PBS. Then, 4 mL of trypsin was applied to dislodge the cells from the flask and 4 mL of RPMI-1640 media without FBS, penicillin and streptomycin supplementation was added. Each cell line was combined into a single 50 mL polypropylene tube and the total cell number was determined. The cells were pelleted by centrifugation at 1000 g for 5 min at 4ºC and the supernatant was carefully aspirated. Then, 5 mL of RPMI-1640 media without FBS, penicillin and streptomycin supplementation was applied to the pellet and the 50 mL polypropylene tube was centrifuged for 5 min at 1000 g at 4ºC, three times to thoroughly wash the cells. Media was aspirated and $2x10^7$ cells ($2x10^6$ cells x 10 mice) were resuspended in 1,000 µL (100µL x 10 mice) of RPMI-1640 media without FBS,

penicillin and streptomycin supplementation. The cells were mixed with 1,000 µL (100 µL x 10 mice) of BD Matrigel™ Matrix Basement Membrane (*BD*, Catalogue Number 356234) and kept on ice. Then, 200 µL of solution was taken up into a 1 mL syringe and a 26G$^{3/8}$ needle (*BD*, Catalogue Number 305110) was attached. The needle was inverted and air bubbles inside the syringe were removed before injecting the mixture subcutaneously into the right flank of the mouse. The size of the tumour in each mouse was measured every week using a plastic *Bel-Art* vernier caliper (*VWR*, Catalogue Number 134150000) and the tumour volume was determined by the formula, Tumour Volume = 0.5 * (Length * Width * Height) (Tomayko *et al.*, 1989), and was graphed in *Microsoft Excel* software. Mice were sacrificed seven weeks after injection, during which blood was collected in a *BD* Vacutainer® (*BD*, Catalogue Number 366643) and incubated overnight at 4ºC until analyzed the following day (reference ***Mouse VEGF Immunoassay*** and ***Mouse adiponectin ELISA***). Tumour xenografts were also collected, placed in 2 mL formalin and sent to the *McMaster University Core Histology Facility* to be embedded in paraffin, sectioned and mounted onto slides (reference ***Immunohistochemical staining of human kidney tissue and mouse xenografts***).

Human Vascular Endothelial Growth Factor (VEGF) Immunoassay. Quantification of human VEGF secreted into the cell culture supernatant by shCONTROL and shLKB1 cells was performed using the Quantikine® Human VEGF Immunoassay kit (*R&D Systems*, Minneapolis MN, Catalogue Number DVE00). Briefly, shCONTROL and shLKB1 cells were seeded at 7.5x10^4 cells/well in a 96-well microtiter plate in 100 µL of

RPMI-1640 media supplemented with 10% FBS. Cells were incubated for 24 h and then the media was aspirated. Wells were washed three times with PBS and 100 µL of RPMI-1640 media supplemented with 1% FBS was added to each well and the cells were incubated for 24 h. Following the incubation, cells were treated in triplicate with various concentrations of adiponectin (0 ng/mL, 30 ng/mL, 60 ng/mL, 90 ng/mL and 120 ng/mL) for 1 h and the supernatant was harvested and centrifuged at maximum speed for 1 min at 4ºC to remove particulates. The VEGF Standard (2000 pg/mL) (*R&D Systems*, Catalogue Number 890220) was reconstituted with 1 mL of Calibrator Diluent RD5K (*R&D Systems*, Catalogue Number 895119) and then diluted into a standard series (1000 pg/mL, 500 pg/mL, 250 pg/mL, 125 pg/mL, 62.5 pg/mL, 31.2 pg/mL, 15.6 pg/mL and 0 pg/mL) in Calibrator Diluent RD5K in eight 50 mL polypropylene tubes. Then, 50 µL of Assay Diluent RD1W (*R&D Systems*, Catalogue Number 895117) was added to each well of the VEGF 96-well microplate (*R&D Systems*, Catalogue Number 890218) followed by 200 µL of each standard (in duplicate) and treatment (in triplicate). The plate was covered with an adhesive cover (*VWR*, Catalogue Number 82018-844) and incubated for 2 h at room temperature. Following the incubation, wells were aspirated and washed three time with 400 µL of Wash Buffer (*R&D Systems*, Catalogue Number 895003) before 200 µL of VEGF Conjugate (*R&D Systems*, Catalogue Number 890219) was applied to each well. Again, the plate was covered, incubated at room temperature for 2 h and the wells were aspirated and washed three times with 400 µL of Wash Buffer. Then, 100 µL of Colour Reagent A (*R&D Systems*, Catalogue Number 895000) and 100 µL of Colour Reagent B (*R&D Systems*, Catalogue Number 895001) were mixed and added to each

well, and the plate was shielded from light for 20 min at room temperature. Finally, 50 µL of Stop Solution (*R&D Systems*, Catalogue Number 895032) was applied to each well and the plate was gently mixed to ensure a uniform colour in each well. The optical density was measured using a SPECTRAmax Plus 384 spectrophotometer at 450 nm and 540 nm and the optical density at 540 nm was subtracted from the optical density at 450 nm to correct for optical imperfections in the plate. Values were analyzed using the standard curve and graphed using *Microsoft Excel* software.

Mouse Vascular Endothelial Growth Factor (VEGF) Immunoassay. Quantification of mouse VEGF in mouse serum (reference ***Tumour growth assay***) was performed using the Quantikine® Mouse VEGF Immunoassay kit (*R&D Systems*, Catalogue Number MMV00). Briefly, blood was collected in a *BD* Vacutainer® and allowed to clot overnight at 4ºC. The blood was then centrifuged for 20 min at 2,000 g at 4ºC before serum was removed and diluted five-fold with Calibrator Diluent RD5T (*R&D Systems*, Catalogue Number 895175). The VEGF Standard (500pg/mL) (*R&D Systems*, Catalogue Number 890784) was reconstituted in 5 mL of Calibrator Diluent RD5T and then diluted into a standard series (500 pg/mL, 250 pg/mL, 125 pg/mL, 62.5 pg/mL, 31.2 pg/mL, 15.6 pg/mL, 7.8 pg/mL and 0 pg/mL) in Calibrator Diluent RD5T in eight 50 mL polypropylene tubes. Then, 50 µL of Assay Diluent RD1N (*R&D Systems*, Catalogue Number 895488) was added to each well of the VEGF 96-well microplate (*R&D Systems*, Catalogue Number 890783) followed by 50 µL of each standard (in duplicate) and diluted serum sample (in triplicate). The plate was covered with an adhesive cover and incubated

for 2 h at room temperature. Following the incubation, wells were aspirated and washed four times with 400 µL of Wash Buffer (*R&D Systems*, Catalogue Number 895024) before 100 µL of Mouse VEGF Conjugate (*R&D Systems*, Catalogue Number 892667) was applied to each well. Again, the plate was covered, incubated at room temperature for 2 h and the wells were aspirated and washed four times with 400 µL of Wash Buffer. Then, 50 µL of Colour Reagent A (*R&D Systems*, Catalogue Number 895000) and 50 µL of Colour Reagent B (*R&D Systems*, Catalogue Number 895001) were mixed and added to each well, and the plate was shielded from light for 30 min at room temperature. Finally, 100 µL of Stop Solution (*R&D Systems*, Catalogue Number 895174) was applied to each well and the plate was gently mixed to ensure a uniform colour in each well. The optical density was measured using a SPECTRAmax Plus 384 spectrophotometer at 450 nm and 540 nm and the optical density at 540 nm was subtracted from the optical density at 450 nm to correct for optical imperfections in the plate. Values were analyzed using the standard curve and graphed using *Microsoft Excel* software.

Mouse adiponectin ELISA. Quantification of mouse adiponectin in mouse serum (reference ***Tumour growth assay***) was performed using the *BioVendor* Mouse Adiponectin ELISA kit (*BioVendor Laboratory Medicine Inc.*, Candler NC, Catalogue Number RD293023100R). Briefly, blood was collected in a *BD* Vacutainer® and allowed to clot overnight at 4ºC. Blood was centrifuged for 20 min at 2,000 g at 4ºC before serum was removed and diluted 10,000-fold with 1X Dilution Buffer. The Mouse Adiponectin Master Standard (8 ng/mL) was reconstituted in 900 µL of 1X Dilution Buffer and then

diluted into a standard series (8 ng/mL, 4 ng/mL, 2 ng/mL, 1 ng/mL, 0.5 ng/mL, 0.25 ng/mL and 0 ng/mL) in 1X Dilution Buffer in seven 50 mL polypropylene tubes. Then, 100 µL of each standard (in duplicate) and diluted serum sample (in triplicate) was added to each well of the Adiponectin 96-well microplate. The plate was covered with an adhesive cover and incubated for 1 h at room temperature with shaking at 300 rpm. Following the incubation, wells were aspirated and washed four times with 350 µL of 1X Wash Solution before 100 µL of Conjugate Solution was applied to each well. Again, the plate was covered, incubated at room temperature for 1h with shaking and the wells were aspirated and washed three times with 350 µL of 1x Wash Solution. Then, 100 µL of Substrate Solution was added to each well and the plate was shielded from light for 10 min at room temperature. Finally, 100 µL of Stop Solution was applied to each well and the plate was gently mixed to ensure a uniform colour in each well. The optical density was measured using a SPECTRAmax Plus 384 spectrophotometer at 450 nm and 630 nm and the optical density at 630 nm was subtracted from the optical density at 450 nm to correct for optical imperfections in the plate. Values were analyzed using the standard curve and graphed using *Microsoft Excel* software.

5.10 **Human tissue and mouse xenograft staining**

Immunohistochemical staining of human kidney tissue and mouse xenografts. Patient's tumour tissue and normal surrounding parenchyma (reference ***Human tissue collection***

and preparation) as well as extracted mouse xenografts (reference ***Tumour growth assay***) were prepared as a single formalin-fixed paraffin-embedded block (*McMaster University Core Histology Facility,* Hamilton ON), sectioned at a thickness of 4 µm and mounted on precoated slides (*VWR*, Catalogue Number 48323-185). Slides were deparaffinized with three changes of Xylene (*Fisher Chemical*, Catalogue Number X3S20) for 10 min each and rehydrated in 100% ethanol (*Fisher Chemical*, Catalogue Number A962) twice for 3 min each. Endogenous peroxidase activity was blocked (0.5% hydrogen peroxide, 80 mM concentrated HCl in methanol) for 10 min at room temperature and slides were rinsed one time in *Ricca Chemical* 70% ethanol (*VWR*, Catalogue Number 2546701), three times in distilled water and one time in 1X TBS (10X TBS: 121.1 g/L Tris (hydroxymethyl) methylamine, 170.0 g/L NaCl and HCl to pH7.6). Heat-induced antigen retrieval was performed in a pressure cooker (*Black & Decker*, Hamilton ON, Catalogue Number HS1000) with citric buffer (2.3 g/L citric acid and 2 N NaOH to pH6.0) that was pre-heated for 25 min, incubated for 30 min and left to cool for an additional 30 min. Slides were rinsed with 1X TBS before being blocked in **N**ormal **G**oat **S**erum (NGS) (*Vector Laboratories*, Burlington ON, Catalogue Number S-1000), which was diluted 1:20 in 1X TBS, for 15 min. The primary antibody was diluted (**Table 5**) in NGS and applied to the slides for 1 h. Slides were rinsed thoroughly with 1X TBS, two times before incubation with the biotinylated secondary antibody (**Table 6**), that was diluted to 1:500 in 1X TBS for 30 min. Following the incubation, slides were rinsed thoroughly with 1X TBS, two times and incubated with one drop of Zymed HRP-Streptavidin (*Invitrogen*, Catalogue Number 50-242Z) in 2 mL 1X TBS for 10 min. The

slides were rinsed thoroughly with 1X TBS one time and dH_2O one time. Immunodetection was performed with ImmPact™ NovaRed™ (*Vector Laboratories*, Catalogue Number SK-4805) prepared in 5 mL dH_2O and was incubated for 5 min. Slides were then placed in dH_2O for 10 min and then counterstained with Hematoxylin Solution, Gill No. 3 (*Sigma-Aldrich*, Catalogue Number GHS316) for 30 sec. Slides were placed in tap water for 5 min and then dehydrated in 100% ethanol twice and Xylene twice. Coverslips (*VWR*, Catalogue Number 48366-067) were applied to the slides with Immunon™ PermaFluor Mountant (*Thermo Scientific*, Catalogue Number 434990) and were left to dry for 1 h before the tissue sections were imaged on a BX41® clinical microscope (*Olympus*, Markham ON, Catalogue Number BX41) using the *Olympus* DP Controller, Image-Pro Plus software. Immunohistochemical staining controls were murine muscle tissue (positive control) and secondary antibody only (negative control).

Antibodies for immunohistochemistry. Primary antibodies used in the immunohistochemical staining of human kidney tissue and mouse xenografts are listed in **Table 5** and the secondary antibodies in **Table 6**

Table 5 | **Primary antibodies used for immunohistochemical staining** of the proteins of interest in human kidney and mouse xenograft tissue.

PROTEIN	ANTI-	DILUTION	MANUFACTURER (CATALOGUE NUMBER)
AdipoR1	Rabbit	1:500	*Phoenix Pharmaceuticals* (H-001-44)
pACCser79	Rabbit	1:25	Cell Signalling (3661S)
LKB1	Mouse	1:100	*Abcam* (ab15095)

Table 6 | **Secondary antibodies used for immunohistochemical staining** of human kidney and mouse xenograft tissue.

ANTI-(PRIMARY)	DILUTION	MANUFACTURER (CATALOGUE NUMBER)
Mouse	1:500	*Vector Laboratories* (BA-9200)
Rabbit	1:500	*Vector Laboratories* (BA-1000)

Hematoxylin and Eosin (H&E) staining. H&E staining of mouse xenografts was performed by the *McMaster University Core Histology Facility* and was imaged on a BX41® clinical microscope using the *Olympus* DP Controller, Image-Pro Plus software.

5.11 **Tissue Microarray staining, scanning and analysis**

Tissue Microarray (TMA) staining. Two TMAs (*US Biomax Inc*., Rockville, MD., Catalogue Numbers KD951 and KD6161) containing duplicate cores for each of the 31 renal carcinoma patients' tumour tissue and eight matched normal renal tissue (KD951) and 294 renal carcinoma patients' tumour tissue and 28 normal renal tissue (KD6161) was stained for LKB1 expression (reference ***Immunohistochemical staining of human kidney tissue and mouse xenografts***).

Aperio Technologies' scanning and analysis. The two TMA slides stained with LKB1 were scanned at a 20x magnification on the ScanScope XT brightfield scanner (*Aperio Technologies*, Vista, CA) located at *The Advanced Optical Microscopy Facility* (AOMF) (Toronto, ON). Digitized high resolution images of LKB1 staining in the TMA patient tissue were generated and then quantified using the Positive Pixel Count Algorithm on ImageScope (Version 10) software (*Aperio Technologies*). ImageScope scored the intensity of LKB1 staining in each tissue core into four categories: Negative (**In**), Weak positive (**Iwp**), Positive (**Ip**) and Strong positive (**Isp**). The percentage of Total Intensity was determined for each category (% Weak positive, % Positive and % Strong positive) by dividing the intensity value (**Iwp**, **Ip** or **Isp**) by Total Intensity (**In** + **Iwp** + **Ip** + **Isp**). These values were used to calculate the H-Score according to the formula, H-Score = [(% Weak positive * 1) + (% Positive * 2) + (% Strong positive * 3) + 1] * 100% (He *et al*., 2010). To focus on the study of clear cell carcinoma, patients diagnosed with a

sarcomatoid renal cell carcinoma, transitional cell carcinoma, papillary renal cell carcinoma and squamous cell carcinoma pathology were excluded from the analysis.

RESULTS

6.1.1 *AdipoR1* and *LKB1* transcript levels are dysregulated in patient RCC

Transcript levels of *AdipoR1*, *AdipoR2*, *LKB1* and *VEGFA* were measured by qRT-PCR in 10 matched patients' RCC tumour tissue and normal surrounding parenchyma sets. The transcript level in tumour tissue was compared to the transcript level in normal surrounding parenchyma and was presented as a relative comparison, with the normal tissue transcript level adjusted to represent 100%. *AdipoR1* transcript level in patient tumour tissue was largely induced compared to normal tissue in all patients examined (**Figure 1**). The mean fold induction in patient tumour tissue was 5,683% compared to 100% in normal, and data ranged from 137% to 25,218%.

Similar to the transcript expression pattern of *AdipoR1*, the *AdipoR2* transcript level in patient tumour tissue was induced over the normal surrounding parenchyma level in eight of the 10 patients (**Figure 2**). The mean fold induction was 23,254% in the tumour tissue and ranged from 161% to 105,522%. Patient 5 and 91 tumour tissue presented a lower *AdipoR2* transcript level compared to normal surrounding parenchyma, however since AdipoR1 predominately mediates the signaling pathway of interest, further examination of AdipoR2 expression in patients was discontinued.

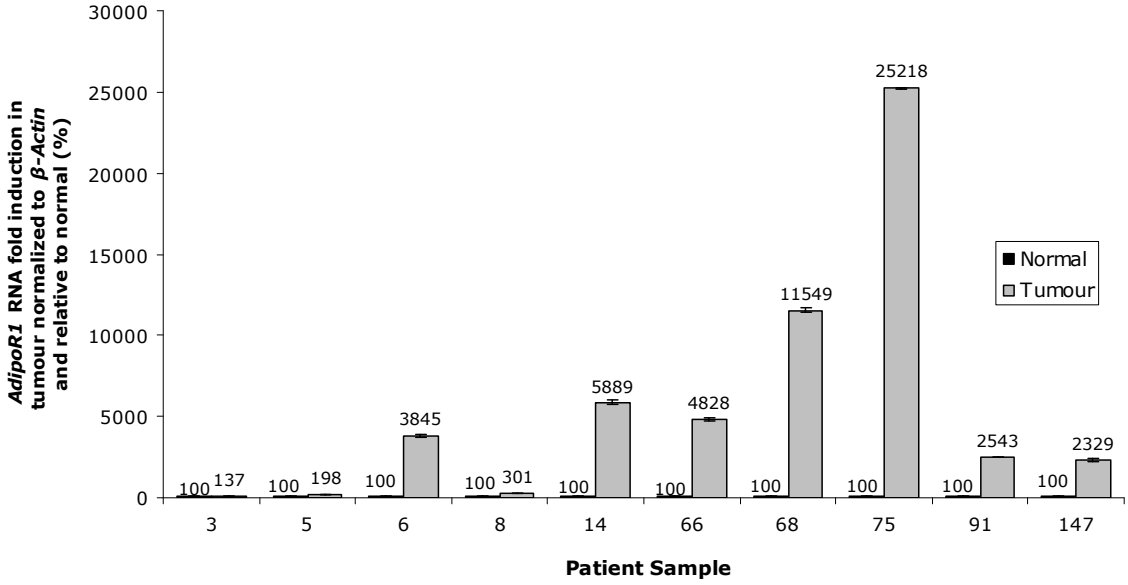

Figure 1 | ***AdipoR1* transcript level is increased in patient RCC tumours**. Total RNA was extracted from patient (3, 5, 6, 8, 14, 66, 68, 75, 91 and 147) tumour tissue (Tumour) and normal surrounding parenchyma (Normal), transcribed into cDNA and analyzed by qRT-PCR using the primer sets for *AdipoR1* and *β-Actin*. Tumour and Normal *AdipoR1* transcript levels were normalized to endogenous *β-Actin* transcript levels. Data represent the mean of triplicate wells ± SEM and are presented as the patient's Tumour *AdipoR1* transcript level relative to Normal, which was set to 100%.

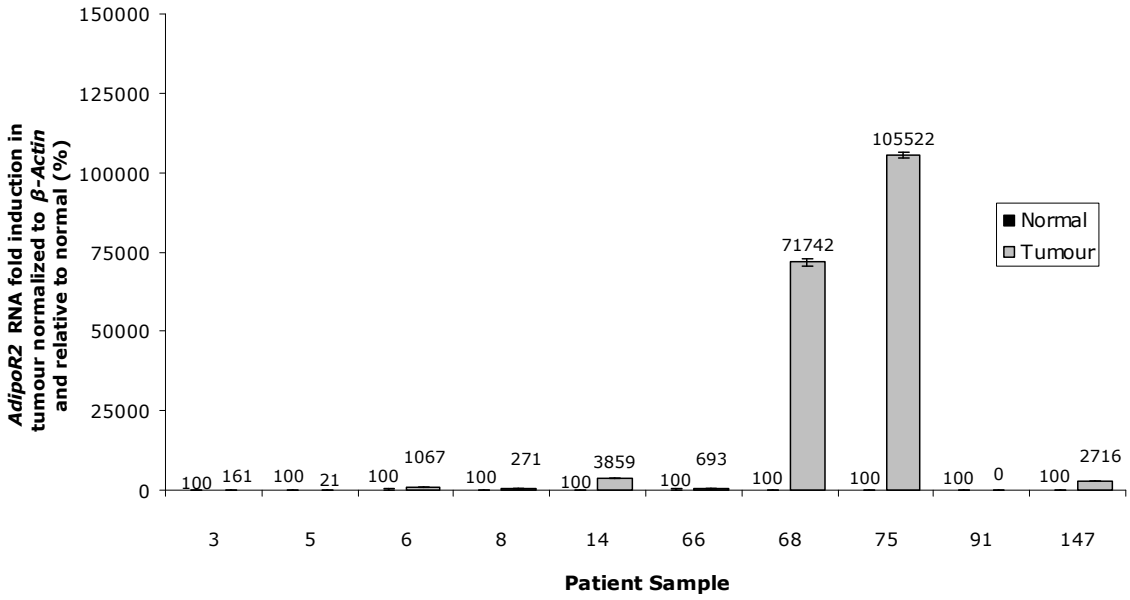

Figure 2 | ***AdipoR2* transcript level is increased in patient RCC tumours**. Total RNA was extracted from patient (3, 5, 6, 8, 14, 66, 68, 75, 91 and 147) tumour tissue (Tumour) and normal surrounding parenchyma (Normal), transcribed into cDNA and analyzed by qRT-PCR using the primer sets for *AdipoR2* and *β-Actin*. Tumour and Normal *AdipoR2* transcript levels were normalized to endogenous *β-Actin* transcript levels. Data represent the mean of triplicate wells ± SEM and are presented as the patient's Tumour *AdipoR2* transcript level relative to Normal, which was set to 100%.

LKB1 transcript level in RCC tumour tissue was significantly reduced compared to normal tissue in all 10 patients examined (**Figure 3**). The mean transcript level of *LKB1* in tumour tissue was 24% compared to 100% in normal tissue, with reduction values ranging from 2% to 66%.

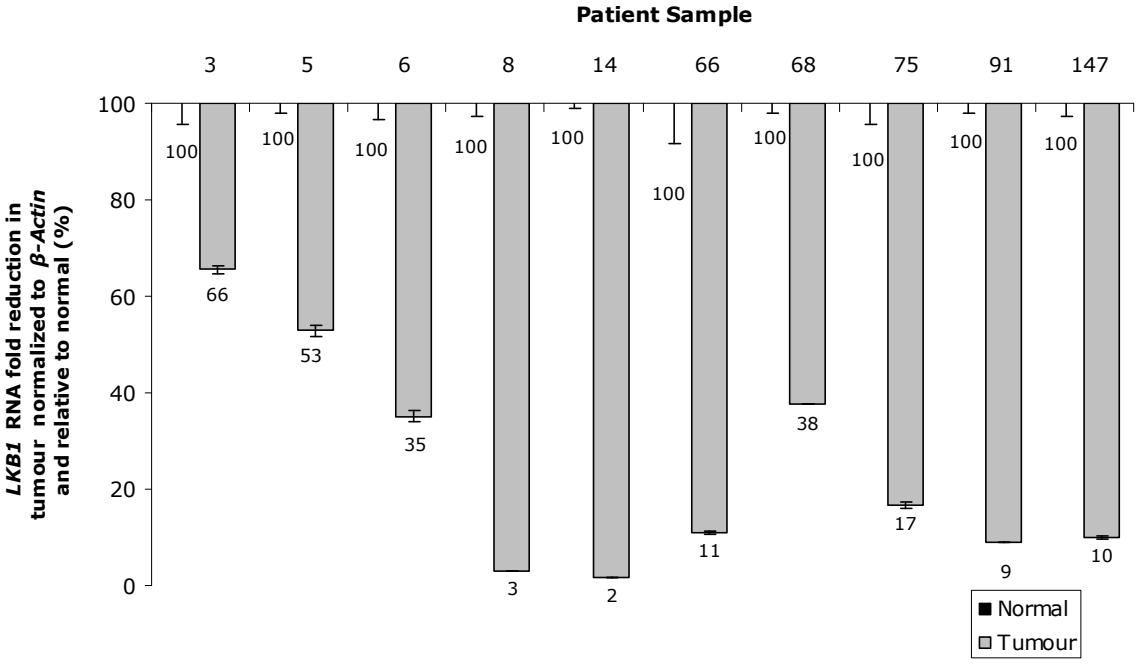

Figure 3 | ***LKB1* transcript level is reduced in patient RCC tumours**. Total RNA was extracted from patient (3, 5, 6, 8, 14, 66, 68, 75, 91 and 147) tumour tissue (Tumour) and normal surrounding parenchyma (Normal), transcribed into cDNA and analyzed by qRT-PCR using the primer sets for *LKB1* and *β-Actin*. Tumour and Normal *LKB1* transcript levels were normalized to endogenous *β-Actin* transcript levels. Data represent the mean of triplicate wells ± SEM and are presented as the patient's Tumour *LKB1* transcript level relative to Normal, which was set to 100%.

VEGFA transcript was examined to distinguish tumour tissue from normal surrounding parenchyma and to confirm that *AdipoR1* and *LKB1* transcript levels were dysregulated specifically in patient tumour tissue. The transcript level in tumour tissue was significantly increased over that of normal tissue, with a mean induction of 65,097% compared to the 100% normal tissue induction, and provided a necessary marker to distinguish tumour tissue from normal tissue (**Figure 4**).

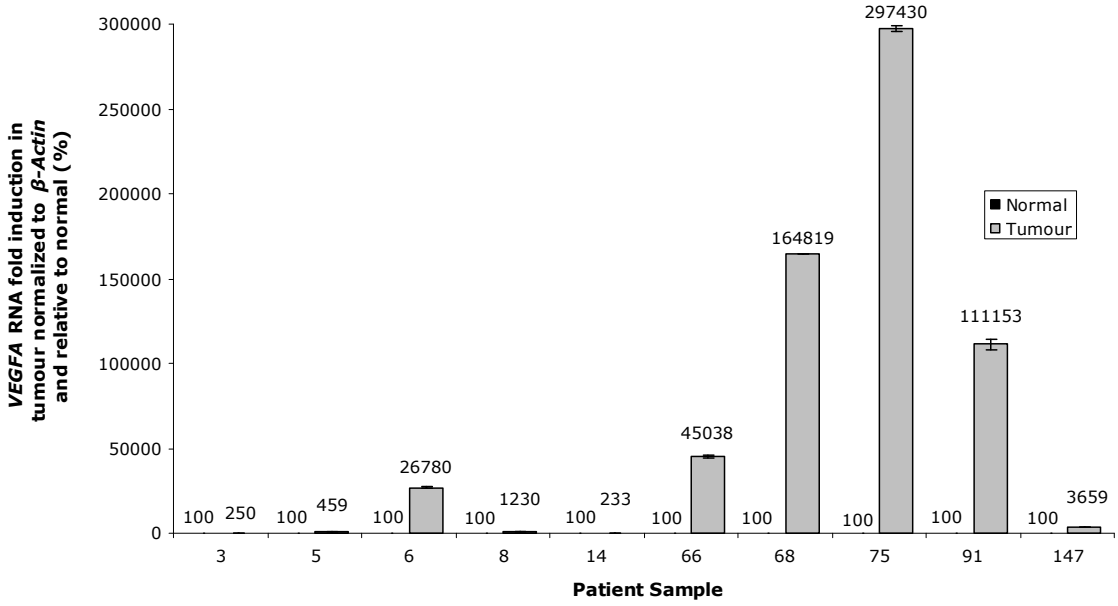

Figure 4 | *VEGFA* transcript level confirmed patient tumour and normal tissues. Total RNA was extracted from patient (3, 5, 6, 8, 14, 66, 68, 75, 91 and 147) tumour tissue (Tumour) and normal surrounding parenchyma (Normal), transcribed into cDNA and analyzed by qRT-PCR using the primer sets for *VEGFA* and *β-Actin*. Tumour and Normal *VEGFA* transcript levels were normalized to endogenous *β-Actin* transcript levels. Data represent the mean of triplicate wells ± SEM and are presented as the patient's Tumour *VEGFA* transcript level relative to Normal, which was set to 100%.

6.1.2 **AdipoR1 and LKB1 protein expression is reduced in patient RCC**

Preliminary experiments examining AdipoR1 protein expression in six matched patient RCC tumour and normal surrounding parenchyma tissue sets (**Figure 5A**), determined that AdipoR1 protein expression was significantly reduced in all six patient RCC tumours compared to normal surrounding parenchyma (**Figure 5B**). Reduction in AdipoR1 protein expression in tumour tissue was drastic to the extent that no bands were visible. Therefore Western blotting conditions were optimized for subsequent experiments (reference ***Western blot analysis***) in order to perform a more accurate comparison of protein expression in patient tumour and normal tissue.

Total protein isolated from the same patient biopsies used to quantify *AdipoR1*, *AdipoR2*, *LKB1* and *VEGFA* transcript levels was analyzed by Western blotting for AdipoR1, LKB1 and CAIX protein expression. Similar to the reduction of AdipoR1 protein expression in patient RCC tumour tissue in the preliminary study, AdipoR1 protein was reduced in eight of the 10 patient tumours (**Figure 6A**), with a mean expression of 69% compared to 100% expression in normal tissue (**Figure 6B**). AdipoR1 protein expression in RCC tumour tissue ranged from 33% to 96% across the eight patients which presented reduced expression. Patient 147 AdipoR1 protein expression was slightly higher in the RCC tumour at 109% compared to normal tissue, and Patient 68 AdipoR1 protein expression in the tumour amounted to 127%.

A

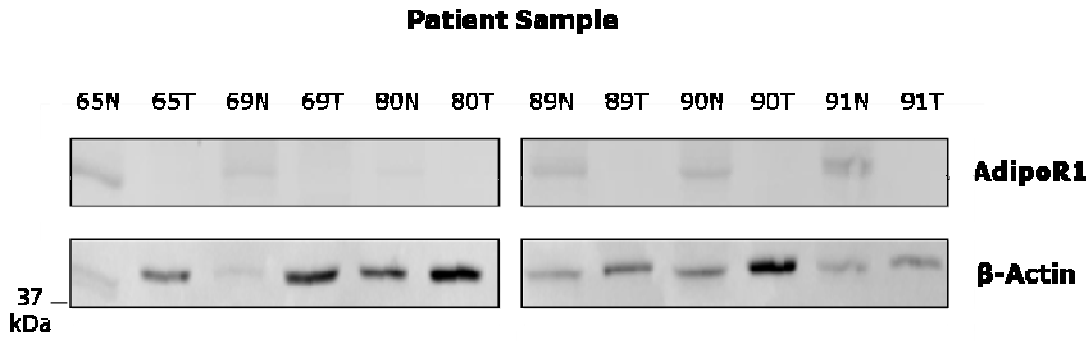

B

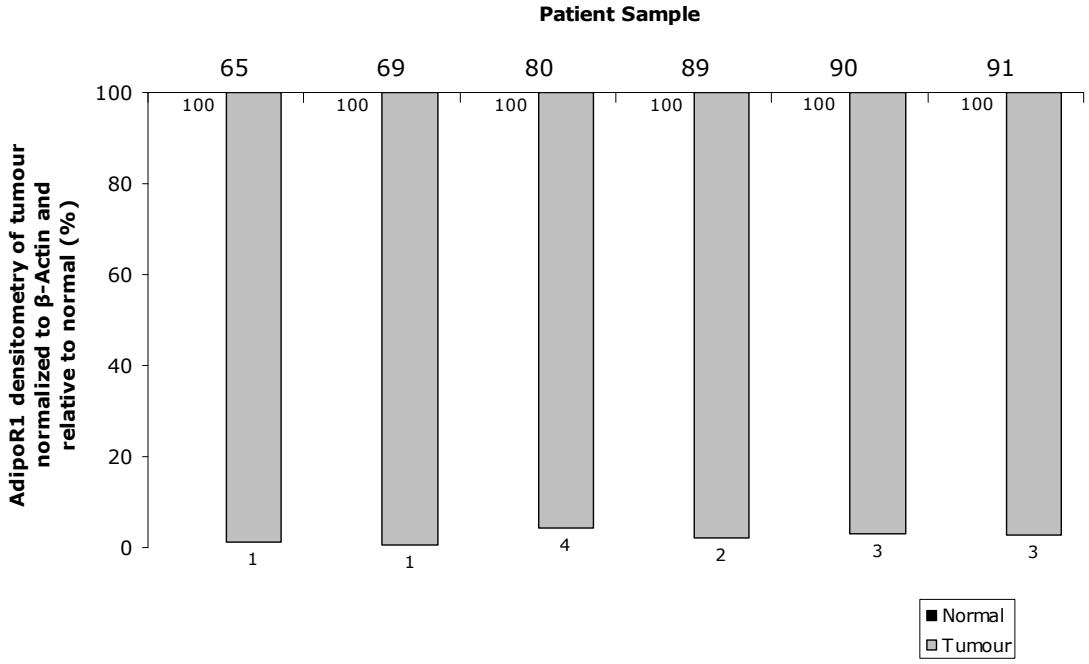

Figure 5 | **AdipoR1 protein expression is reduced in patient RCC tumours**. (**A**) Total protein was extracted from patient (65, 69, 80, 89, 90 and 91) tumour tissue (T, Tumour) and normal surrounding parenchyma (N, Normal), brought to 40µg, separated by SDS-PAGE and analyzed by Western blotting for AdipoR1 and β-Actin. (**B**) The intensity of the bands was quantified by densitometry and the Tumour and Normal AdipoR1 values were normalized to endogenous β-Actin values. Data represent the densitometric quantification and are presented as the patient's Tumour AdipoR1 protein expression level relative to Normal, which was set to 100%.

A

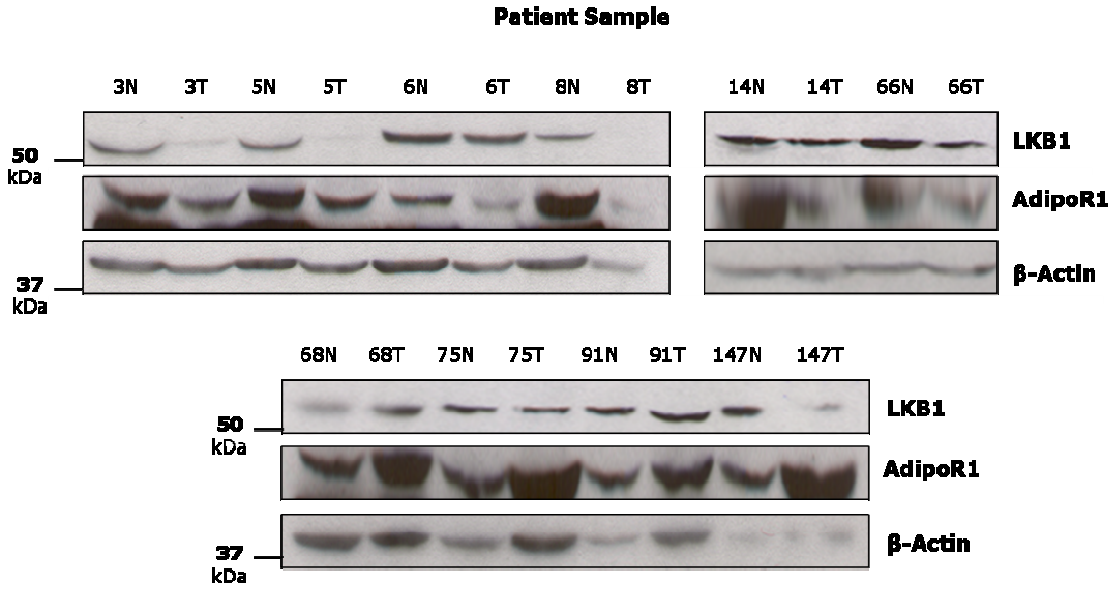
Patient Sample
3N 3T 5N 5T 6N 6T 8N 8T
14N 14T 66N 66T
50 kDa
37 kDa
LKB1
AdipoR1
β-Actin
68N 68T 75N 75T 91N 91T 147N 147T
50 kDa
37 kDa
LKB1
AdipoR1
β-Actin

B

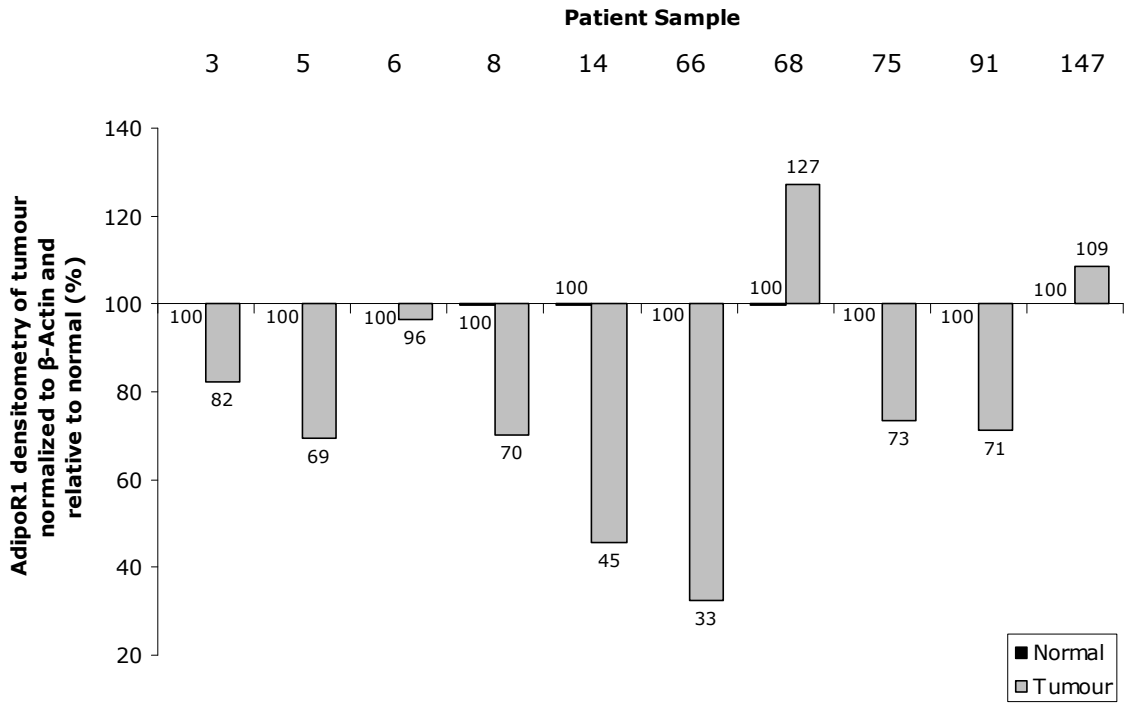
Patient Sample
3 5 6 8 14 66 68 75 91 147
AdipoR1 densitometry of tumour normalized to β-Actin and relative to normal (%)
140
120
100
80
60
40
20
100 82
100 69
100 96
100 70
100 45
100 33
100 127
100 73
100 71
100 109
Normal
Tumour

C

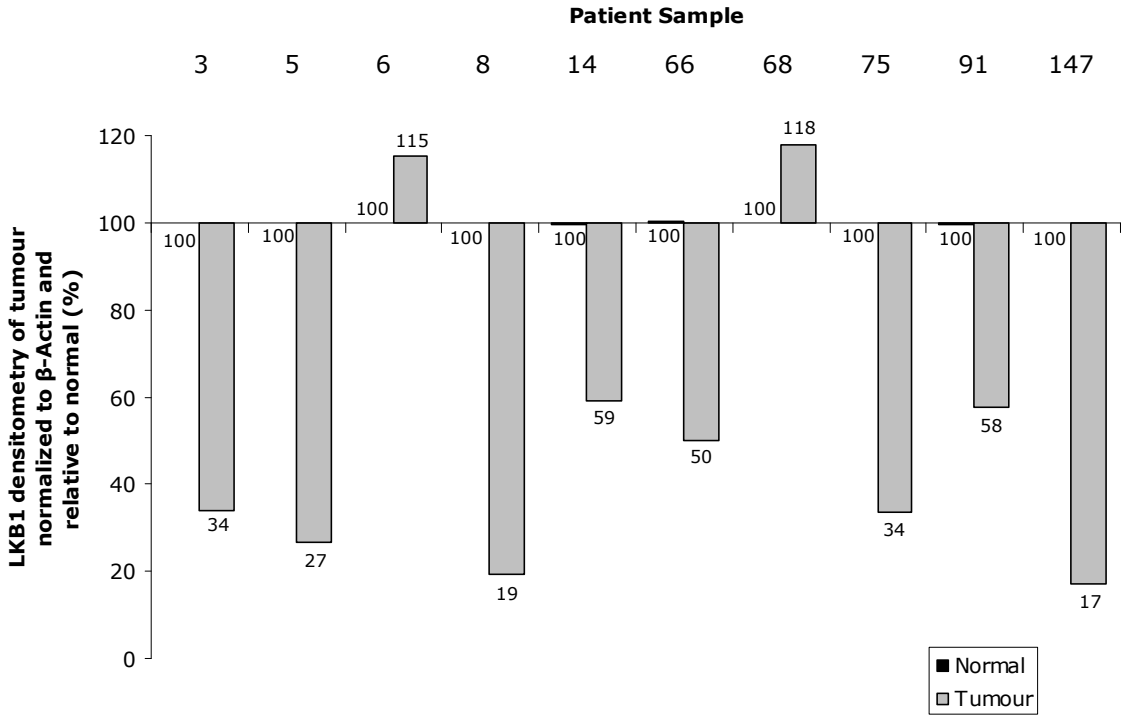

Figure 6 | **AdipoR1 and LKB1 protein expression is reduced in patient RCC tumours**. (**A**) Total protein was extracted from patient (3, 5, 6, 8, 14, 66, 68, 75, 91 and 147) tumour tissue (T, Tumour) and normal surrounding parenchyma (N, Normal), brought to 40μg, separated by SDS-PAGE and analyzed by Western blotting for AdipoR1, LKB1 and β-Actin. The intensity of the bands was quantified by densitometry and the Tumour and Normal AdipoR1 and LKB1 values were normalized to endogenous β-Actin values. Data represent the densitometric quantification and are presented as the patient's Tumour (**B**) AdipoR1 and (**C**) LKB1 protein expression level relative to Normal, which was set to 100%.

LKB1 protein expression was also reduced in eight of the 10 patient RCC tumours, with a mean expression of 37% compared to 100% expression in normal tissue (**Figure 6C**). Both Patient 6 and 68 presented greater LKB1 protein expression in the tumour compared to normal tissue, however, Patient 68 coincided as one of the two patients that presented increased AdipoR1 protein expression in tumour tissue.

Carbonic anhydrase IX (CAIX) protein expression was examined in patient RCC tumour tissue and normal surrounding parenchyma in order to support the *VEGFA* transcript differentiation of patient tumour and normal tissue, and further, confirm that AdipoR1 and LKB1 protein expression were downregulated specifically in tumour tissue. CAIX expression was not quantified by densitometry due to the apparent difference in banding pattern on the developed membrane between tumour and normal tissue samples in eight of the 10 patients (**Figure 7**). Increased CAIX expression was not evident in Patient 6 and 8 tumour tissue.

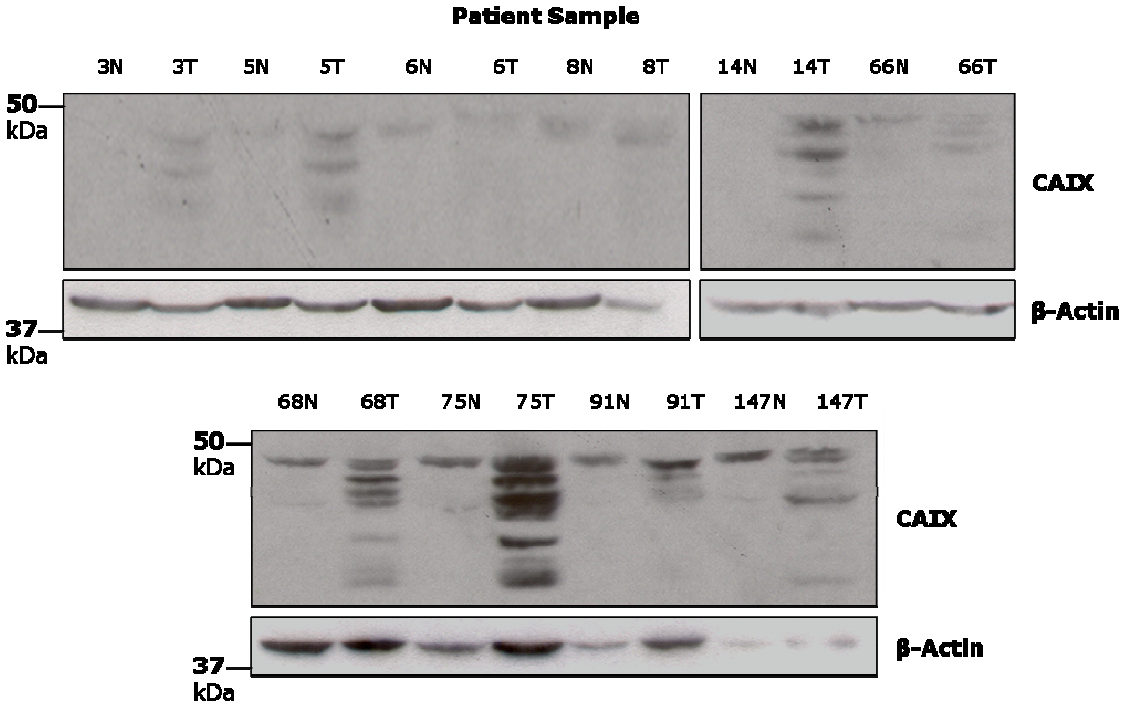

Figure 7 | **CAIX expression distinguished RCC tumour from normal tissue**. Total protein was extracted from patient (3, 5, 6, 8, 14, 66, 68, 75, 91 and 147) tumour tissue (T) and normal surrounding parenchyma (N), brought to 40µg, separated by SDS-PAGE and analyzed by Western blotting for carbonic anhydrase IX (CAIX) and β-Actin.

6.1.3 **AdipoR1 and LKB1 staining is reduced in patient RCC**

Consecutive histological sections of five patients' (4, 5, 8, 9 and 10) RCC tumour tissue and normal surrounding parenchyma were stained for AdipoR1, LKB1 and **p**hosphorylated **A**cetyl-**C**oA **C**arboxylase (p-ACC) to observe protein presence and localization in the tissue. AdipoR1 staining was evident in the normal surrounding parenchyma of Patient 4 with reduction in intensity in the tumour tissue (**Figure 8A**), however, AdipoR1 staining was weaker across all other patient tissue samples with minimal reduction in the corresponding RCC tumour tissue (**Figure 8B-E**).

LKB1 staining was evident in the tubules of normal tissue in all five patients, while staining was practically obliterated in the matched RCC tumour tissue (**Figure 9A-E**). Quantification of LKB1 staining on tissue microarrays KD6161 and KD951 (**Figure 10A**), containing tissue cores from 201 RCC patients and 26 normal patients (**Figure 10B**), confirmed that the mean H-Score of LKB1 expression was significantly reduced in RCC tumour tissue (H-Score: 209) compared to normal renal tissue (H-Score: 227) (**Figure 10C**).

A

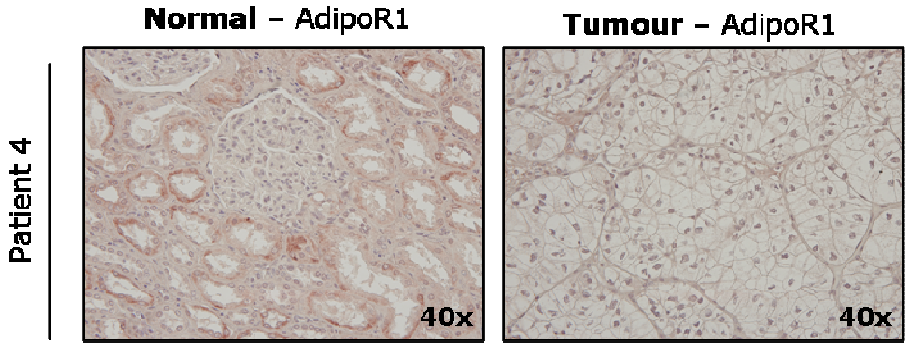
Normal – AdipoR1
Tumour – AdipoR1
Patient 4
40x
40x

B

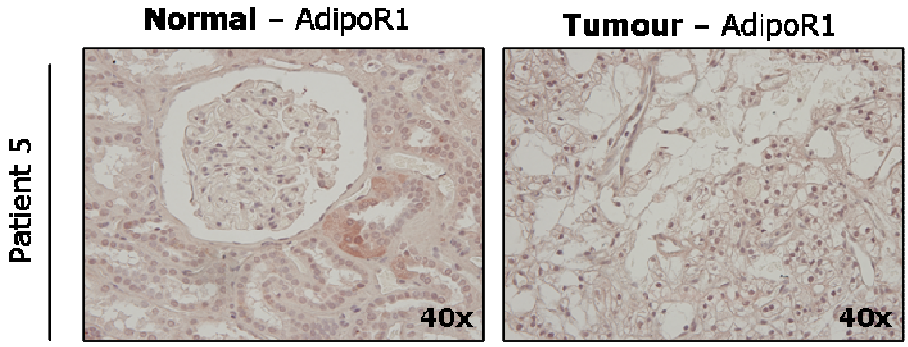
Normal – AdipoR1
Tumour – AdipoR1
Patient 5
40x
40x

C

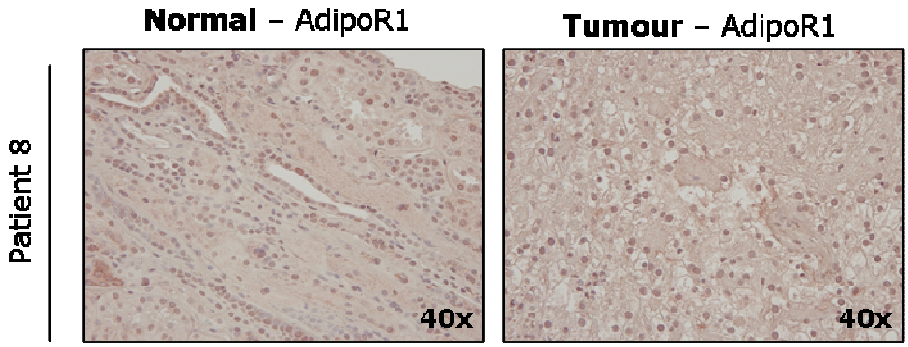
Normal – AdipoR1
Tumour – AdipoR1
Patient 8
40x
40x

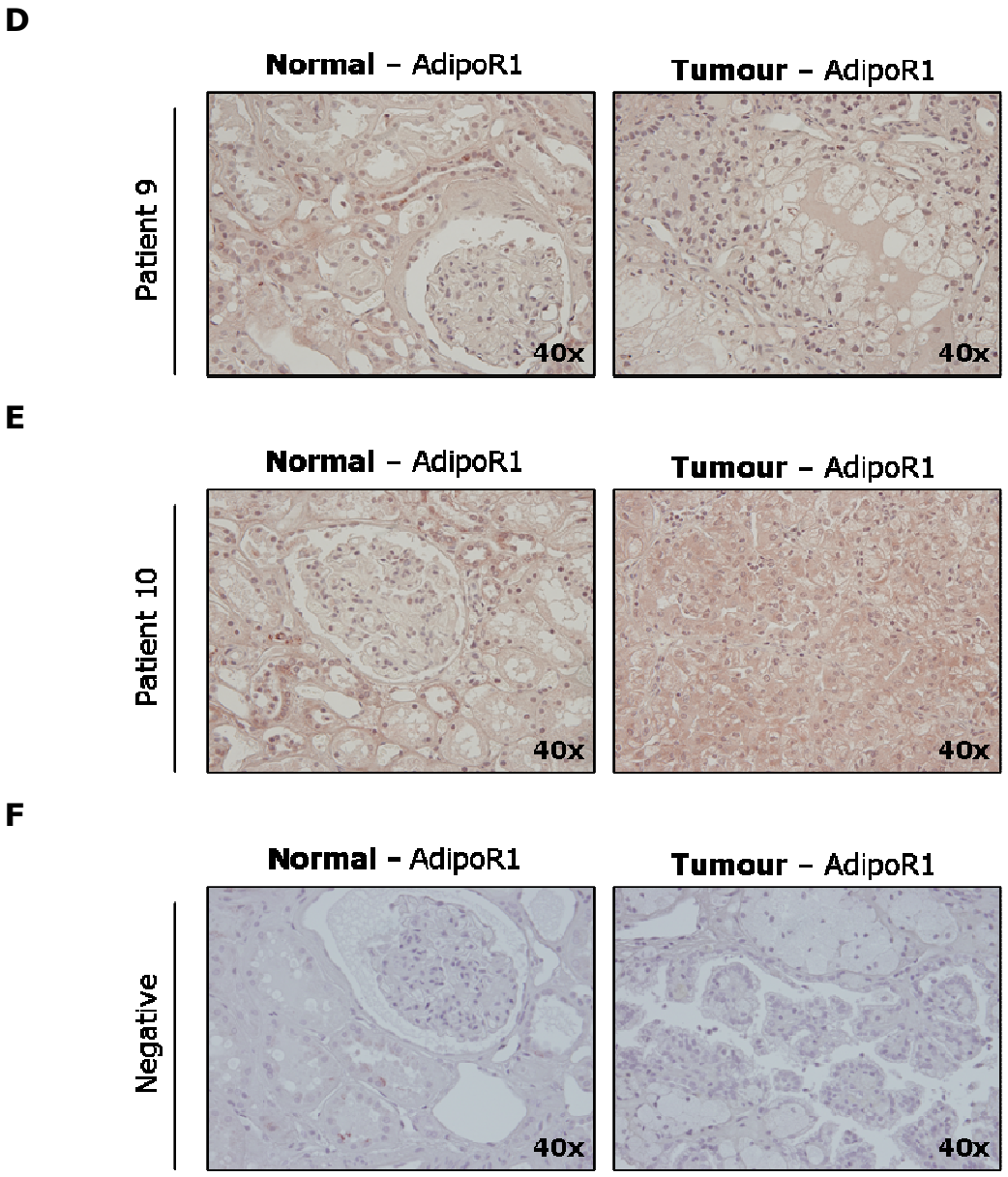

Figure 8 | **AdipoR1 expression is slightly reduced in histological sections of patient RCC tumours**. (**A**) Patient 4, (**B**) 5, (**C**) 8, (**D**) 9 and (**E**) 10 tumour tissue (Tumour) and normal surrounding parenchyma (Normal) were fixed in formalin, embedded in a single paraffin block, sectioned to a thickness of 4μm, immunohistochemically stained for AdipoR1 and imaged with a 40x objective. The positive control was murine muscle tissue stained for AdipoR1 (not shown) and the (**F**) negative control was secondary antibody staining only on patient tumour and normal tissue.

A

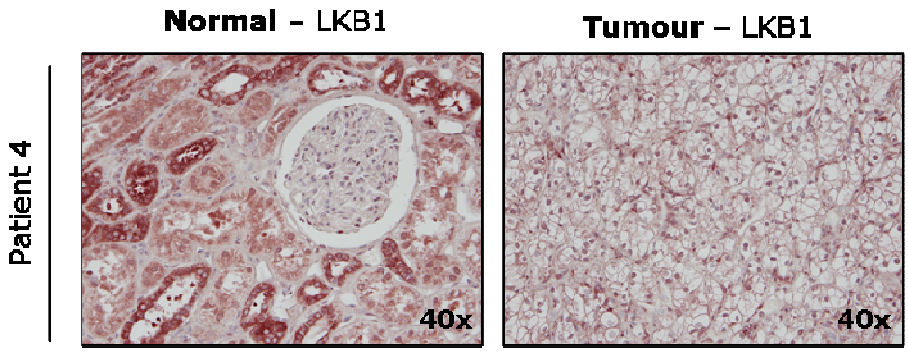
Normal – LKB1
Tumour – LKB1
Patient 4
40x
40x

B

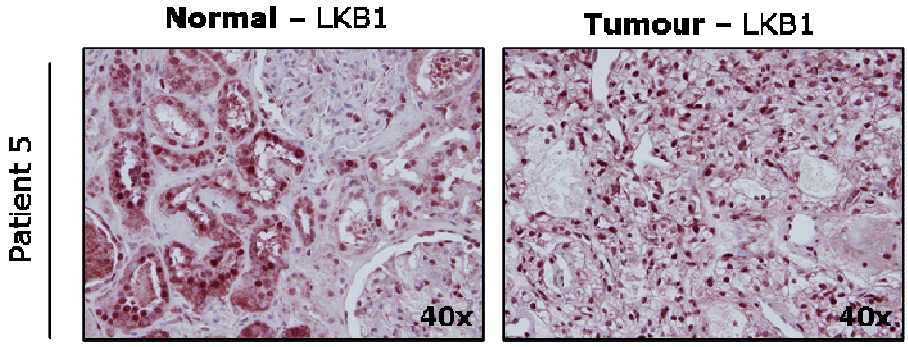
Normal – LKB1
Tumour – LKB1
Patient 5
40x
40x

C

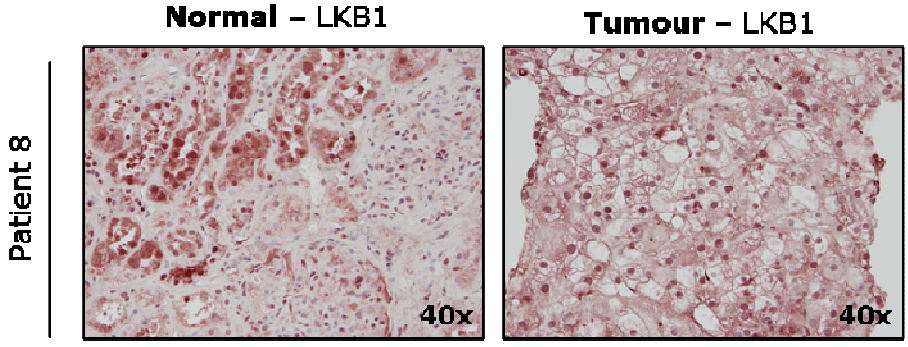
Normal – LKB1
Tumour – LKB1
Patient 8
40x
40x

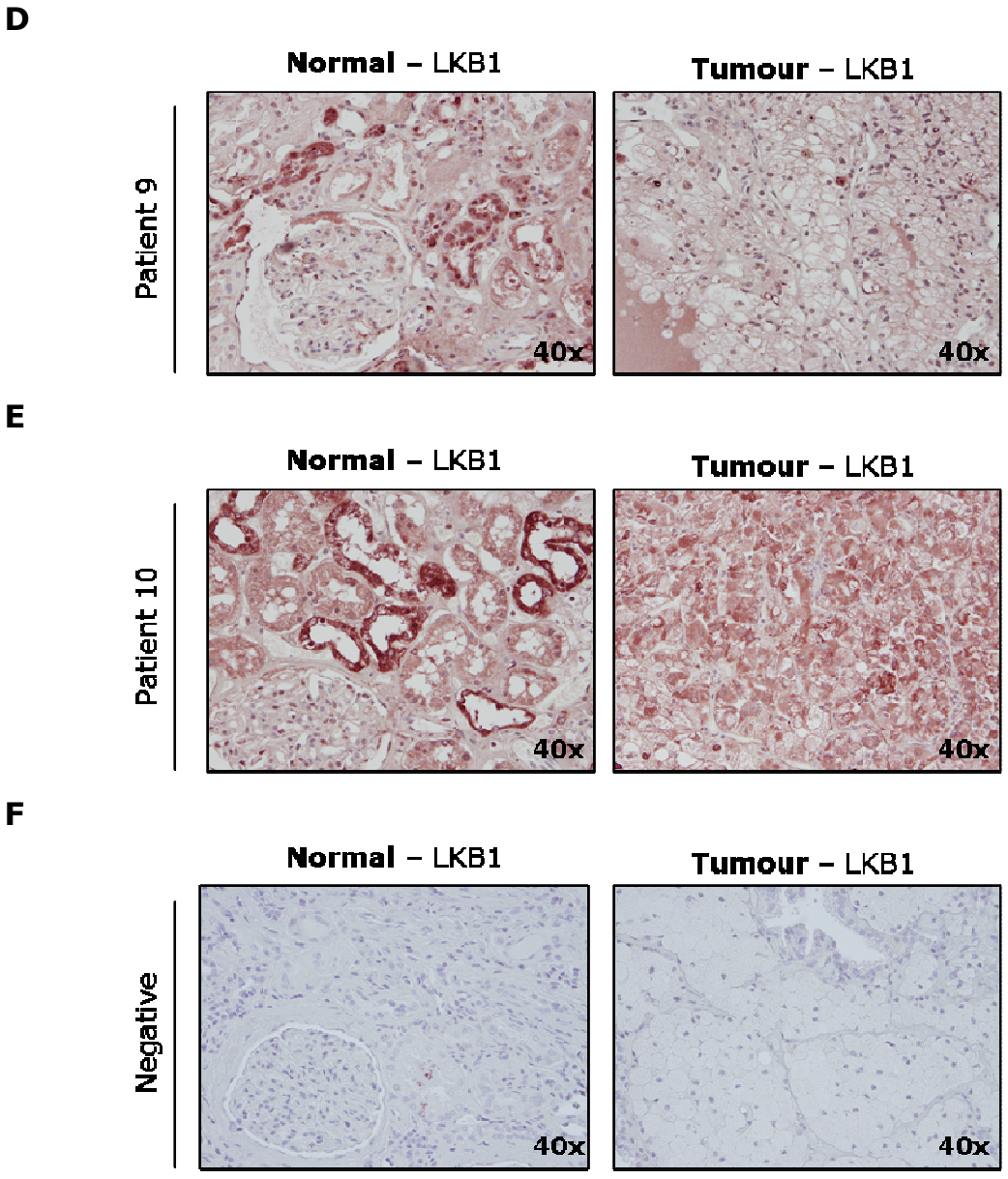

Figure 9 | **LKB1 expression is reduced in histological sections of patient RCC tumours**. (**A**) Patient 4, (**B**) 5, (**C**) 8, (**D**) 9 and (**E**) 10 tumour tissue (Tumour) and normal surrounding parenchyma (Normal) were fixed in formalin, embedded in a single paraffin block, sectioned to a thickness of 4μm, immunohistochemically stained for LKB1 and imaged with a 40x objective. The positive control was murine muscle tissue stained for LKB1 (not shown) and (**F**) the negative control was secondary antibody staining only on patient tumour and normal tissue.

A

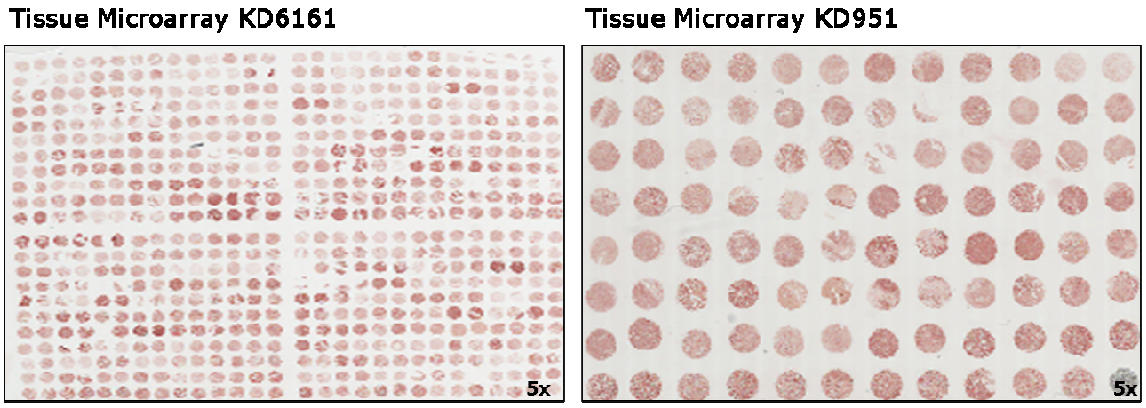
Tissue Microarray KD6161
Tissue Microarray KD951
5x
5x

B

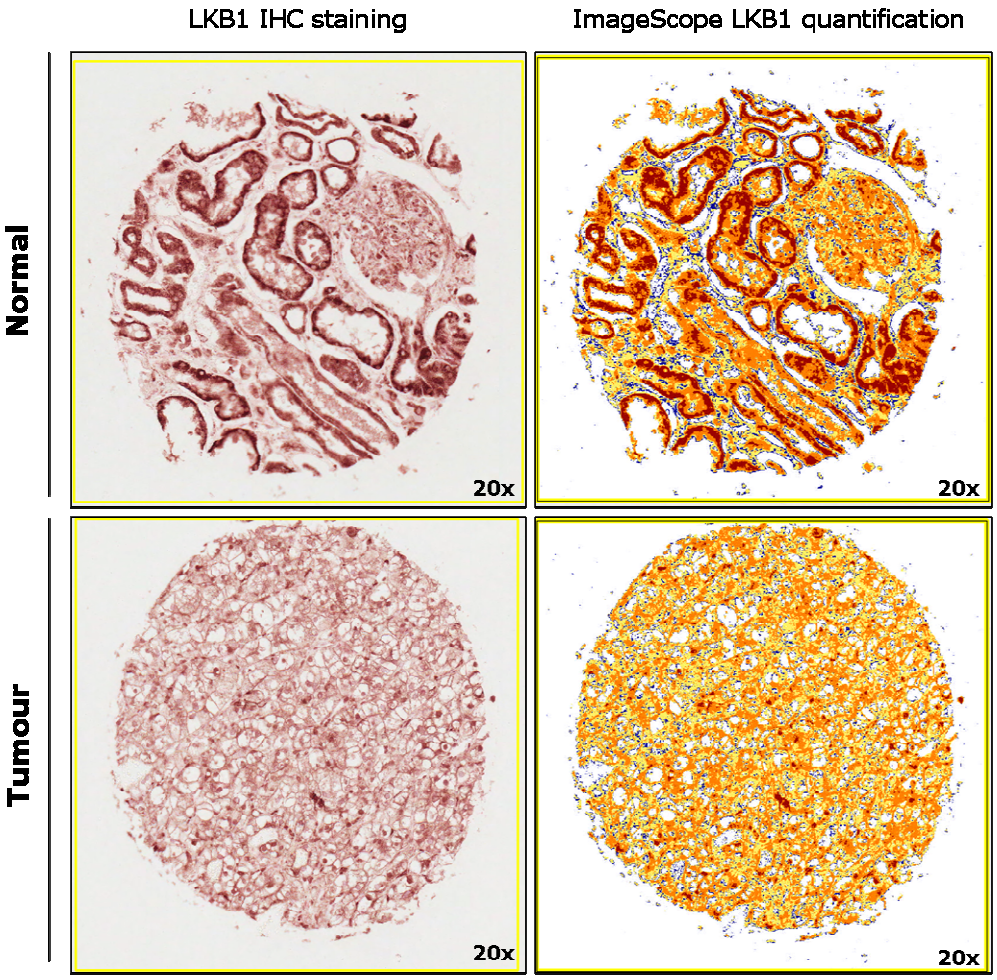
LKB1 IHC staining
ImageScope LKB1 quantification
Normal
Tumour
20x
20x
20x
20x

C

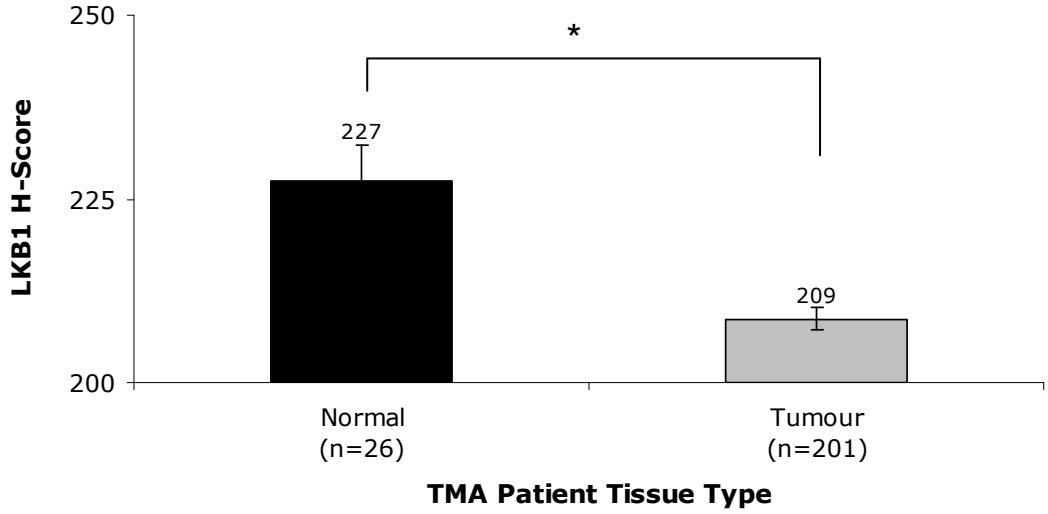

Figure 10 | **TMA confirms LKB1 reduction in 201 patient RCC tumours.** (**A**) Two TMAs containing duplicate cores of patient RCC tumour tissue and patient normal renal tissue were immunohistochemically stained for LKB1, scanned at a 20x magnification on the ScanScope XT brightfield scanner and quantified on ImageScope software using the Positive Pixel Count algorithm. (**B**) Images of a representative RCC tumour and normal tissue core are shown following LKB1 staining (left) and quantification with the Positive Pixel Count algorithm (right) where colour represents staining intensity categories: red = strong positive, orange = positive, yellow = weak positive and blue = negative. (**C**) Average H-score for LKB1 staining was determined across the duplicate tissue cores for each sample and the data represent the mean H-score of 26 normal patient tissue samples and 201 RCC patient tumour tissue samples ± SEM. Independent t-test significance (*) was $p < 0.05$.

Staining of p-ACC was examined to infer the effect of RCC on activated AMPK, however, inconsistent and most likely non-specific staining of tissue structures was observed throughout the normal and tumour tissue histological sections (**Figure 11A-E**).

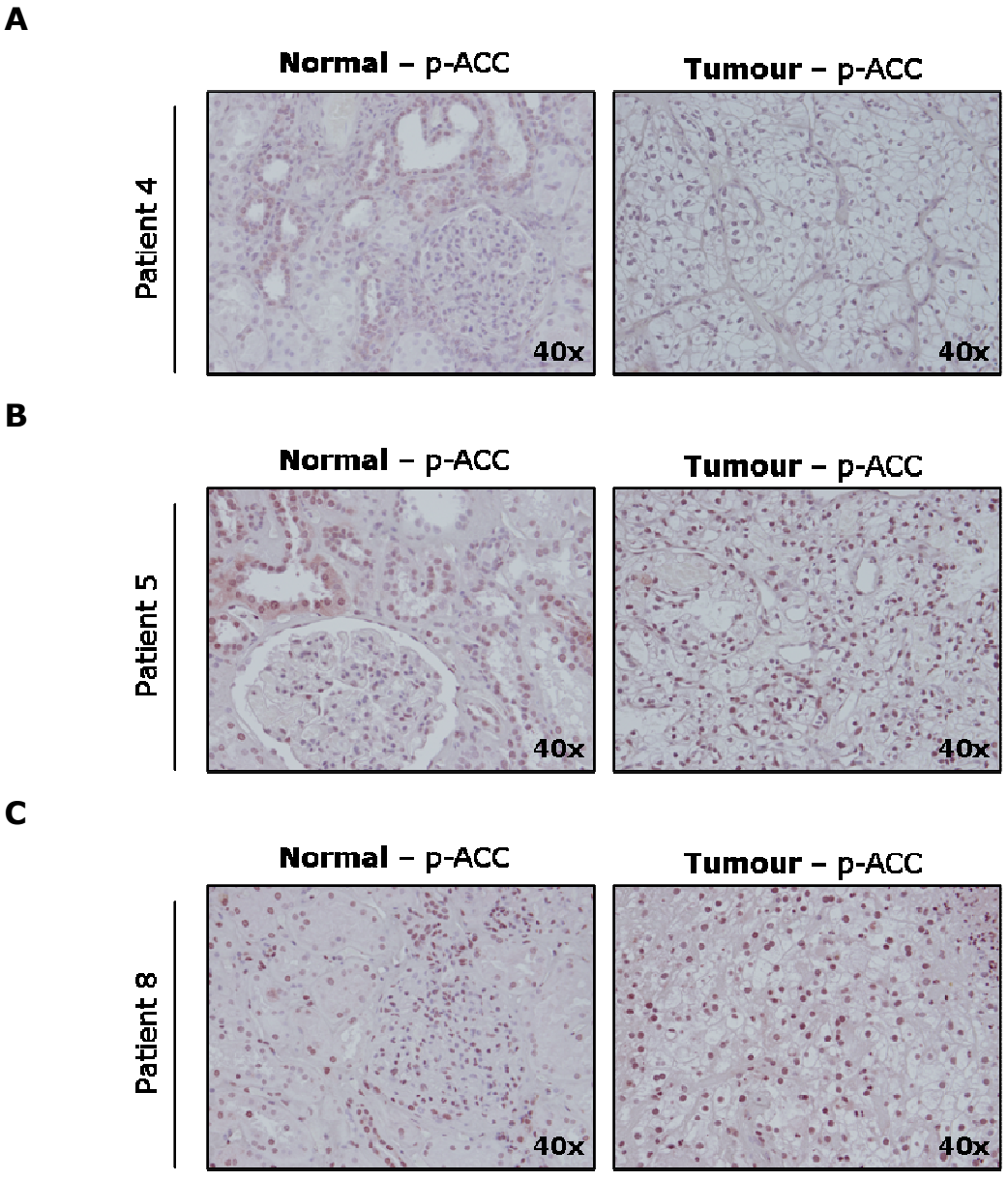

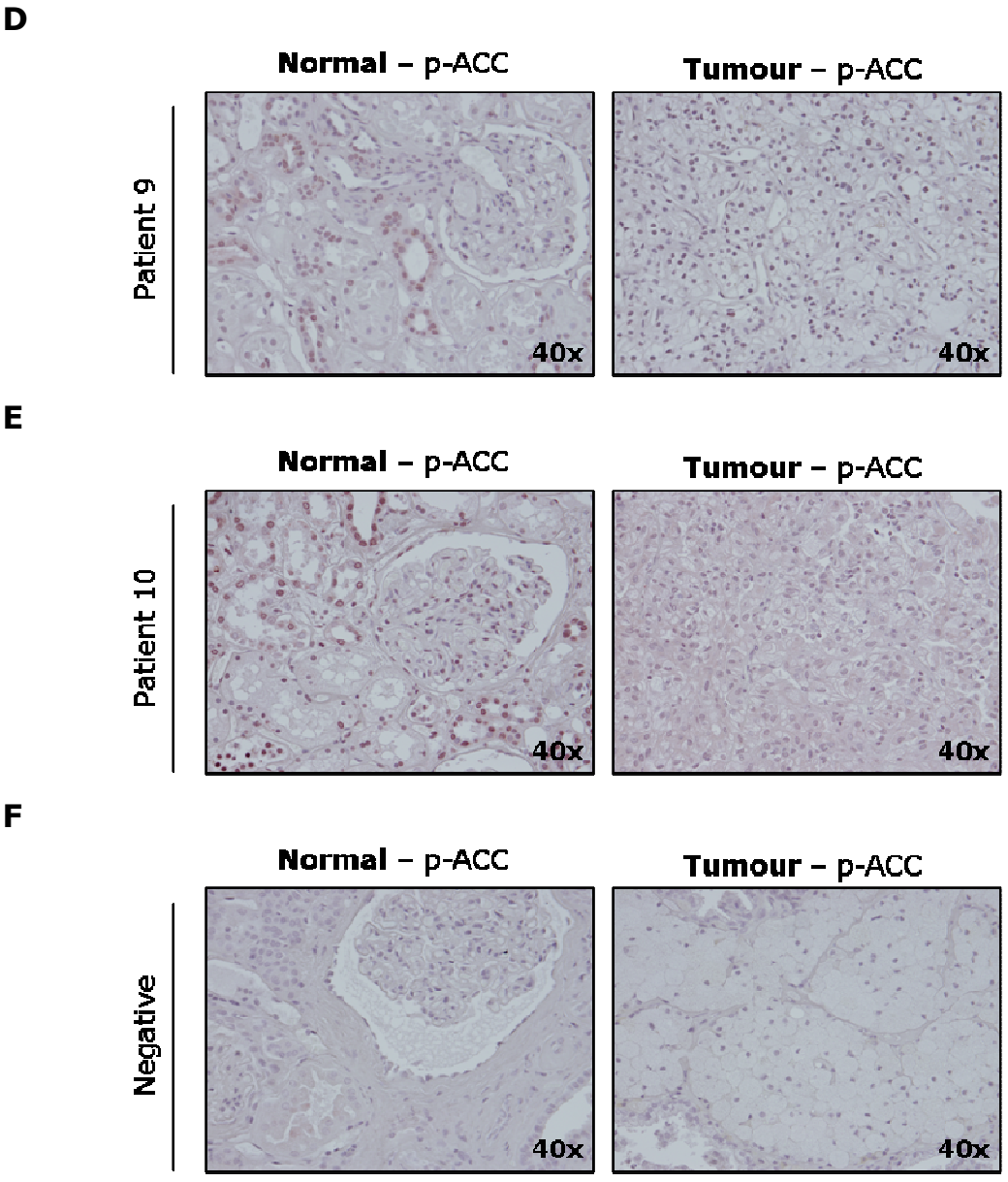

Figure 11 | p-ACC staining in histological sections of patient RCC tumour and normal tissue was not conclusive. (**A**) Patient 4, (**B**) 5, (**C**) 8, (**D**) 9 and (**E**) 10 tumour tissue (Tumour) and normal surrounding parenchyma (Normal) were fixed in formalin, embedded in a single paraffin block, sectioned to a thickness of 4µm, immunohistochemically stained for phosphorylated ACCser79 (p-ACC) and imaged with a 40x objective. The positive control was murine muscle tissue stained for p-ACC (not shown) and (**F**) the negative control was secondary antibody staining only on patient tumour and normal tissue.

6.2.1 **CRL-1932 is the *in vitro* cell model of human RCC**

Prior to utilizing the CRL-1932 and CRL-1933 cell lines derived from human RCC in *in vitro* studies, the cell lines were examined for the expression of both adiponectin receptors, AdipoR1 and AdipoR2. Indeed, the presence of both AdipoR1 and AdipoR2 was apparent in the cell lines, permitting their application in following experiments (**Figure 12**).

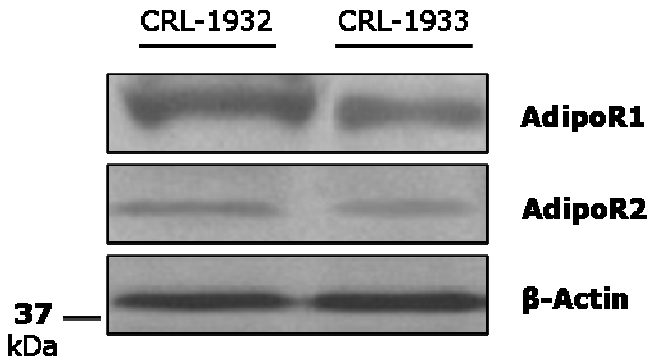

Figure 12 | CRL-1932 and CRL-1933 cell lines express AdipoR1 and AdipoR2. Total protein was extracted from CRL-1932 and CRL-1933 cell lines, brought to 40 µg, separated by SDS-PAGE and analyzed by Western blot for AdipoR1, AdipoR2 and β-Actin.

Although the expression of both adiponectin receptors in the CRL-1932 and CRL-1933 cell lines was evident, it was crucial to demonstrate that the receptors were functional. In order to demonstrate function, downstream cellular effects of adiponectin signalling, including the reduction of phosphorylated mTOR (p-mTOR) and activation of AMPKα (p-AMPKα), were examined in the cell lines (**Figure 13A**). The expression level of p-mTOR was reduced to 25% with adiponectin treatment compared to 100% in the untreated (**Figure 13B**), while p-AMPKα expression increased to 320% with adiponectin treatment compared to 100% in the untreated in CRL-1932 cells (**Figure 13C**). Adiponectin treatment of CRL-1933 cells did not phosphorylate AMPKα and inhibit p-mTOR to the magnitude observed in CRL-1932 cells (data not shown). Thus, for the reasons that the CRL-1932 cell line expressed AdipoR1 and AdipoR2 as well as effectively responded to adiponectin, CRL-1932 cells were selected as the *in vitro* model.

A

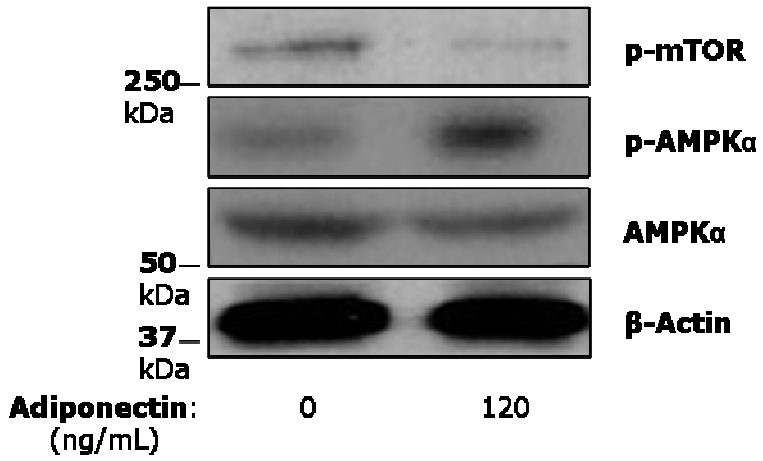

B

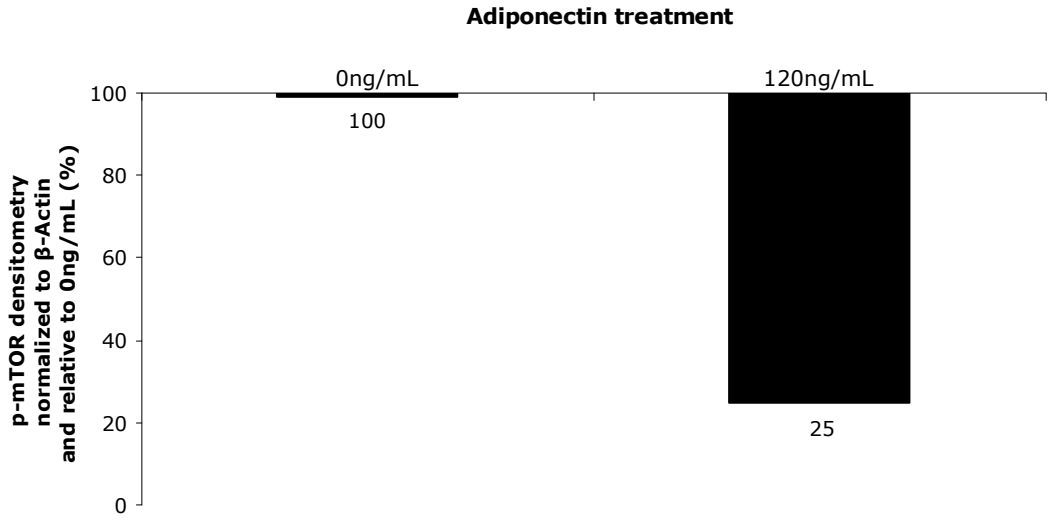

C

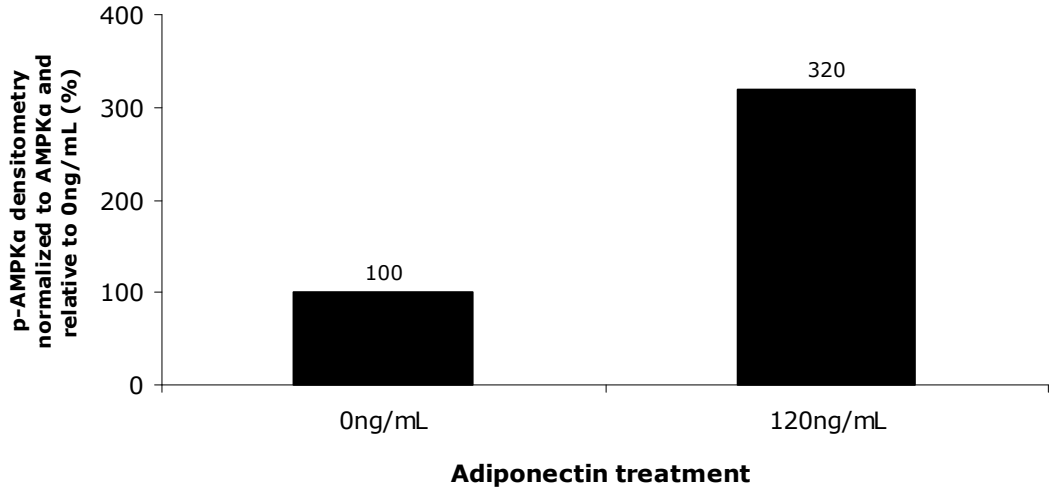

Figure 13 | **Adiponectin activates AMPKα and inhibits mTOR in CRL-1932 cells**. (**A**) CRL-1932 cells were either untreated (0 ng/mL) or treated (120 ng/mL) with adiponectin for 1 hour before total protein was extracted from the cells. Lysates (40µg) were separated by SDS-PAGE and analyzed by Western blotting for phosphorylated mTORser2448 (p-mTOR), activated AMPKαthr172 (p-AMPKα), total AMPKα and β-Actin. The intensity of the bands was quantified by densitometry and (**B**) p-mTOR values were normalized to endogenous β-Actin values and (**C**) p-AMPKα values were normalized to AMPKα values. Data represent the densitometric quantification and are presented as the 120 ng/mL treatment relative to no treatment, which was set to 100%.

6.2.2 **AdipoR1 and LKB1 knockdown in shVAdipoR1 and shLKB1 cell lines**

Stable CRL-1932 cell lines with knockdown of AdipoR1, AdipoR2 or LKB1 expression were generated by either a retroviral infection with shVAdipoR1, shVAdipoR2 and shVLKB1 plasmids or infection with shLKB1 lentiviral particles. AdipoR1 protein expression in shVAdipoR1 knockdown cells was successfully reduced to 60% (**Figure 14A**), compared to the 100% expression in shVControl cells (**Figure 14B**), however attempts to knockdown AdipoR2 protein expression in shVAdipoR2 cells were not effective. Knockdown of LKB1 protein expression in shVLKB1 cells was evident, however, LKB1 expression did not remain stable through successive cell passages (data not shown).

LKB1 protein expression in shLKB1 cells was reduced in all three trials of infection with shLKB1 lentiviral particles (**Figure 15A**) to an average of 53%, compared to the 100% expression in shCONTROL cells (**Figure 15B**). The 53% reduction in LKB1 protein expression remained stable throughout successive cell passages, even when cultured without puromycin selection (**Figure 20**). Therefore, the shLKB1 cell line was selected for use in all future experiments.

A

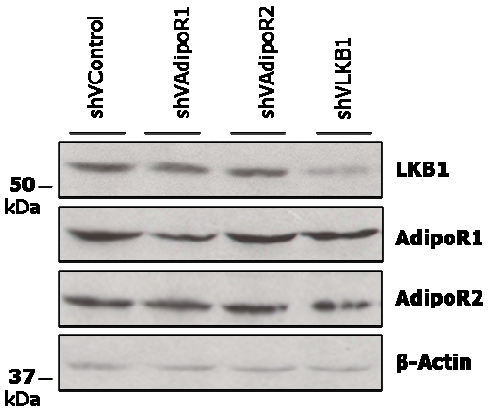

B

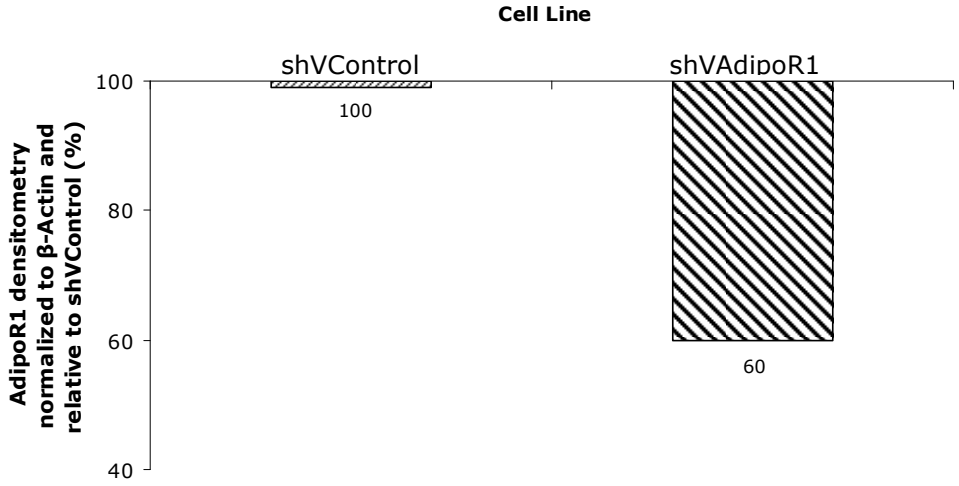

Figure 14 | **Retroviral infection knockdown of AdipoR1 in shVAdipoR1 cells**. (**A**) The 293T viral packaging cell line was co-transfected with the viral plasmids pVPack-VSV-G and pVPack-GP in addition to one of the shRNA plasmids specific to the knockdown of AdipoR1 (shVAdipoR1), AdipoR2 (shVAdipoR2), LKB1 (shVLKB1) or scrambled (shVControl). The resultant retrovirus was used to infect CRL-1932 cells and knockdown AdipoR1, AdipoR2 or LKB1 expression. Total protein was extracted from the cell lines, brought to 40 µg, separated by SDS-PAGE and analyzed by Western blotting for AdipoR1, AdipoR2, LKB1 and β-Actin. (**B**) The intensity of the bands was quantified by densitometry and the shVControl and shVAdipoR1 AdipoR1 values were normalized to endogenous β-Actin values. Data represent the densitometric quantification and are presented as shVAdipoR1 relative to shVControl, which was set to 100%.

A

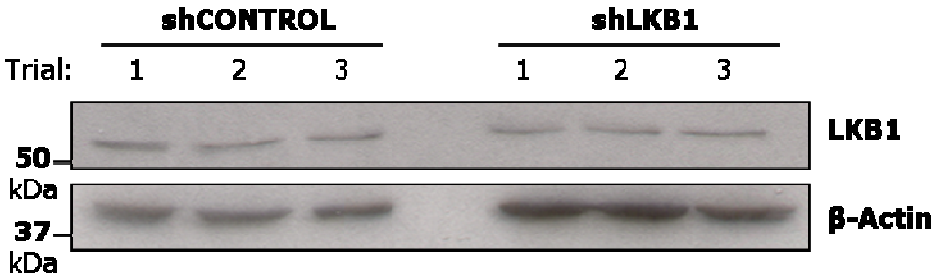

B

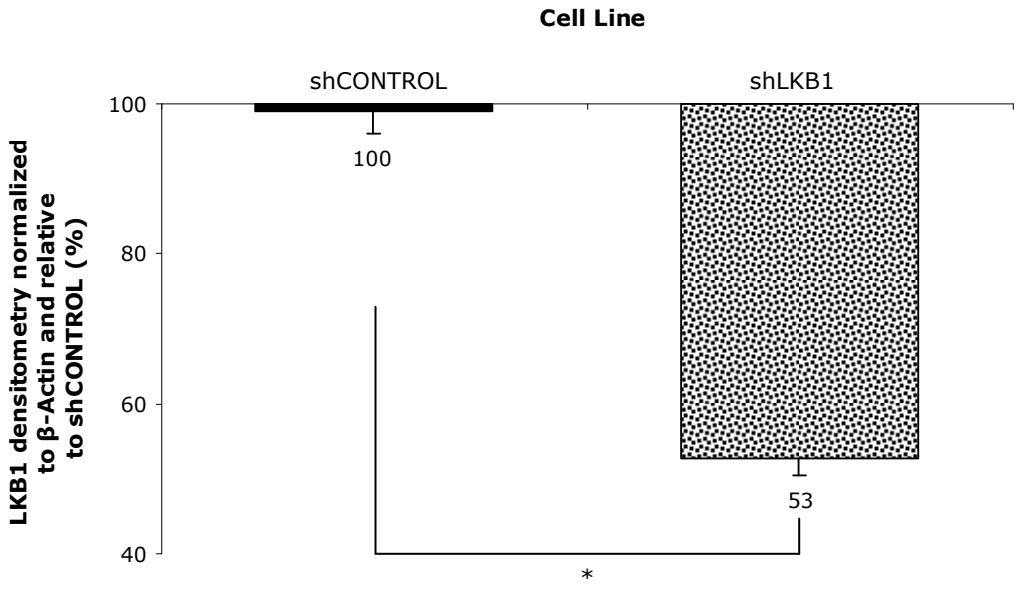

Figure 15 | **Lentiviral particle infection knockdown of LKB1 in shLKB1 cells**. (**A**) CRL-1932 cells were infected with lentiviral particles containing a scrambled shRNA sequence (shCONTROL) or sequence specific to the knockdown of LKB1 (shLKB1). Total protein was extracted from the cells, brought to 40 µg, separated by SDS-PAGE and analyzed by Western blotting for LKB1 and β-Actin. (**B**) The intensity of the bands was quantified by densitometry and the LKB1 values were normalized to endogenous β-Actin values. Data represent the mean densitometric quantification of three trials ± SEM and are presented as shLKB1 relative to shCONTROL, which was set to 100%. Independent t-test significance (*) was $p < 0.05$.

6.2.3 **AdipoR1 and LKB1 transcript and protein levels in shVAdipoR1 and shLKB1 cell lines**

AdipoR1 and *LKB1* transcript levels were quantified in the shLKB1 and shVAdipoR1 stable knockdown cell lines and compared to the transcript level of the respective infected control cell line. Both *AdipoR1* and *LKB1* transcript levels were reduced to 78% and 88% respectively, in shVAdipoR1 cells compared to the 100% transcript level in shVControl cells (**Figure 16A**). Similarly, *LKB1* and *AdipoR1* transcript levels were reduced to 45% and 78% respectively, in the shLKB1 cell line compared to the 100% transcript level in the shCONTROL cell line (**Figure 16B**). Reduction in the transcript level of *LKB1* in shVAdipoR1 cells, and *AdipoR1* in shLKB1 cells was not to the magnitude of reduction of the gene targeted for knockdown.

In contrast to the reduced *LKB1* transcript level observed in shVAdipoR1 cells, LKB1 protein expression in shVAdipoR1 cells (**Figure 17A**) was not reduced when compared to shVControl cells (**Figure 17B**). On the other hand, similarly to the reduced *AdipoR1* transcript level in shLKB1 cells, AdipoR1 protein expression in shLKB1 cells was reduced to 45% (**Figure 17C**) compared to 100% expression in shCONTROL cells (**Figure 17D**).

A

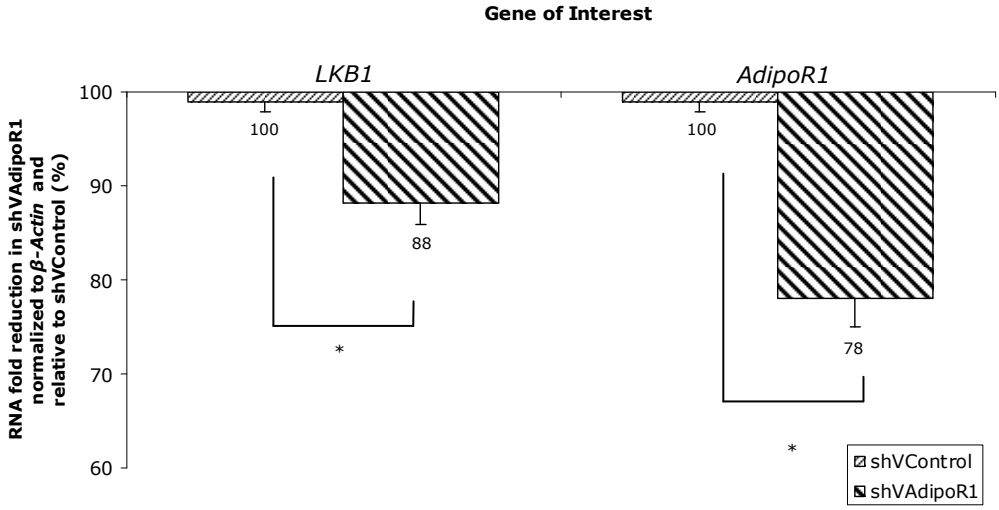

B

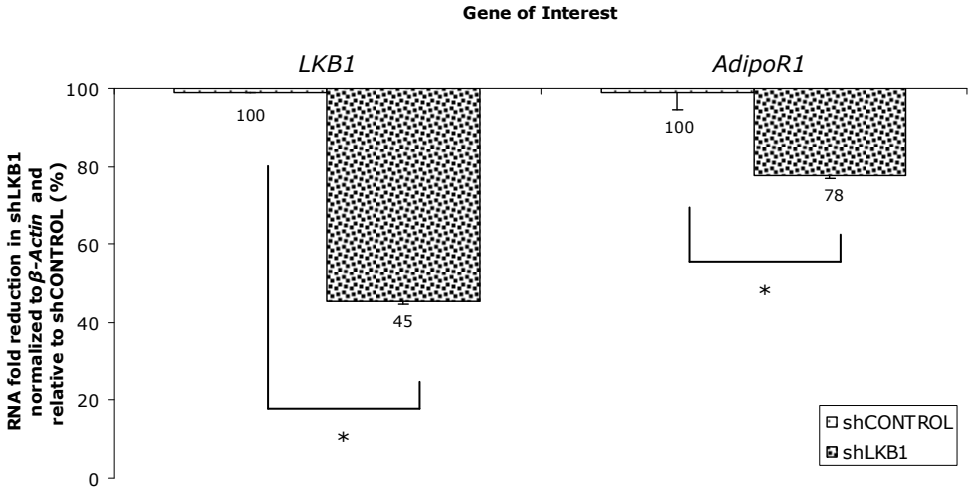

Figure 16 | ***AdipoR1* and *LKB1* transcript levels are reduced with AdipoR1 or LKB1 knockdown**. Total RNA was extracted from shVAdipoR1, shVControl, shLKB1 and shCONTROL cells, transcribed into cDNA and analyzed by qRT-PCR using the primer sets for *LKB1*, *AdipoR1*, *β-Actin* and *18S*. (**A**) The shVControl and shVAdipoR1 *LKB1* and *AdipoR1* transcript levels were normalized to the endogenous *β-Actin* transcript level and (**B**) the shCONTROL and shLKB1 *LKB1* and *AdipoR1* transcript levels were normalized to the endogenous *β-Actin* transcript level. Data represent the mean of triplicate wells ± SEM and are presented as the transcript level of the knockdown relative to the respective control, which was set to 100%. Independent t-test significance (*) was $p < 0.05$.

A


shVControl
shVAdipoR1
Trial:
1
1
2
3
50 –
kDa
37 –
kDa
LKB1
β-Actin

B

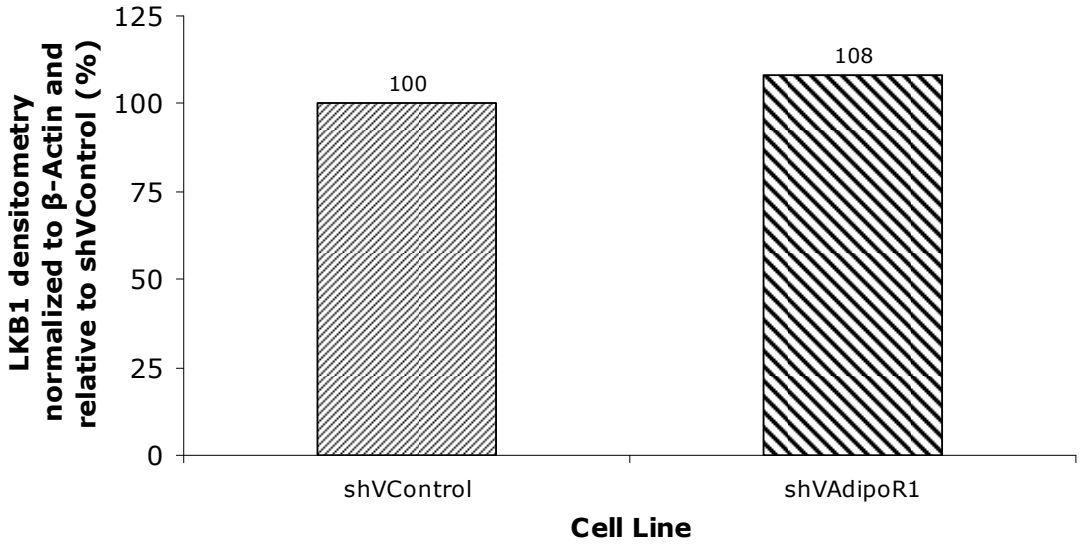
LKB1 densitometry normalized to β-Actin and relative to shVControl (%)
125
100
75
50
25
0
100
108
shVControl
shVAdipoR1
Cell Line

C

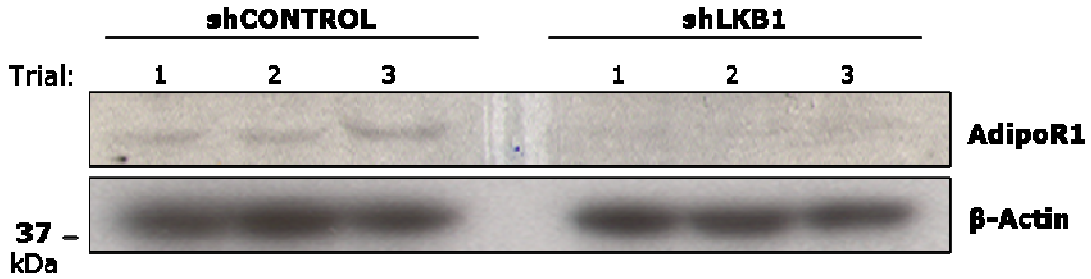

D

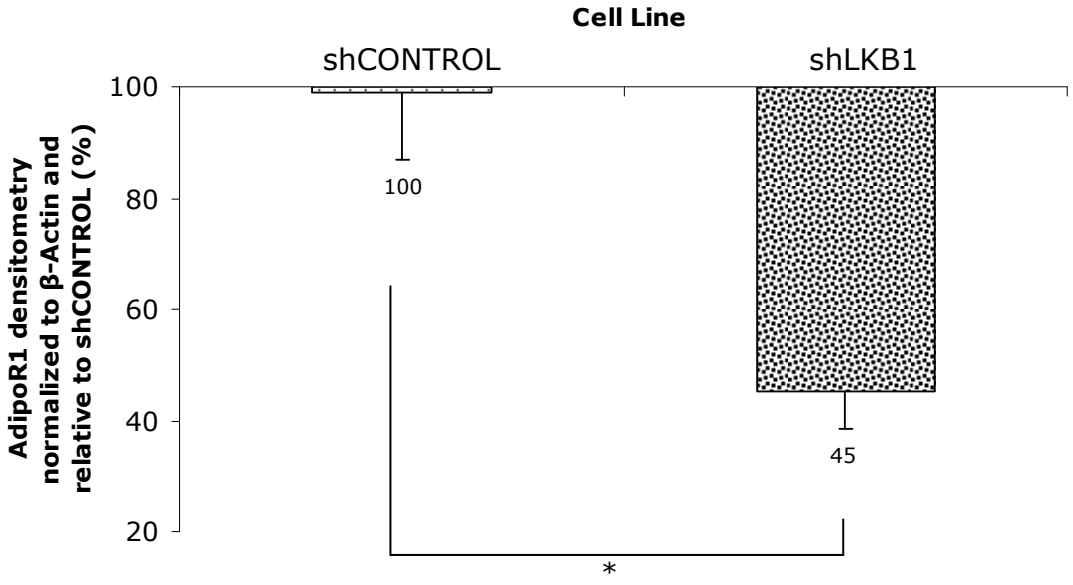

Figure 17 | **AdipoR1 protein expression is reduced with LKB1 knockdown, LKB1 protein expression is not reduced with AdipoR1 knockdown**. Total protein was extracted from shVAdipoR1, shVControl, shLKB1 and shCONTROL cells, brought to 40 µg, separated by SDS-PAGE and analyzed by Western blotting for (**A**) LKB1 and β-Actin or (**C**) AdipoR1 and β-Actin. (**B**) Intensity of the bands was quantified by densitometry and the shVAdipoR1 and shVControl LKB1 values were normalized to endogenous β-Actin values. Data represent the densitometric quantification and are presented as shVAdipoR1 relative to shVControl, which was set to 100%. (**D**) The shLKB1 and shCONTROL AdipoR1 values were normalized to endogenous β-Actin values. Data represent the mean densitometric quantification of three trials ± SEM and are presented as shLKB1 relative to shCONTROL, which was set to 100%. Independent t-test significance (*) was $p < 0.05$.

6.2.4 **Adiponectin signalling is disrupted with LKB1 knockdown**

Due to the fact that the shLKB1 cell line presented reduced LKB1 and AdipoR1 transcript and protein expression, the cell line was selected to investigate the effect of AdipoR1 and LKB1 reduction on adiponectin signalling events. Expression levels of p-AMPKα and p-ACC were examined in shCONTROL and shLKB1 cell lines treated with or without adiponectin. Escalating doses of adiponectin increased p-AMPKα levels in shCONTROL cells, but did not significantly affect p-AMPKα levels in shLKB1 cells (**Figure 18**). Increasing doses of adiponectin did not affect p-ACC levels in a dose-dependent manner in either cell line. However, p-ACC protein expression was significantly increased in shCONTROL cells over shLKB1 cells regardless of treatment.

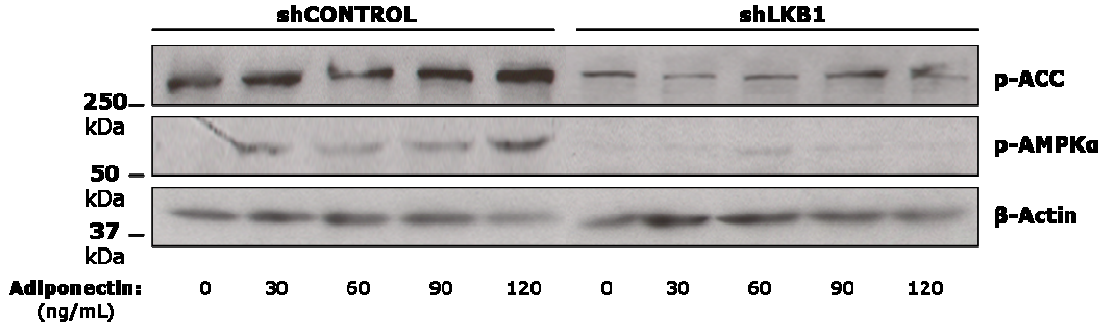

Figure 18 | Adiponectin-mediated phosphorylation of AMPKα and ACC is disrupted with LKB1 knockdown. The shCONTROL and shLKB1 cells were either untreated (0 ng/mL) or treated (30 ng/mL, 60 ng/mL, 90 ng/mL and 120 ng/mL) with adiponectin for 1 hour before total protein was extracted from the cells. Lysates (40 µg) were separated by SDS-PAGE and analyzed by Western blotting for activated AMPKαthr172 (p-AMPKα), phosphorylated ACCser79 (p-ACC) and β-Actin.

Baseline level of secreted VEGF prior to adiponectin treatment was significantly higher in shLKB1 cells (918 pg/mL) compared to shCONTROL cells (800 pg/mL) (**Figure 19A**). Treatment of shLKB1 and shCONTROL cells with increasing doses of adiponectin demonstrated reduced VEGF secretion in shCONTROL cells in a dose-responsive manner, however VEGF secretion in shLKB1 cells was not affected (**Figure 19B**).

A

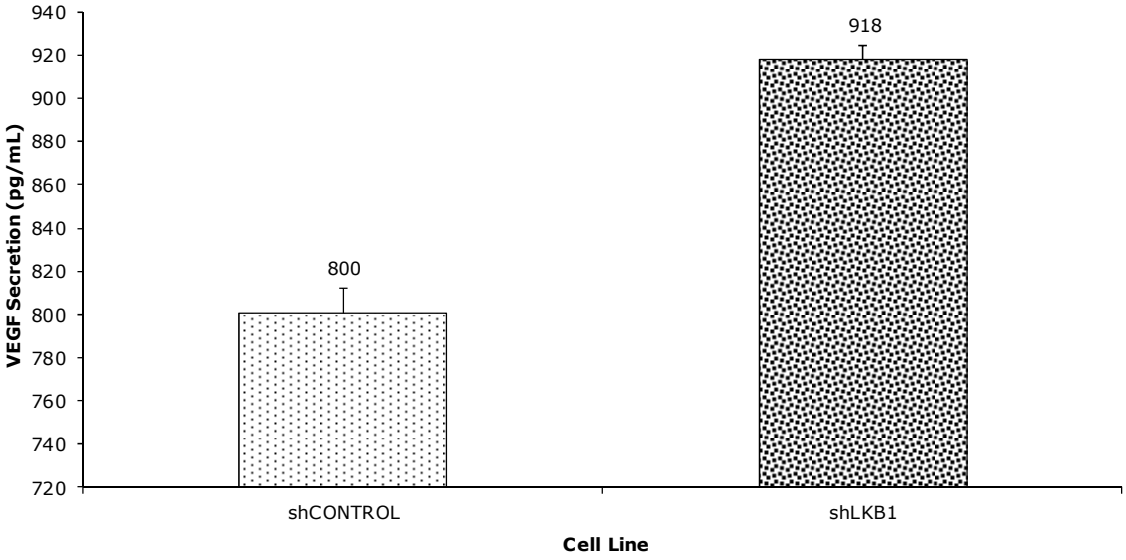

B

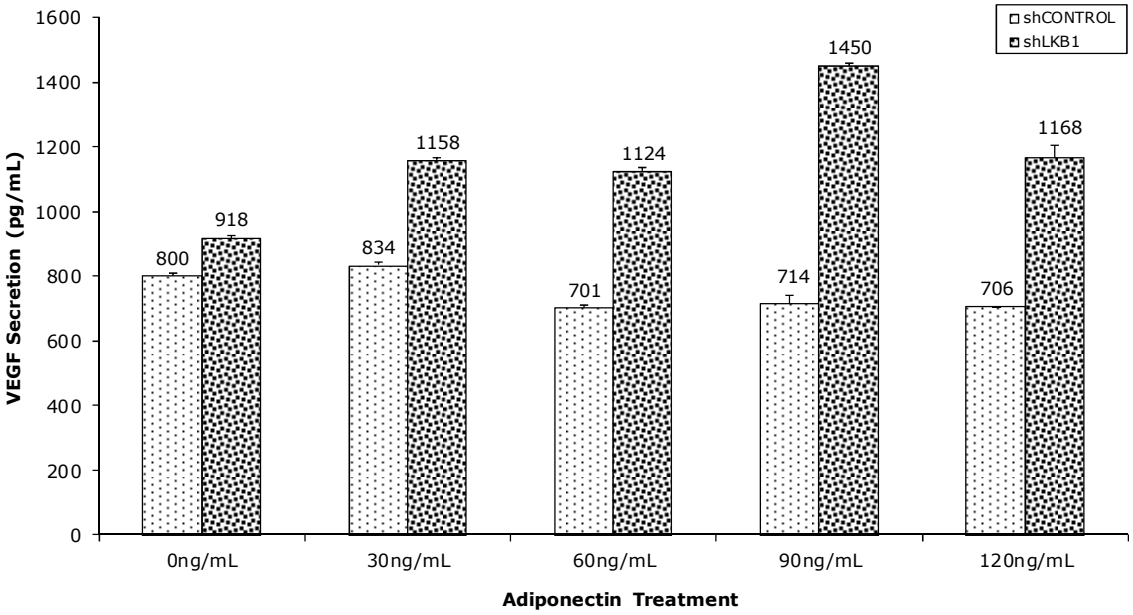

Figure 19 | **LKB1 knockdown increases VEGF secretion and disrupts adiponectin-mediated inhibition of VEGF secretion**. The shCONTROL and shLKB1 cell lines were either (**A**) untreated (0 ng/mL) or (**B**) treated with adiponectin (30 ng/mL, 60 ng/mL, 90 ng/mL and 120 ng/mL) for 24 hours before the supernatant was harvested and measured for human VEGF using an ELISA. Data represent the mean VEGF secretion in three wells ± SEM and are presented as shLKB1 compared to shCONTROL.

6.2.5 **LKB1 knockdown increases RCC tumourigenic potential**

The stable knockdown of LKB1 in shLKB1 cells was confirmed by culturing the cell line without puromycin selection over a period of 15 days. LKB1 protein expression in shLKB1 cells was significantly reduced compared to shCONTROL cells at every time point examined (0, 3, 6, 9, 12 and 15 days) (**Figure 20**).

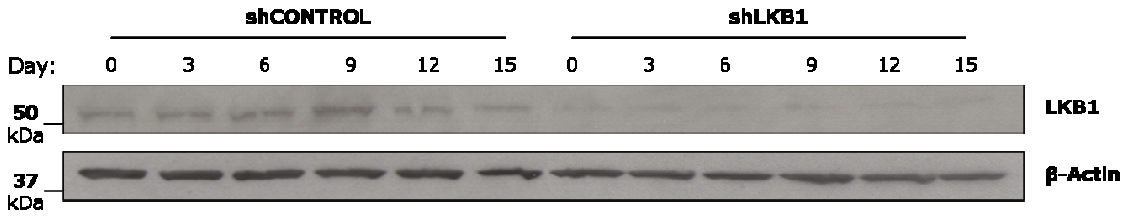

Figure 20 | LKB1 knockdown in shLKB1 cells remains stable over 15 days. The shCONTROL and shLKB1 cell lines were grown without puromycin selection for 0, 3, 6, 9, 12 and 15 days before total protein was extracted from the cells. Lysates (40 µg) were separated by SDS-PAGE and analyzed by Western blotting for LKB1 and β-Actin.

The shLKB1 cell line was examined using traditional proliferation, invasion, xenograft and ELISA assays in order to determine the effect of AdipoR1 and LKB1 knockdown on tumourigenicity. The growth assay demonstrated greater cell numbers for shLKB1 cells compared to shCONTROL cells at all time points examined (0 h, 24 h, 48 h, 72 h, 96 h, 120 h and 144 h) (**Figure 21A**), and reached significance after only 24 hours of growth (**Figure 21B**). At the final time point of the proliferation assay (144 h), the number of shLKB1 cells was approximately double (cells: $9.2x10^5$) that of shCONTROL cells (cells: $5.0x10^5$).

The ability of shLKB1 and shCONTROL cells to migrate through a Matrigel™ coated chamber was examined, quantified and expressed as an Invasion Percentage. It was apparent from the images of the Invasion and Control Chamber membranes that the percentage of shLKB1 cells that invaded through the Matrigel™ was significantly greater than the percentage of shCONTROL cells (**Figure 22A**). Indeed, the shLKB1 Invasion Percentage of 252% was significantly greater than the 9% Invasion Percentage of shCONTROL cells (**Figure 22B**).

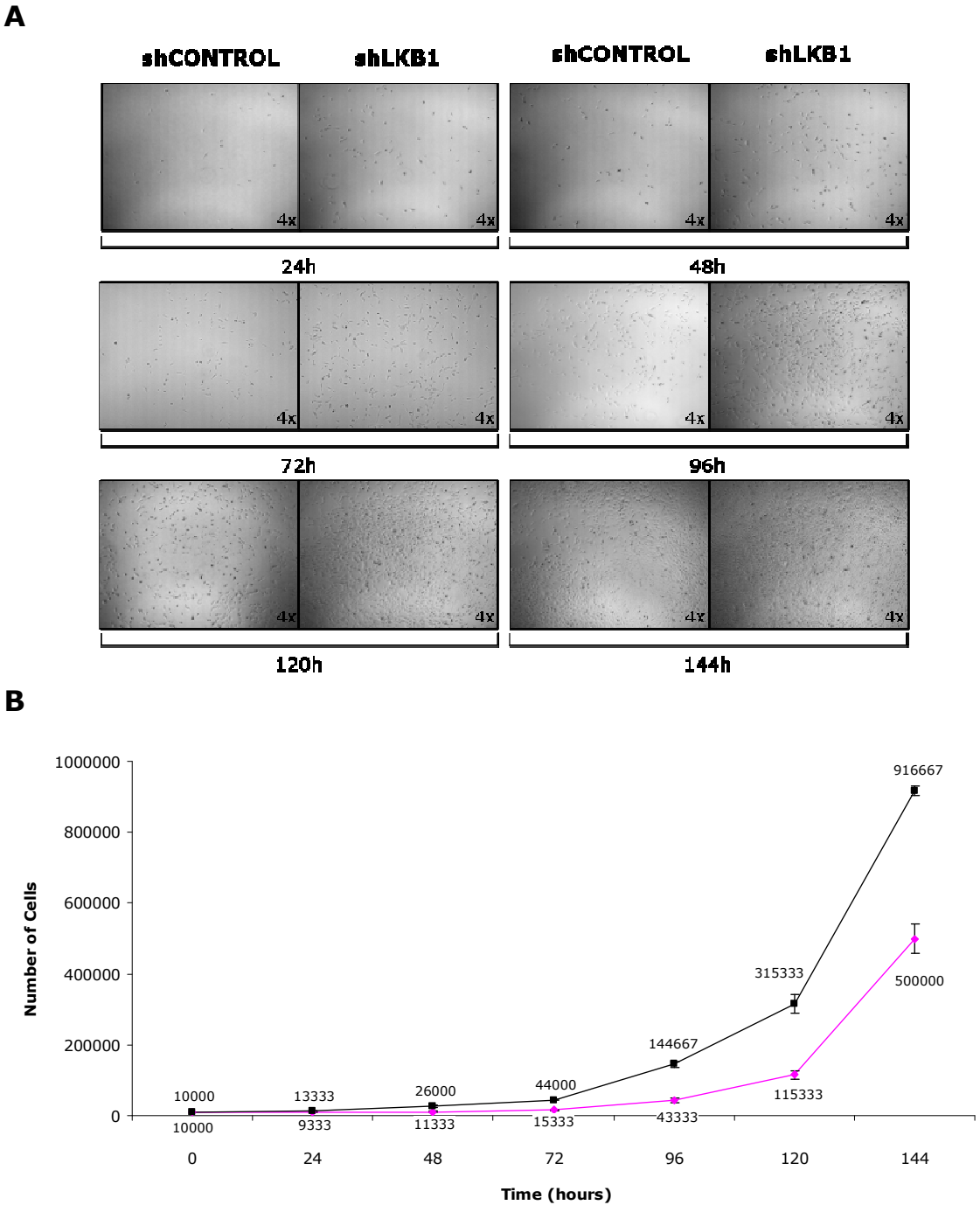

Figure 21 | **LKB1 knockdown increases cell proliferation**. (**A**) The shCONTROL (◇) and shLKB1 (□) cell lines were seeded to 1.0x10^4 cells per well, incubated (0 h, 24 h, 48 h, 72 h, 96 h, 120 h and 144 h), visualized to approximate cell density and (**B**) counted to determine cell number. Data represent the mean cell number in three wells ± SEM and are presented as shLKB1 compared to shCONTROL.

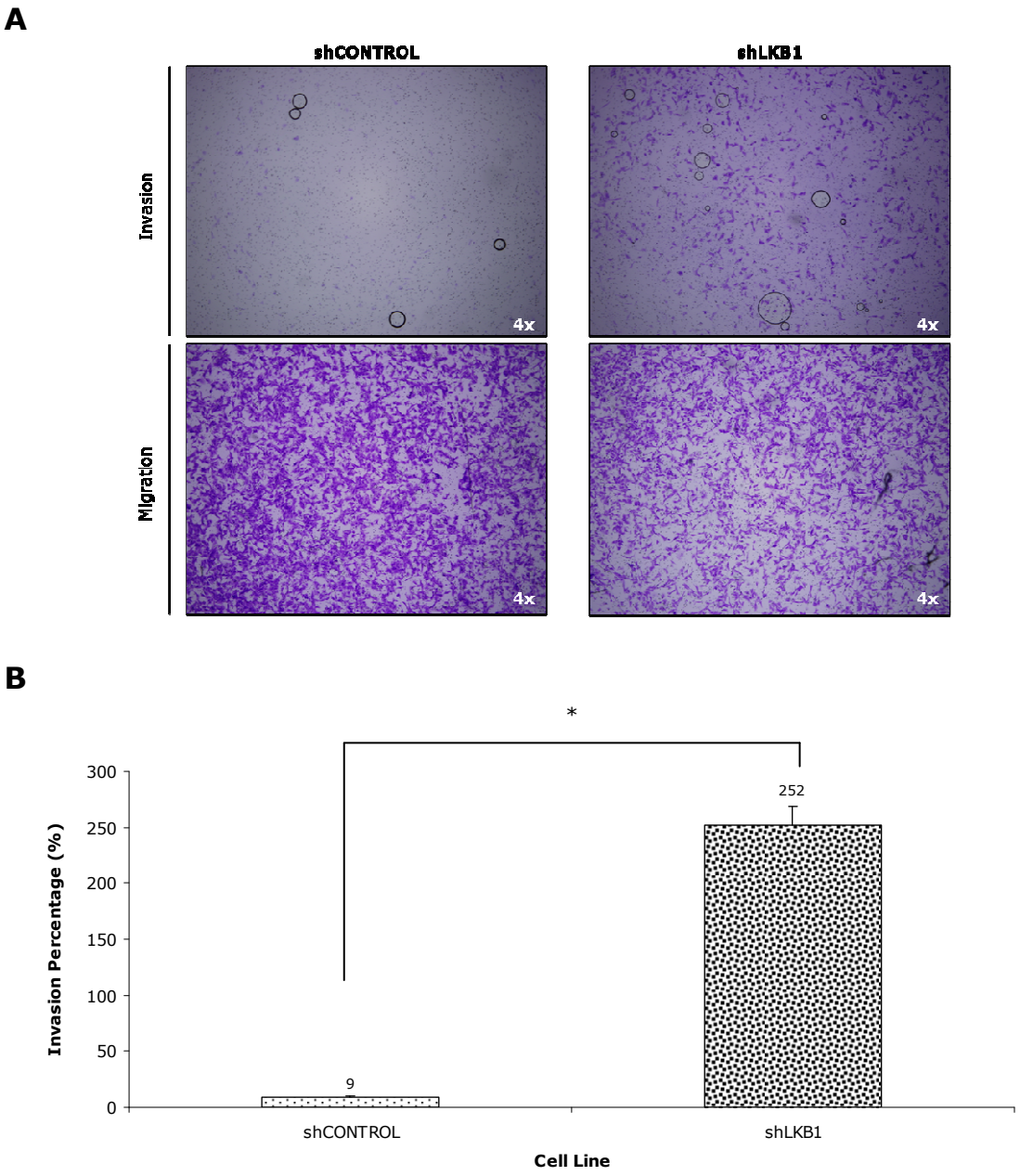

Figure 22 | **LKB1 knockdown increases cell migration and invasion**. (**A**) The shCONTROL and shLKB1 cell lines were seeded to $2.5x10^4$ cells per Invasion and Control Chamber, incubated with 10% FBS as the chemoattractant for 22 hours, fixed, stained, imaged to quantify the number of invaded or migrated cells and (**B**) analyzed for Invasion Percentage [(Number of cells in Invasion membrane/Number of cells in Migration membrane)*100]. Data represent the mean Invasion Percentage of three sets of Invasion and Control Chambers ± SEM and are presented as LKB1 knockdown compared to control. Independent t-test significance (*) was $p < 0.05$.

The ability of shLKB1 cells to grow tumours was analyzed by subcutaneously injecting $2x10^6$ shLKB1 or shCONTROL cells into 10 BALB/c Nu/Nu mice. The 10 mice injected with shLKB1 cells generated a greater tumour volume than the majority of mice injected with shCONTROL cells (**Figure 23A**). Mean tumour volume of shLKB1 xenografts was significantly greater than shCONTROL xenografts for all time points examined (1, 2, 3, 4, 5, 6 and 7 weeks) and at study completion, the mean tumour volume of shLKB1 xenografts was 270.1 mm^3 compared to shCONTROL xenograft 52.2 mm^3 (**Figure 23B**). The mean tumour weight of shLKB1 xenografts (weight: 0.297 g) was significantly greater than shCONTROL xenografts (weight: 0.077 g) (**Figure 23C**), while the mean body weight of shLKB1 mice (weight: 23.6 g) was similar to that of shCONTROL mice (weight: 23. 3g) (**Figure 23D**).

A

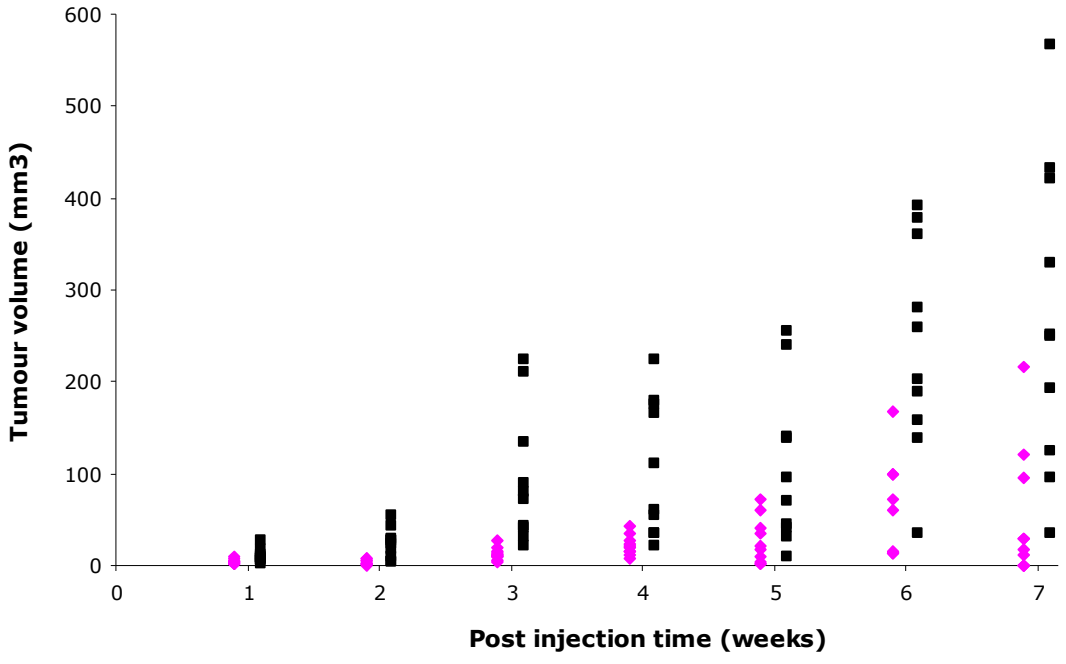

B

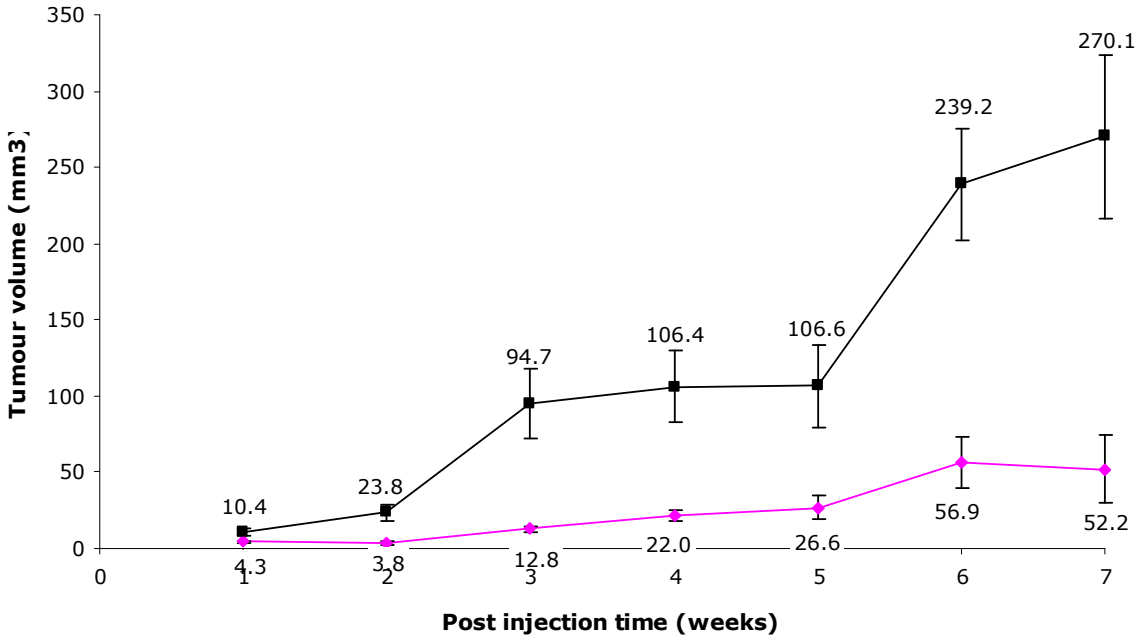
Tumour volume (mm3)
350
300
250
200
150
100
50
0
0
1
2
3
4
5
6
7
Post injection time (weeks)
10.4
23.8
94.7
106.4
106.6
239.2
270.1
4.3
3.8
12.8
22.0
26.6
56.9
52.2

C

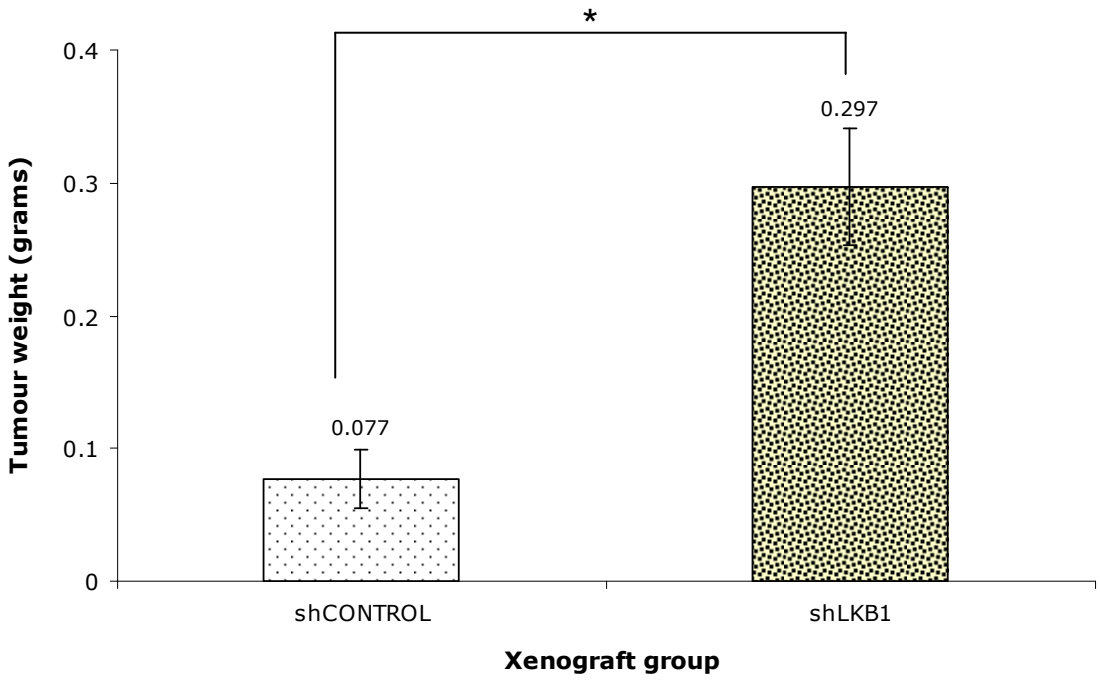
*
Tumour weight (grams)
0.4
0.3
0.2
0.1
0
0.297
0.077
shCONTROL
shLKB1
Xenograft group

D

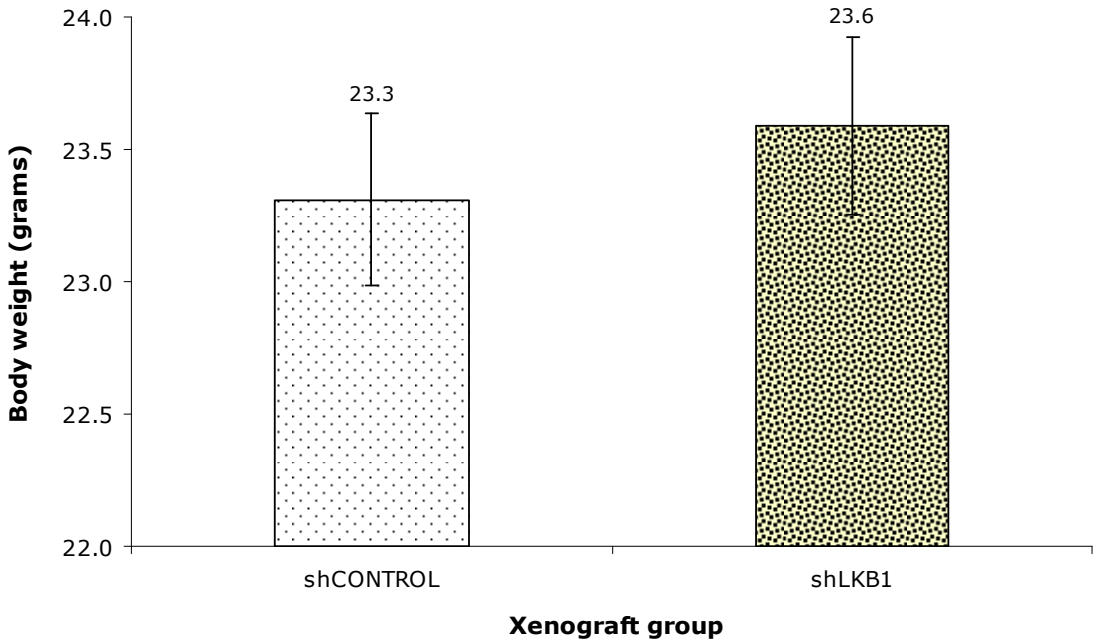

Figure 23 | LKB1 knockdown increases xenograft size and proliferation. (**A**) A total of $2x10^6$ shCONTROL (◇) or shLKB1 (□) cells were subcutaneously injected into 10 BALB/c Nu/Nu male mice and measured once a week to calculate tumour volume [0.5(length*width*height)]. Data represent the tumour volume of each nude mouse. (**B**) Data represent the mean tumour volume of 10 mice ± SEM. (**C**) Tumours were excised from shCONTROL and shLKB1 mice seven weeks post injection and weighed. Data represent the mean tumour weight for 10 mice ± SEM and independent t-test significance (*) was $p < 0.05$. (**D**) The shCONTROL and shLKB1 mice were weighed immediately prior to sacrifice. Data represent the mean body weight for 10 mice ± SEM.

Three mice from each xenograft group with tumour volumes closest to the mean (shCONTROL mice: 203, 205 and 206) (shLKB1 mice: 211, 215 and 216) (**Figure 24A**) were selected as a representative set to display tumour size, LKB1 immunohistochemical staining and hematoxylin and eosin (H&E) staining. The greater tumour volume of shLKB1 xenografts over shCONTROL xenografts, quantified in **Figure 23C**, was evident through the skin of the nude mice, and clear once excised (**Figure 24B**). Staining for LKB1 in histological sections of all xenografts confirmed that LKB1 knockdown remained stable in shLKB1 xenografts throughout the seven week study (**Figure 24D**), and corresponded with an active tissue pathology compared to the apparent regions of dead cells or regions devoid of cells in shCONTROL xenografts (**Figure 24C**).

A

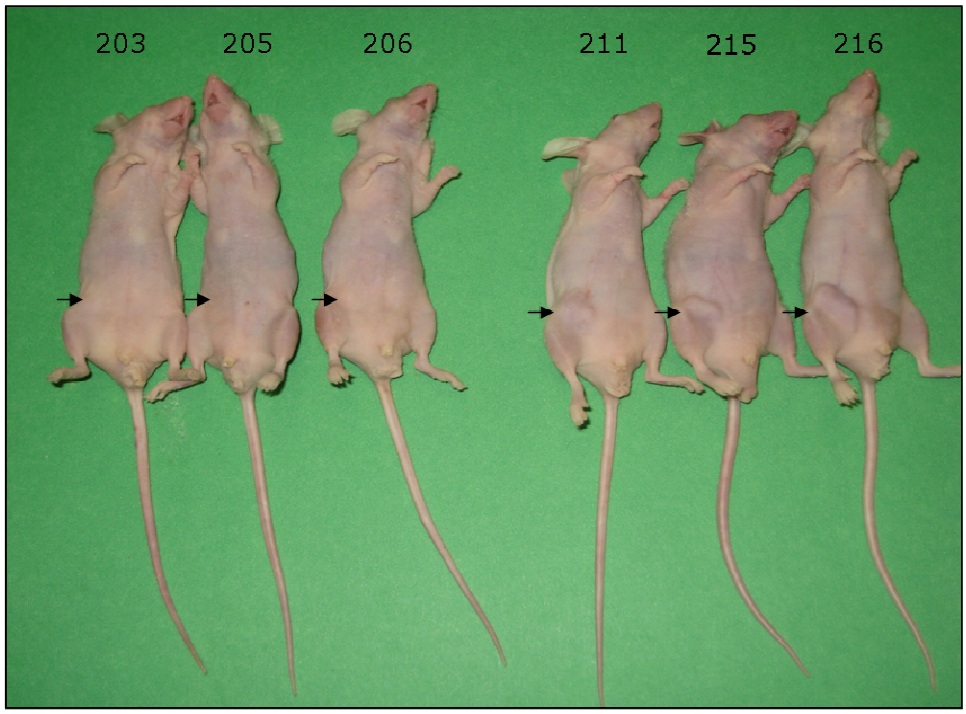

B


shCONTROL
shLKB1
203
205
206
211
215
216

C

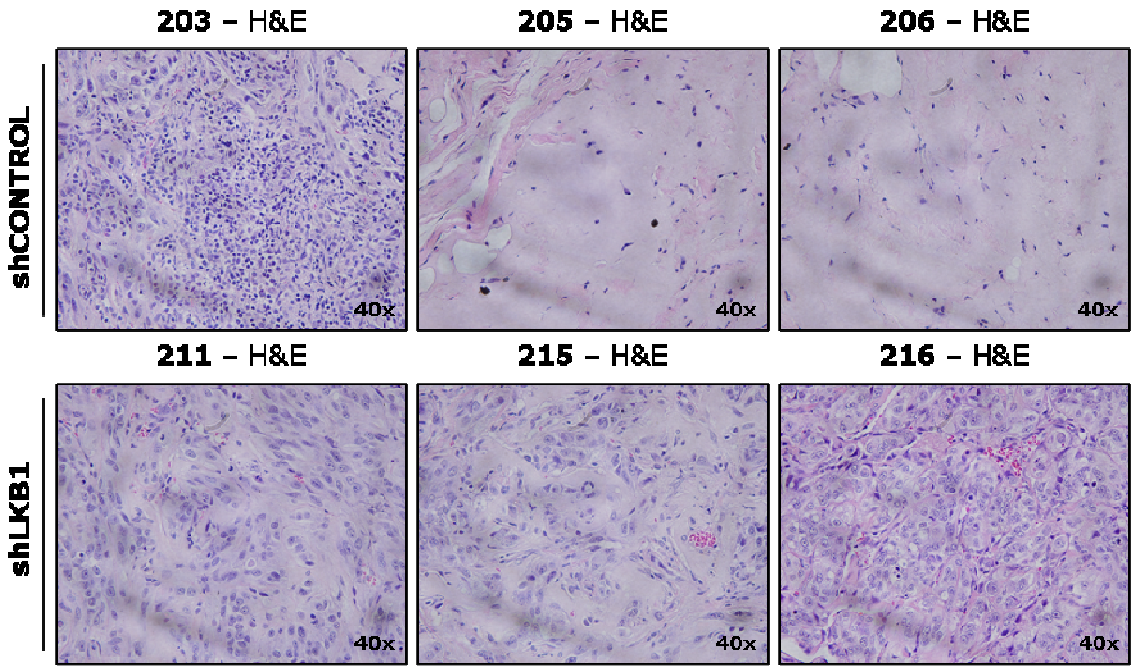
203 – H&E
205 – H&E
206 – H&E
shCONTROL
211 – H&E
215 – H&E
216 – H&E
shLKB1
40x

D

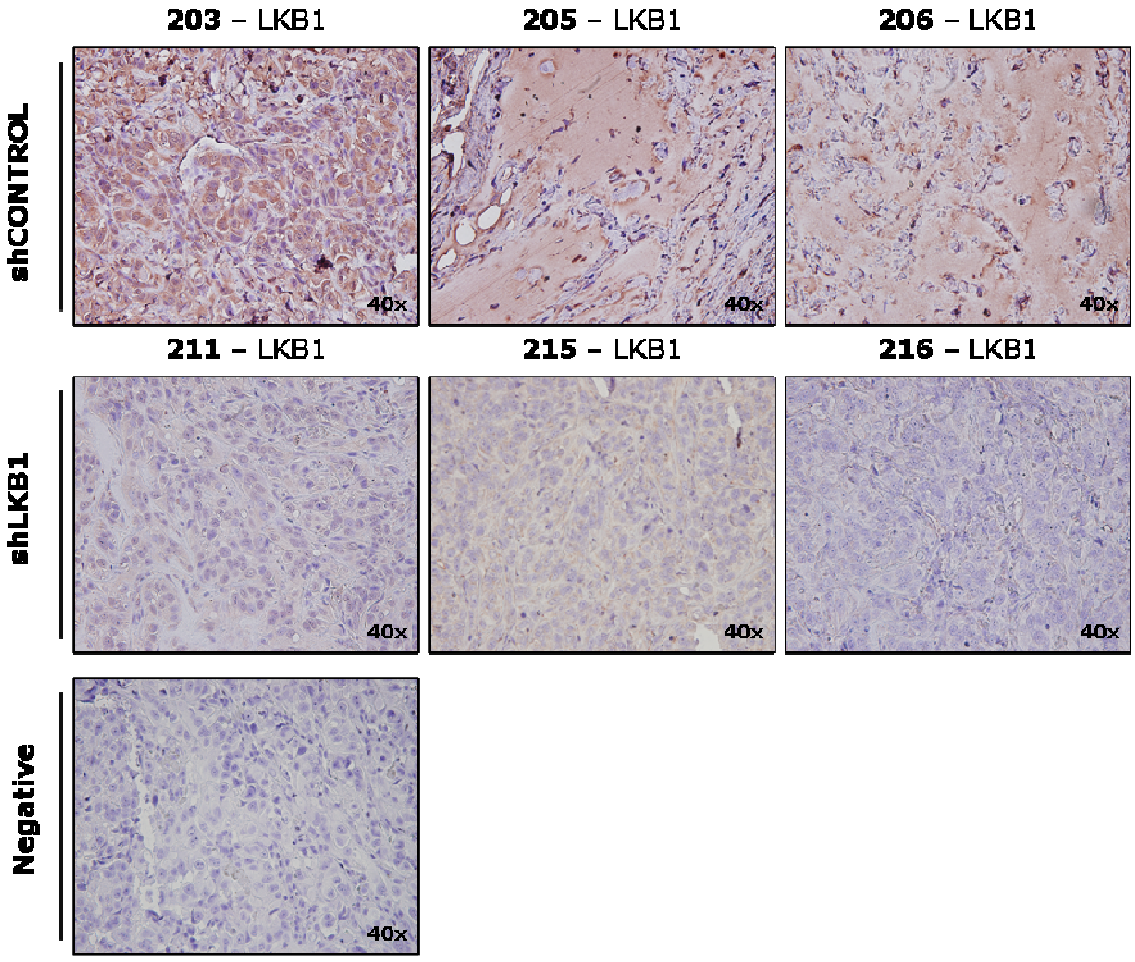

Figure 24 | **shLKB1 xenografts retain LKB1 knockdown**. (**A**) 20 BALB/c Nu/Nu male mice were subcutaneously injected with $2x10^6$ shCONTROL or shLKB1 cells. Three representative shCONTROL (mouse number: 203, 205 and 206) and shLKB1 (mouse number: 211, 215 and 216) mice are shown with xenograft, seven weeks post injection (→) (**B**) Xenografts were excised, fixed in formalin, embedded in a paraffin block, sectioned to a thickness of 4μm, stained with (**C**) hematoxylin and eosin (H&E) and (**D**) LKB1 by immunohistochemistry and imaged with a 40x objective. Negative control was mouse xenograft stained with only secondary antibody.

The mean levels of VEGF in serum from shLKB1 and shCONTROL xenograft injected mice were 59.7 pg/mL and 71.5 pg/mL respectively, however were not significantly different (**Figure 25A**). Mean serum adiponectin level in shLKB1 xenograft mice was 9.1 µg/mL compared to 11.1 µg/mL in shCONTROL mice, however, was not significant (**Figure 25C**). The association between tumor weight and serum levels of VEGF (**Figure 25B**) or adiponectin (**Figure 25D**) were examined, however no significant relationship was observed.

A

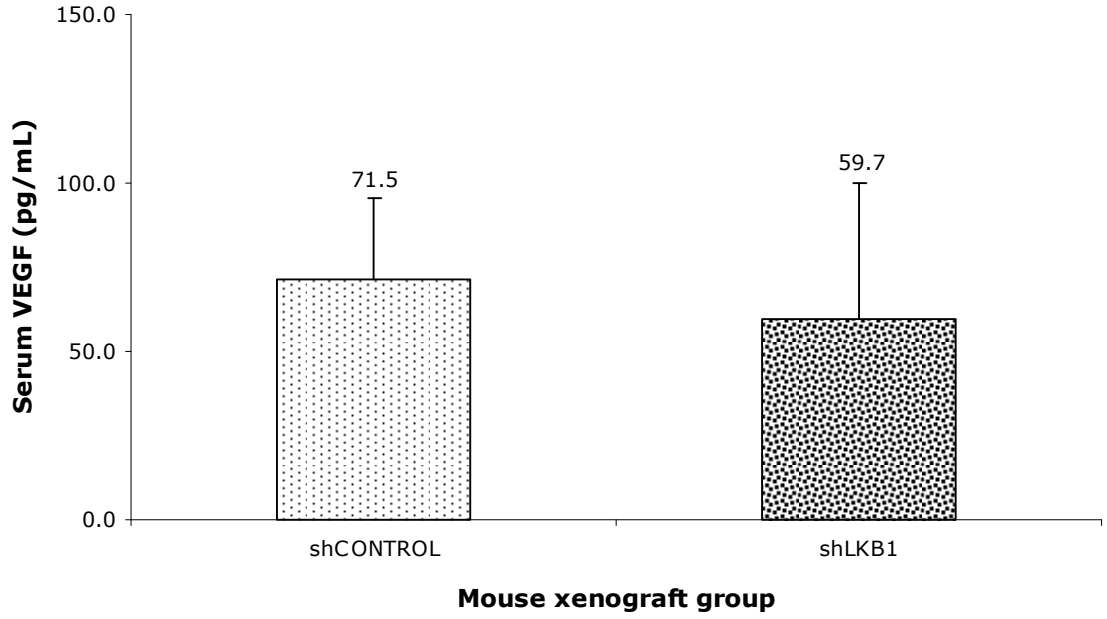

B

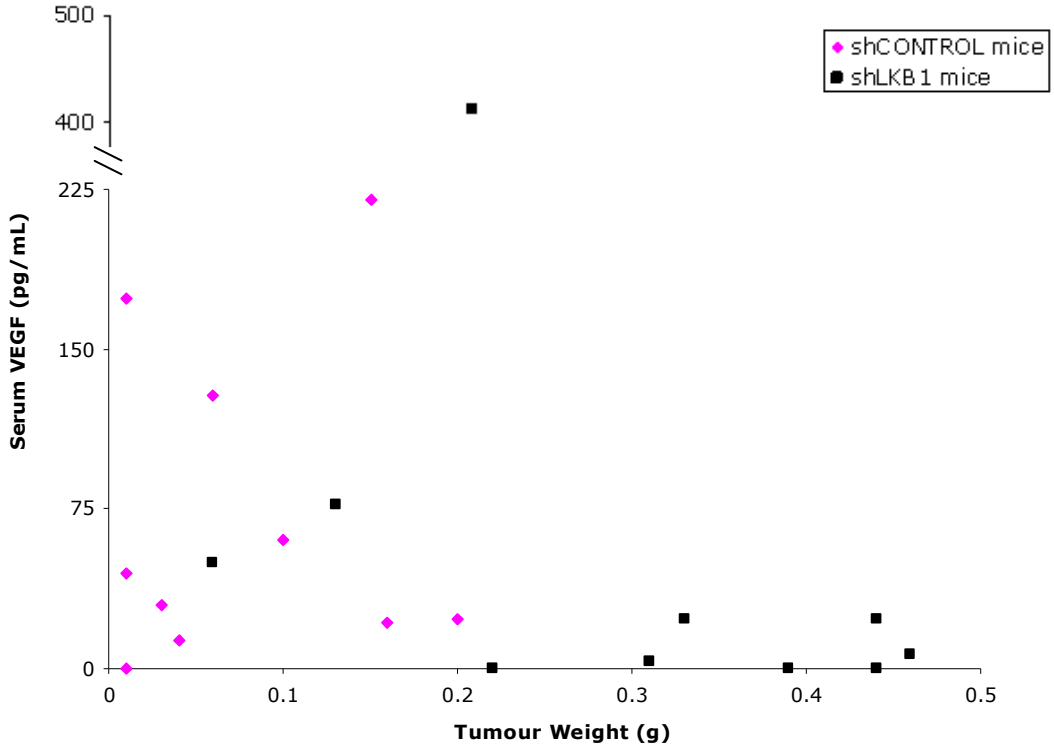
500
400
225
150
75
0
Serum VEGF (pg/mL)
0
0.1
0.2
0.3
0.4
0.5
Tumour Weight (g)
shCONTROL mice
shLKB1 mice

C

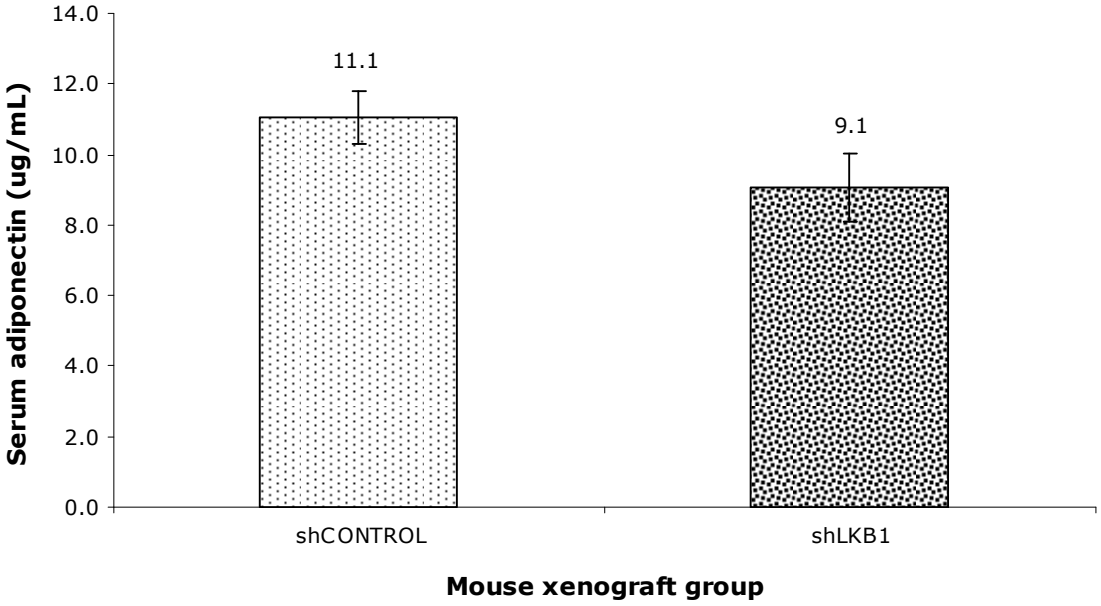
14.0
12.0
10.0
8.0
6.0
4.0
2.0
0.0
Serum adiponectin (ug/mL)
11.1
9.1
shCONTROL
shLKB1
Mouse xenograft group

D

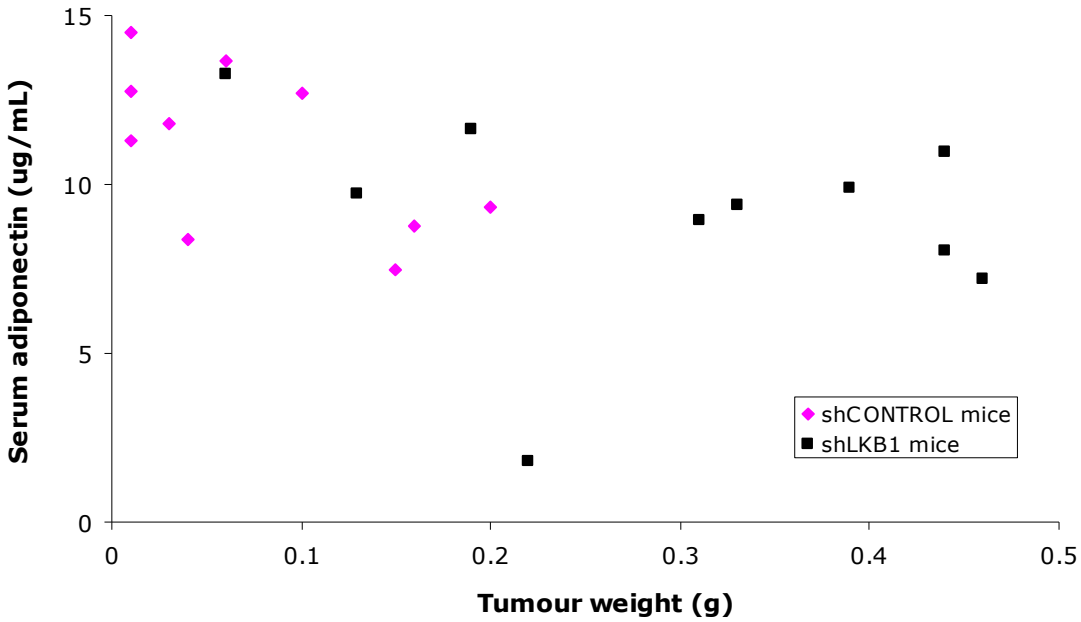

Figure 25 | LKB1 knockdown did not significantly affect serum VEGF and adiponectin levels. Serum from 20 BALB/c Nu/Nu male mice subcutaneously injected with $2x10^6$ shCONTROL (n=10) or shLKB1 (n=10) cells was collected seven weeks post injection, incubated at 4°C overnight to clot, centrifuged to isolate serum and measured for mouse (**A**) VEGF and (**C**) adiponectin using ELISAs. Data represent the mean serum concentration from 10 mice measured in triplicate ± SEM and are presented as shLKB1 compared to shCONTROL. (**B**) Relationship of individual shCONTROL (◇) and shLKB1 (□) mouse tumour weight to serum VEGF concentration and (**D**) tumour weight to serum adiponectin concentration was explored.

FUTURE DIRECTIONS

The preliminary examination of a novel AdipoR1 to LKB1 signalling pathway, through the hypothesized AdipoR1-CK2β-CDC37-Hsp90-LKB1 signalling cascade, was examined in CRL-1932 cells treated with increasing doses of adiponectin (**Figure 26A**). Activation of pathway members CDC37 (p-CDC37) and CK2β (p-CK2β) was determined as an increase in phosphorylation status above untreated. Dose-dependent activation of p-CDC37 was demonstrated with all treatment doses of adiponectin excluding 90ng/mL (**Figure 26B**), while increased p-CK2β expression was observed at every dose of adiponectin (**Figure 26C**). In addition, an increase in LKB1 protein expression was observed with increasing adiponectin treatment doses.

A

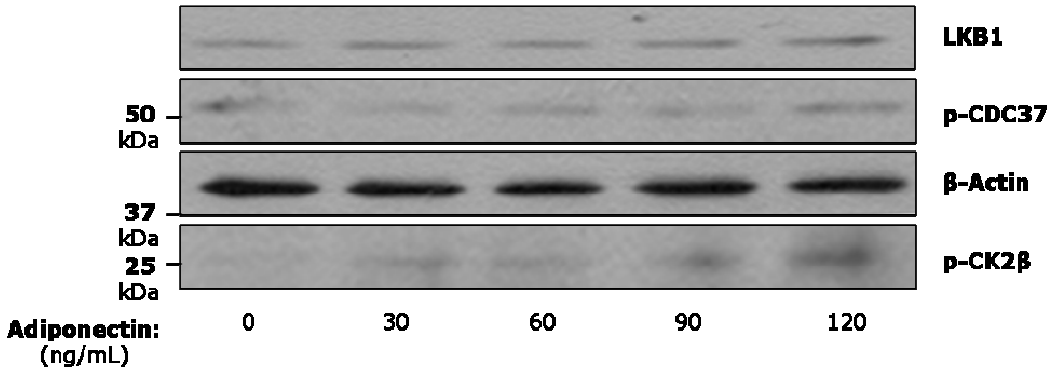

B

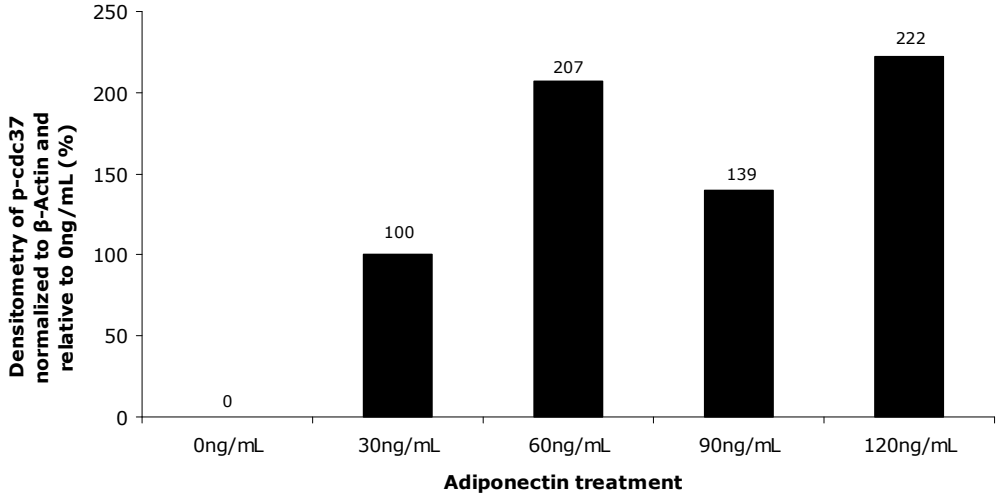

C

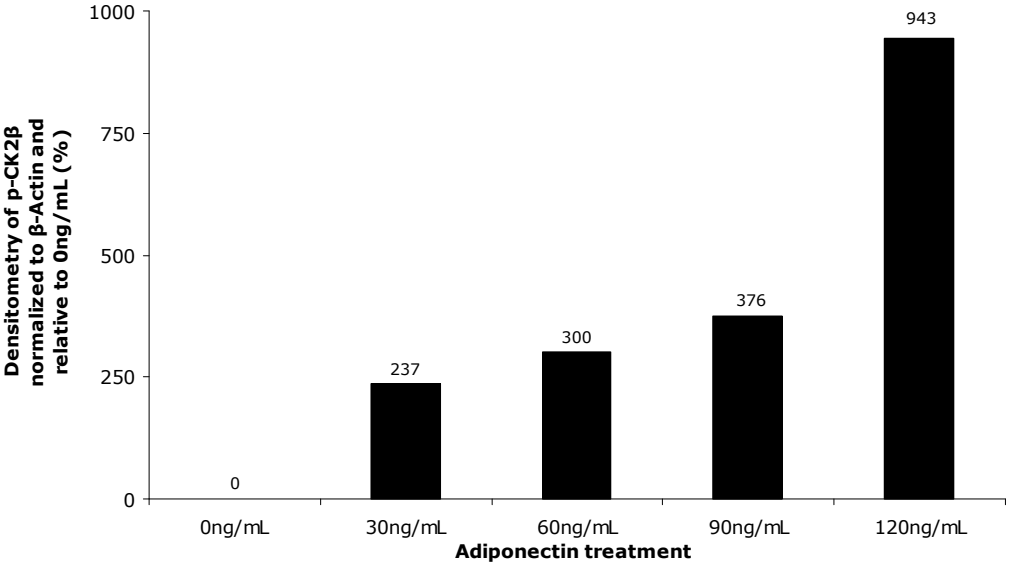

Figure 26 | **Adiponectin treatment stimulates activation of CK2β and CDC37**. (**A**) CRL-1932 cells were either untreated (0 ng/mL) or treated (30 ng/mL, 60 ng/mL, 90 ng/mL and 120 ng/mL) with adiponectin for 1 hour before total protein was extracted from the cells. Lysates (40 µg) were separated by SDS-PAGE and analyzed by Western blotting for LKB1, activated CDC37ser13 (p-CDC37), activated CK2βser209 (p-CK2β) and β-Actin. The intensity of the bands was quantified by densitometry and the (**B**) p-CDC37 and (**C**) p-CK2β values were normalized to endogenous β-Actin values. Data represent the densitometric quantification and are presented as the treatments relative to the untreated, which was set to 0%.

To further validate that adiponectin signals through the proposed AdipoR1-CK2β-CDC37-Hsp90-LKB1 pathway, CRL-1932 cells were treated with adiponectin to activate pathway members, and with or without the TBB inhibitor of CK2 activation. Then, cells were examined for p-CDC37 and p-AMPKα levels (**Figure 27A**). Expectedly, activated AMPKα (**Figure 27B**) and CDC37 (**Figure 27D**) expression levels reduced in a dose-responsive manner with escalating treatment doses of TBB. Similarly, LKB1 protein expression levels reduced in a dose responsive manner (**Figure 27C**).

A

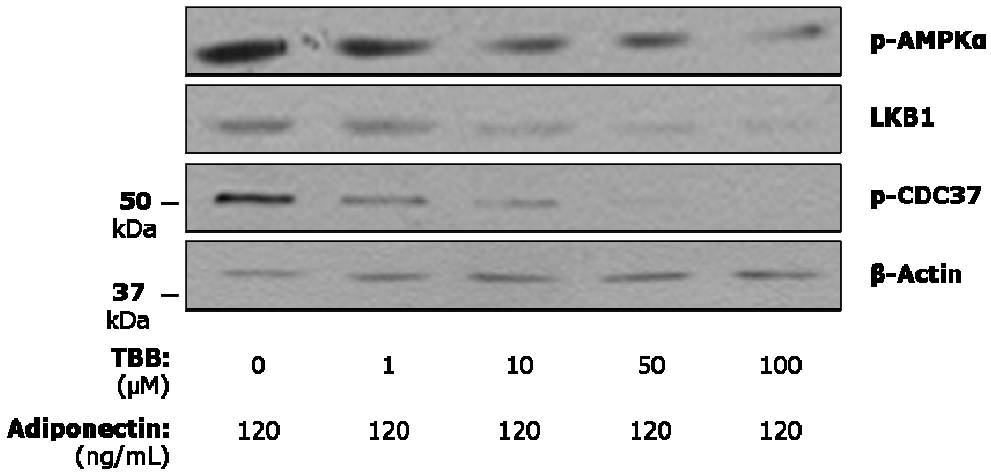

B

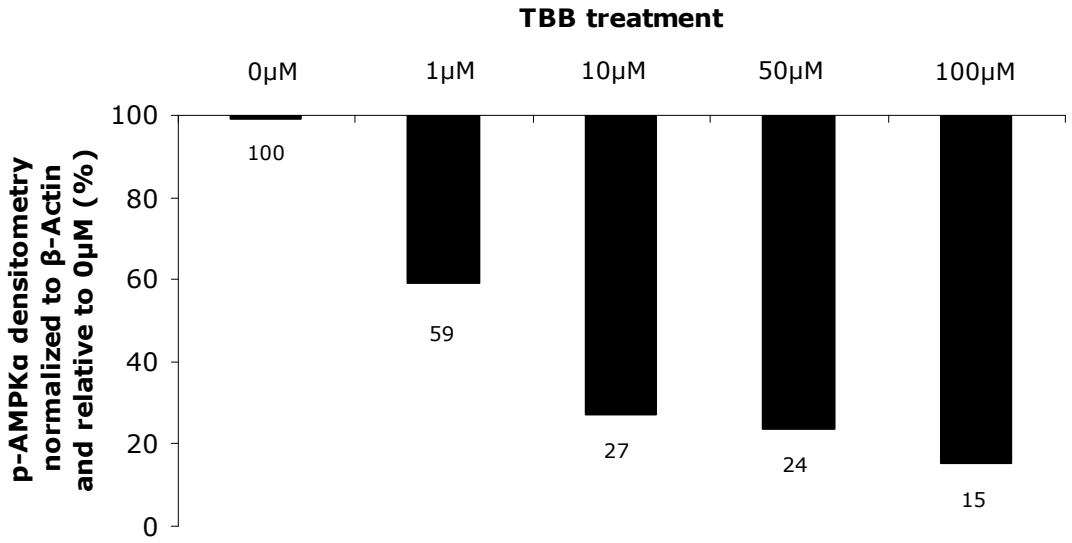
TBB treatment
0μM
1μM
10μM
50μM
100μM
p-AMPKα densitometry normalized to β-Actin and relative to 0μM (%)
100
80
60
40
20
0
100
59
27
24
15

C

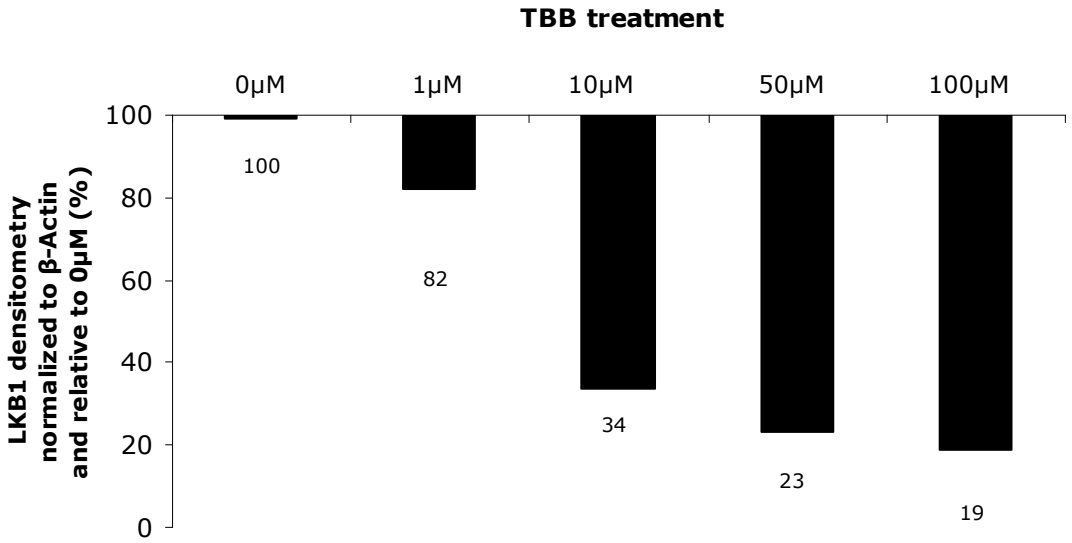
TBB treatment
0μM
1μM
10μM
50μM
100μM
LKB1 densitometry normalized to β-Actin and relative to 0μM (%)
100
80
60
40
20
0
100
82
34
23
19

D

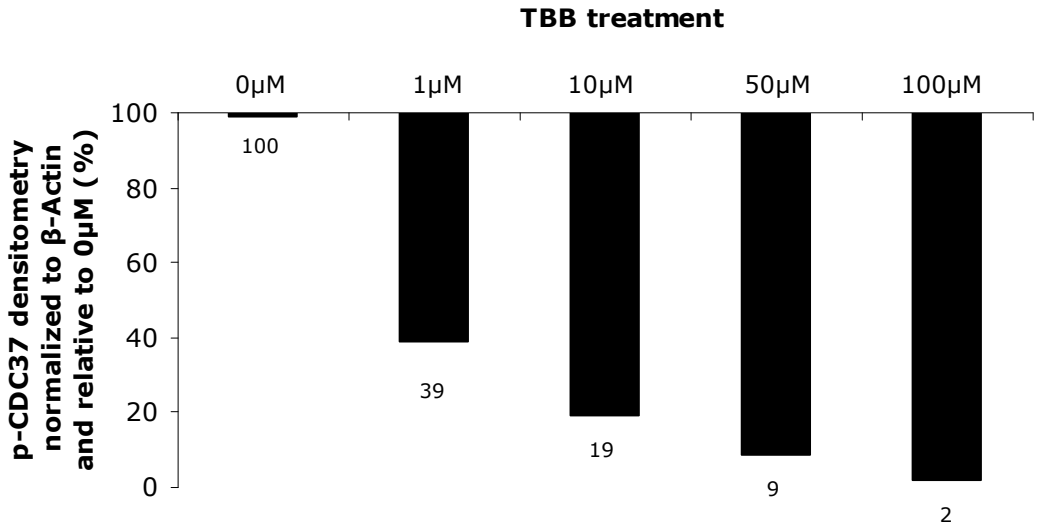

Figure 27 | **CK2 inhibition reduces adiponectin-mediated activation of AMPKα, CDC37 and LKB1 protein expression**. (**A**) CRL-1932 cells were treated with adiponectin (120 ng/mL) for 1 hour before cells were untreated (0 μM) or treated (1 μM, 10 μM, 50 μM and 100 μM) with the TBB inhibitor of CK2 activation for 1 hour. Total protein was extracted from the cells, lysates (40 μg) were separated by SDS-PAGE and analyzed by Western blotting for activated AMPKαthr172 (p-AMPKα), LKB1, activated CDC37ser13 (p-CDC37) and β-Actin. The intensity of the bands was quantified by densitometry and the (**B**) p-AMPKα (**C**) LKB1 and (**D**) p-CDC37 values were normalized to endogenous β-Actin values. Data represent the densitometric quantification and are presented as the treatments relative to the untreated, which was set to 100%.

DISCUSSION

This study on RCC had many benefits, which included that the quantification of mRNA and protein levels was performed on the same sample of patient tissue, and that each pair of tumour and normal tissues was obtained from the same patient's kidney. The matched nature of the RCC tumour and normal tissue samples did not necessitate statistical adjustment to control for differences in age, BMI and other potentially confounding factors, which is required in studies comparing independent populations of RCC patients and patients with normal kidney function. Therefore, we were able to directly compare transcript levels of *AdipoR1, LKB1* and *VEGFA* in the 10 patients' RCC tumours to the transcript level in the matched normal surrounding parenchyma tissue.

AdipoR1 transcript levels were largely induced in all 10 patients examined, with a mean relative fold induction of 5,683% compared to 100% in normal tissue (**Figure 1**). In the same manner, a study by Williams *et al.* (2008) demonstrated an induction of *AdipoR1* mRNA in patient colon tumour tissue when compared to the matched normal tissue. However, in contrast to the induction of *AdipoR1* in RCC and colon tumours, *AdipoR1* transcript levels were reduced by approximately 50% in the gastric tumour tissue of 67 patients, compared to the normal matched tissue (Otani *et al.*, 2010). This contrast supports the findings from the Pinthus *et al.* (2008) study, which demonstrated a

reduction in AdipoR1 protein expression in RCC tumours compared to the matched normal tissue. Indeed, our examination of AdipoR1 protein expression in both a preliminary trial with six RCC patients (**Figure 5A**) and in the 10 RCC patients examined for *AdipoR1* transcript levels (**Figure 6A**), revealed a significant reduction of AdipoR1 protein expression in 6/6 and 8/10 RCC tumours. Specifically, densitometric quantification of AdipoR1 determined a mean expression of 2% (**Figure 5B**) and 69% (**Figure 6B**) in the RCC tissue compared to 100% expression in the matched normal tissues. Furthermore, immunohistochemical staining of AdipoR1 in histological sections of RCC patients tissues revealed a slight reduction in AdipoR1 staining in RCC tumour tissue, particularly of Patient 4, when compared to staining in the matched normal tissue (**Figure 8**). A similar study by Chou *et al.* (2010) on nine matched RCC tumour and normal tissue sets also concluded extremely minor reductions in the immunohistochemical staining of AdipoR1. Nonetheless, despite only minor reduction of AdipoR1 immunohistochemical staining in RCC tumour tissues, the reduction of AdipoR1 protein expression in RCC is puzzling given the reciprocal relationship often observed between serum levels of a ligand and tissue expression of its receptors. Accordingly, it is expected that the reduced serum level of adiponectin in RCC, observed by Spyridopoulos *et al.* (2007) and Horiguchi *et al.* (2008), would promote an upregulation of AdipoR1 protein expression. But this was not observed in our study or in others. Yet again, despite levels of adiponectin being reduced in RCC patients, adiponectin does continue to exist in the circulation, and downregulation of AdipoR1 protein expression may be an ideal strategy for RCC cells to escape the tumour-

suppressive effects of adiponectin. An alternative explanation to the decreased AdipoR1 protein expression level, and paradoxical increased *AdipoR1* transcript level, comes from observations made on dystrophin. Mutations to the dystrophin gene, which cause Duchenne muscular dystrophy and Becker muscular dystrophy, result in a truncated non-functional protein that is degraded (Koenig *et al.*, 1989). In an attempt to compensate for this reduction in protein, transcription of the mutated dystrophin gene is enhanced, however, the mutated dystrophin protein cannot overcome the loss of function caused by the mutation, and protein levels do not rise (Koenig *et al.*, 1989). Thus, it is reasonable to suggest that in RCC the AdipoR1 protein is disrupted and attempts to restore AdipoR1 protein expression by increasing transcription are not effective.

Although mutations to the AdipoR1 gene in cancer have not yet been identified, the reduction of LKB1 protein levels that have been documented in a variety of cancers result from somatic mutations and epigenetic silencing of LKB1. Specifically, the Sanchez-Cespedes *et al.* (2002) study identified 6/20 primary lung tumours to harbour somatic mutations in LKB1, resulting in gene inactivation. As well, a study by Morton *et al.* (2010) identified a biallelic loss of LKB1 due to somatic mutations in 8/27 primary lung and a downregulation of LKB1 protein expression in the remaining 19/27 lung adenocarcinomas due to epigenetic silencing of the LKB1 promoter. A similar conclusion on the downregulation of LKB1 expression due to epigenetic silencing in tumours was presented by Shorning *et al.* (2011), after the frequency of LKB1 downregulation in

endometrial tumours, on a tissue microarray, was significantly greater than could be explained by the frequency of sporadic somatic mutation. Certainly, a more detailed analysis on the promoter region of LKB1 is required to determine the occurrence and frequency of epigenetic silencing of LKB1 in RCC. Further analysis is also required on the potential of the various mutations and epigenetic silencing events to affect the development and/or progression of many different types of cancers, from lung to endometrial to RCC, given the plethora of pathways that LKB1 regulates.

Although the cause of the downregulation of LKB1 in RCC is not known, it is quite evident that the level of LKB1 expression is drastically reduced in RCC. *LKB1* transcript levels were significantly reduced in all 10 RCC tumours, to a mean expression level of 24% (**Figure 3**). As well, LKB1 protein expression was reduced in 8/10 patients to a mean expression of 37% (**Figure 6C**). Furthermore, the immunohistochemical staining of LKB1 in patients' RCC tumour tissue was practically obliterated when compared to the substantial staining of LKB1, predominantly in the tubules, in the matched normal tissue (**Figure 9**). Similar to this reduction of LKB1 immunohistochemical staining in RCC tumour tissue, studies by Conde *et al.* (2007) and Amin *et al.* (2008) confirmed a reduction of LKB1 staining in 80% and 84%, respectively, of patient lung tumours examined. Quantification of the immunohistochemical staining of LKB1 on two tissue microarrays containing 201 patients' RCC tumours, confirmed a significant reduction of LKB1 protein expression in RCC tissue compared to normal patient kidney tissue

(**Figure 10C**). The clinical significance and statistical power of increasing our study population from 15 RCC patients (10 examined for LKB1 transcript and protein levels and 5 examined for LKB1 immunohistochemical staining) to 201 RCC patients was enormous, and confirmed that the downregulation of LKB1 was a statistically significant event in RCC. Interestingly, a study by Kline *et al.* (2010) confirmed a reduction in the cytoplasmic, but not nuclear, fraction of LKB1 in head and neck squamous cell carcinomas compared to normal tissue. This reduction in cytoplasmic, but not nuclear, LKB1 levels is significant, considering Tiainen *et al.* (2002) demonstrated that the active form of LKB1 is present in the cytoplasm, while the non-active form resides in the nucleus. Thus, quantification of the cytoplasmic and nuclear level of LKB1 in our RCC patient tumours would confirm that the reduction of LKB1 levels in RCC tumours is a reduction of the active form of LKB1, and thus is biologically relevant. Indeed, observation of the immunohistochemical staining of LKB1 revealed a reduction in the cytoplasmic fraction of LKB1 in RCC tumour tissue in 4/5 patients, suggesting that the measured reductions of LKB1 are relevant in cancer (**Figure 9**).

Although the vast majority of the study's patients presented a reduction in LKB1, one patient, Patient 68, expressed both an 18% greater protein expression level of LKB1 (**Figure 6C**) and 27% greater protein expression level of AdipoR1 (**Figure 6B**) compared to the matched normal tissue. This suggests that the downregulation of AdipoR1 and LKB1 in RCC is not the only factor, and other events may contribute to the

development of RCC. Indeed, mutations to the *VHL*, *MET*, *FLCN*, *TSC1*, *TSC2*, *FH* and *SDH* genes are known to disrupt metabolic signalling pathways and promote the development of kidney cancer (Linehan *et al.*, 2010). Taken together, it is unreasonable to assume that the development of all RCCs depends exclusively on the downregulation of AdipoR1 and LKB1 expression. However, with the tremendous potential to activate numerous signalling pathways related to cancer development and progression by disrupting the tumour suppressor LKB1, along with the significant reduction of AdipoR1 and LKB1 expression in RCC tumours, it is likely that AdipoR1 and LKB1 are important and understated factors in the development and/or progression of RCC.

The primary downstream substrate of LKB1 is AMPK, which, when activated by stimuli including adiponectin, exerts several cellular functions that are known to restrain both tumour formation and progression through the inhibition of mTOR (Mirouse *et al.*, 2011). Disruption to this AMPK-mediated pathway results in the constitutive activation of mTOR, an event established in RCC, which drives tumourigenesis through a variety of signalling pathways. One pathway stabilizes the α-subunit of the **h**ypoxia **i**nducible **f**actor-**1** (HIF-1α), which leads to an increase in *VEGF* transcription and ultimately promotes angiogenesis (Shackelford *et al.*, 2009). Consistent with these hallmarks of RCC, the *VEGF* transcript level in all 10 RCC patient tumours was upregulated to a mean induction of 65,097% compared to 100% in the matched normal tissue (**Figure 4**). This overexpression of *VEGF* was confirmed by previous studies on RCC tumours (Pinthus *et*

al., 2008) as well as on lung tumours (Amin *et al.*, 2008), and ultimately provided an indispensable marker to distinguish patient tumour tissue from normal tissue in this study. The distinction of RCC tumour and normal kidney tissues was also aided by the examination of **c**arbonic **a**nhydrase **IX** (CAIX), a protein constitutively induced in RCC tumour tissue (Bui *et al.*, 2003). Indeed, CAIX expression was apparent in 8/10 patient RCC tumours and absent in all 10 patients' matched normal tissue (**Figure 7**). Thus, increased *VEGF* and CAIX levels in RCC tumours confirmed the discrimination between tumour and normal tissues as well as verified that the downregulation of AdipoR1 and LKB1 was specifically in RCC tumour tissue. Attempts to correlate the level of AdipoR1 expression in tumour tissue by Chou *et al.* (2010) and Takahata *et al.* (2007) to determine the pathophysiological significance of AdipoR1 protein expression on tumour size, histological grade and treatment outcome in a cohort of RCC and breast cancer patients, were not significant. These failed correlation attempts were likely attributed to the limited number of patients in the studies and the high variability in patient background associated with random selection. Future studies on RCC with a greater patient enrolment may significantly conclude a relationship between AdipoR1 and LKB1 expression levels, and clinical and pathological features.

The reduction of LKB1 in RCC also impacts the activity of AMPK in RCC. Surely, the inactivation of AMPK is in the interest of RCC cells, considering AMPK functions to restore the cellular AMP:ATP ratio by reducing energy consuming processes that the cells depend on (Vaahtomeri *et al.*, 2011). Indeed, numerous studies have shown the

downregulation of AMPK activity in a variety of cancers, through examining the levels of p-ACC at the serine 79 residue (Viollet *et al.*, 2010). The quantity of p-ACC relates to the degree of AMPK functionality for the reason that ACC catalyzes the carboxylation of acetyl CoA to malonyl CoA, for fatty acid synthesis, which is inhibited by activated AMPK through the phosphorylation of ACC on its serine 79 residue (Mao *et al.*, 2006). Thus, in order to infer the activity of AMPK in RCC, the patients' tumour and normal tissues were immunohistochemically stained with p-ACC. Unfortunately, inconsistent and non-specific staining was observed in the tumour and normal tissues, and thus no accurate conclusion on the activity of AMPK in RCC was achieved (**Figure 11**). However, immunohistochemical staining with a different p-ACC antibody in a study by Conde *et al.* (2007), revealed staining in all normal lung tissue samples and a reduction of p-ACC staining in 69% of the lung tumours examined. Thus, repeating the immunohistochemical staining of p-ACC on our RCC tumour and normal tissues with the antibody utilized by Conde *et al.* (2007) is warranted to confirm that the activity of AMPK is reduced in RCC.

Given the effectiveness of AMPK activators on inhibiting the proliferation of RCC cells, AMPK activity is likely reduced in this study's patients' RCC tissue. Specifically, one AMPK activator, 5-**a**mino**i**midazole-4-**c**arbox**a**mide **r**ibonucleotide (AICAR), that functions to mimic cellular AMP and activate AMPK has been demonstrated to induce apoptosis and inhibit proliferation of RCC cells (Woodard *et al.*, 2010). Interestingly, AICAR does not activate any of the other members of the AMPK family of kinases (Alessi *et al.*, 2006), suggesting specifically AMPK has a role in preventing RCC

tumourigenesis. Another AMPK activator, the anti-diabetic drug metformin, has been demonstrated to reduce the risk of developing cancer (Sahra *et al.*, 2010), and has been shown to reduce the proliferation of RCC cells by activating the AMPK-mediated inhibition of mTOR (Woodard *et al.*, 2010).

The human CRL-1932 RCC cell line utilized in the above mentioned studies on AMPK activation was also used in our study. In fact, the CRL-1932 cell line is one of the most common *in vitro* cell lines utilized in the research of human RCC. CRL-1932 cells were isolated from the renal cell adenocarcinoma of a 58-year old male and are known to possess a hyperactivation of mTOR (Robb *et al.* 2007). Indeed, the level of phosphorylated mTOR in CRL-1932 cells was apparent, compared to the level of p-mTOR following adiponectin treatment (**Figure 13A**), which was reduced by the adiponectin-induced AMPK-mediated inhibition of mTOR. Interestingly, AdipoR1 and LKB1 protein levels were detected in CRL-1932 cells, which would seemingly contrast our observations in RCC tumours. An explanation for this could actually come from our examination of AdipoR1 and LKB1 protein expression levels in the RCC patient tumours. Indeed, AdipoR1 and LKB1 protein was detected in all RCC tumour tissues, but the detection was to a significantly reduced level when compared to the level in the matched normal tissue. Thus, without a reference to the protein expression level of AdipoR1 and LKB1 in the normal tissue section of the kidney from which the CRL-1932 cell line was isolated, it cannot be concluded that AdipoR1 and LKB1 protein expression is not reduced in CRL-1932 cells.

In order to undeniably recapitulate our observations that AdipoR1 and LKB1 protein expression levels are reduced in RCC, viral-mediated knockdown of AdipoR1 and LKB1 was performed in CRL-1932 cells. The retroviral-mediated knockdown of AdipoR1 reduced protein expression to 60% in shVAdipoR1 cells compared to 100% in the shVControl control cell line (**Figure 14B**). As well, the lentiviral particle-mediated knockdown of LKB1 in shLKB1 cells reduced protein expression to 53%, relative to 100% in the shCONTROL control cell line (**Figure 15B**). As expected, the *AdipoR1* transcript level in shVAdipoR1 cells was reduced to 78% compared to shVControl (**Figure 16A**), and the *LKB1* transcript level in shLKB1 cells was reduced to 45% relative to shCONTROL (**Figure 16B**). Surprisingly, however, the *LKB1* transcript level in shVAdipoR1 cells was also reduced to 88% (**Figure 16A**), as was the *AdipoR1* transcript level in shLKB1 cells to 78% (**Figure 16B**). Taken together, the indirect knockdown of LKB1 and AdipoR1, respectively, suggests that the regulation of AdipoR1 and LKB1 expression is linked in RCC. Yet, bearing in mind that the *AdipoR1* transcript level in RCC tumours did not relate to the AdipoR1 protein expression, reduction of *LKB1* and *AdipoR1* in shVAdipoR1 and shLKB1 cells, respectively, was confirmed at the protein level. Similar to the discrepancy between *AdipoR1* transcript and protein levels in RCC patient tumours, the 88% reduction in *LKB1* transcript level in shVAdipoR1 cells did not translate into a reduction in LKB1 protein expression, when compared to shVControl cells (**Figure 17B**). On the other hand, the reduced *AdipoR1* transcript level in shLKB1 cells related to a 45% AdipoR1 protein expression level, relative to 100% in

shCONTROL cells (**Figure 17D**). Although the mechanism by which LKB1 may reduce the expression level of AdipoR1 is not known, it may be of great clinical significance given that RCC tumours present a downregulation of both AdipoR1 and LKB1 protein expression.

Given that the shLKB1 cell line presented a reduction in both AdipoR1 and LKB1 protein expression, similar to the majority of the study's RCC patient tumours, the cell line was selected to investigate the effect of AdipoR1 and LKB1 knockdown on the adiponectin-AMPK signalling pathway as well as on the tumourigenic potential of RCC cells. Reduction of AdipoR1 and LKB1 in shLKB1 cells significantly impaired the cell's ability to phosphorylate and activate AMPKα in response to adiponectin (**Figure 18**). As well, AMPK activity, inferred through the levels of p-ACC, was significantly reduced in shLKB1 cells compared to shCONTROL. These results confirmed the dependence of AMPK on LKB1, and not on the alternative upstream kinases CaMKKβ and TAK1, to phosphorylate its threonine 172 residue in response to adiponectin treatment and enable the phosphorylation of ACC and inhibition of mTOR, inferred through a reduction in VEGF secretion. Indeed, treatment of shLKB1 cells with increasing doses of adiponectin did not affect VEGF secretion levels, in contrast to the shCONTROL cells, which presented a dose-dependent reduction in VEGF secretion (**Figure 19B**). This lack of ability to inhibit VEGF secretion closely resembles the increased *VEGFA* transcript level in RCC patient tumours and justifies the highly angiogenic property of RCC tumours.

The effect of AdipoR1 and LKB1 knockdown on the tumourigenic potential of RCC was assessed by traditional proliferation, invasion, tumour growth assays. Briefly, the number of shLKB1 cells in the growth assay was significantly greater than the number of shCONTROL cells at all time points examined (**Figure 21**), which is in line with a disruption to the AMPK-mediated inhibition of mTOR in RCC. However, in a study by Pierre *et al.* (2009), the lentiviral-mediated knockout of AdipoR1 in a human granulosa cell line significantly reduced cellular proliferation and induced cell death. Importantly however, the complete knockout of AdipoR1 protein has yet to be observed in RCC. In fact, AdipoR1 protein expression was detected in all 10 of this study's patient RCC tumours (**Figure 6**) and in the CRL-1932 *in vitro* cell model of human RCC (**Figure 12**), suggesting that the complete knockout of AdipoR1 is not physiologically relevant in RCC. Nonetheless, confirming the ability of the knockdown of AdipoR1 and LKB1 in RCC to disrupt the adiponectin-induced AMPK-mediated inhibition of mTOR is beneficial, and could be achieved by demonstrating reduced cellular proliferation in shCONTROL, but not in shLKB1, cells following adiponectin treatment. Furthermore, it is of interest to confirm that the difference in cellular proliferation is not attributed to a resistance to cell death in shLKB1 cells. Thus, analysis on the cell death potential of shLKB1 and shCONTROL cells using either an LDH release assay, TUNEL assay or western blot analysis for caspases is critical.

In addition to the increased proliferation of shLKB1 cells, the knockdown of AdipoR1 and LKB1 significantly increased the ability of RCC cells to invade through Matrigel™ (**Figure 22A**). Specifically, shLKB1 cells presented an Invasion Percentage of 252% compared to 9% in the shCONTROL cells (**Figure 22B**). This increased Invasion Percentage could be attributed to shLKB1 cells possessing a greater level and activity of **m**atrix **m**etallo**p**roteinases (MMPs), which has been observed in metastatic human breast tumours (Iwata *et al*. 1996). Indeed, an increase in both the level and activity of MMPs, specifically that of MMP-2 and MMP-9, is associated with an increased potential for cells to invade, due to the ability of MMP-2 and MMP-9 to degrade a variety of extracellular proteins, which can lead to the pathological process of metastasis (Iwata *et al.*, 1996). Unfortunately, attempts to measure the level and activity of MMP-2 and MMP-9 in shLKB1 and shCONTROL cells were not successful. Thus, quantification of the level and activity of MMP-2 and MMP-9 via alternative methodologies, including western blot analysis and/or zymography, is required to conclude whether the level and activity of MMP-2 and MMP-9 explains the significantly greater Invasion Percentage in shLKB1 cells. Regardless of the mechanism, an increased invasion potential advocates for an increased potential of shLKB1 cells, and similarly, RCC with downregulated AdipoR1 and LKB1, to metastasize.

The *in vivo* tumour growth potential of RCC cells with reduced AdipoR1 and LKB1 expression was examined in 10 BALB/c Nu/Nu mice subcutaneously injected with either shLKB1 or shCONTROL cells. It was expected from the increased cellular proliferation

of shLKB1 cells *in vitro* (**Figure 21**) that the shLKB1 xenografts would proliferate faster than shCONTROL xenografts. Indeed, mice injected with shLKB1 cells generated a significantly greater tumour volume at all of the time points examined, compared to the mice injected with an identical number of shCONTROL cells (**Figure 23B**). Specifically, at seven weeks post injection, when the study was terminated, the mean tumour weight of shLKB1 xenografts was 0.297 g, which was significantly greater than the mean shCONTROL xenograft tumour weight of 0.077 g (**Figure 23C**). The study was terminated at seven weeks to ensure that the knockdown of LKB1 remained stable in the shLKB1 xenografts, and thus, would not confound results. Indeed, the stable reduction of LKB1 was confirmed by the immunohistochemical staining of LKB1 in the shLKB1 xenografts (**Figure 24D**) as well as by the Western blot analysis of LKB1 in shLKB1 cells (**Figure 20**). The significant difference in tumour volume between shLKB1 and shCONTROL xenografts was evident through the skin of the injected mice (**Figure 24A**), and made apparent the advantage of utilizing BALB/c Nu/Nu mice in *in vivo* tumour growth assays. Interestingly, histological sections of shLKB1 xenografts stained with H&E presented an active cellular tissue pathology containing a high density of extended cells (**Figure 24C**). In contrast, shCONTROL xenografts, specifically mouse number 205 and 206, had a significantly reduced number of cells of significant regions of cell death, as apparent in mouse number 203. Certainly, the analysis of proliferation markers, *VEGFA* transcript levels as well as p-AMPKα, p-ACC and p-mTOR expression levels in these xenografts would be extremely valuable in order to confirm the effect of AdipoR1 and LKB1 knockdown on the AMPK-mediated inhibition of mTOR.

Although not examined at the transcript level, the level of VEGF was measured in the serum of the mice with shLKB1 and shCONTROL xenografts. Surprisingly, the mean level of VEGF in shLKB1 mice was not significantly different than the level of VEGF in shCONTROL mice (**Figure 25A**). A significant difference in VEGF levels was expected considering the adiponectin-AMPK signalling pathway is known to be disrupted in shLKB1 cells (**Figure 18**), leading to a loss of AMPK-mediated inhibition of mTOR and allowing for the increase in VEGF secretion (**Figure 19A**). However, it is possible that the high variability in shLKB1 and shCONTROL xenograft sizes across the 10 mice (**Figure 23A**), or the presence of other sources of VEGF, did not allow the serum level of VEGF to reach significance. Thus, the relationship between tumour weight and serum VEGF level was plotted for every individual mouse, with the expectation that the majority of shLKB1 mice would be located in the top right quadrant of the graph while the majority of shCONTROL mice would fall into the bottom left quadrant (**Figure 25B**). Although the majority of the shLKB1 mice aligned on the right side of the graph, due to possession of a greater tumour weight, serum level of VEGF was not significantly greater than that of the shCONTROL mice. However, it is also possible, and likely, the shLKB1 tumours secreted greater VEGF levels, however due to the small size of the tumour in relation to the size of the mouse, VEGF secreted from shLKB1 tumours could not significantly increase systemic VEGF levels. Similarly, the serum level of adiponectin in shLKB1 mice was not significantly different from the level in shCONTROL mice (**Figure 25C**). On the other hand, the relationship between tumour weight and serum

adiponectin level in each individual mouse revealed a trend towards shLKB1 mice presenting a greater tumour weight and lower serum adiponectin level compared to shCONTROL mice (**Figure 25D**). Yet, with three shLKB1 mice presenting a similar tumour weight and serum adiponectin level to the majority of shCONTROL mice, concluding an effect of AdipoR1 and LKB1 reduction in RCC on serum adiponectin levels was not convincing.

Further investigations included a potential signalling mechanism by which AdipoR1 cooperates with AMPK to elicit tumour-suppressive effects. Based on conclusions from previous research studies, including that the intracellular portion of AdipoR1 binds CK2β (Heiker *et al.* 2009), CK2β is the only known kinase to phosphorylate and activate CDC37 (Miyata *et al.*, 2004), CDC37 and HSP90 cooperate to protect active LKB1 (Boudeau *et al.*, 2003), and that LKB1 is the primary upstream kinase of AMPK (Hawley *et al.*, 1996), the hypothetical signalling pathway of AdipoR1-CK2β-CDC37-HSP90-LKB1-AMPK was proposed. In an effort to investigate the existence and functionality of the signaling pathway, escalating doses of adiponectin were applied to CRL-1932 cells, in order to activate AdipoR1 and, suggestively, members of the signalling pathway. Indeed, increased activated levels of CK2β and CDC37, as well as an increased protein expression level of LKB1 were observed with increasing doses of adiponectin (**Figure 26**), which are events in accordance with the hypothetical signalling pathway. What is more, the inhibition of CK2 abolished the adiponectin-mediated increase in activated CDC37 and AMPKα, as well as reduced LKB1 protein expression levels (**Figure 27**).

Although concluding the existence of this signalling pathway is premature, since additional experiments with alternative inhibitors and knockdown cell lines need to be conducted, it is feasible that this proposed pathway may present a novel mechanism by which adiponectin activates AMPK. This signalling pathway would also justify why reduction of any pathway member in cancer would disrupt the tumour-suppressive actions of the adiponectin-AMPK signalling axis. Indeed reduction to AdipoR1 protein expression has been identified in various cancers, and was specifically identified to be reduced in RCC in this study (**Figure 6**). As well a human testicular tumour was identified to possess a mutation in the catalytic domain of LKB1 that prevented the assembly of the CDC37-HSP90-LKB1 complex. Also, it is established that mutations and epigenetic silencing events contribute to a downregulation of LKB1 in a variety of cancers, which result in a reduction in AMPK activation. Taken together, this hypothetical signalling pathway may be the first explanation for how adiponectin directly mediates AMPK activation and induces tumour suppression. As well, it would explain why disruption to the members of the pathway has been documented in cancer and suggests a complete disruption of this pathway in a variety of cancers, including RCC.

Overall, it is well established that excess body weight associates with an increased risk of developing RCC. This association may be explained by the reduced serum level of adiponectin in both obese and RCC patients, and the tumour-suppressive effects of adiponectin, in cooperation with AMPK. However, the adiponectin-AMPK tumour suppression signalling pathway relies on AdipoR1 to transduce the adiponectin signal

through the plasma membrane and LKB1 to activate AMPK. RCC patient tumours present a significant reduction in both AdipoR1 and LKB1 expression, suggesting that the adiponectin-AMPK signalling axis is disrupted in RCC. Indeed, RCC cells with reduced AdipoR1 and LKB1 expression were unable to execute established events of adiponectin-AMPK signalling and the cells presented significantly increased proliferation, invasion and tumour growth abilities. The proposed signalling pathway of AdipoR1-CK2β-CDC37-HSP90-LKB1 may detail the mechanism by which adiponectin activates AMPK, and the reason for which adiponectin, AdipoR1 and LKB1 reduction in RCC may prevent AMPK activation. Collectively, the findings in this study suggest that disruption to the tumour-suppressive adiponectin-AMPK signalling pathway in RCC, via reduced adiponectin levels and downregulated AdipoR1 and LKB1 expression, is a contributing factor to the association of obesity and the development of RCC.

REFERENCES

Ahmad KA, Wang G, Unger G, Slaton J, Ahmed K. Protein Kinase CK2 – A key suppressor of apoptosis. *Advances in Enzyme Regulation* 2008. 48:179-187

Alessi DR, Sakamoto K, Bayascas JR. LKB1-Dependent Signaling Pathways. *Annual Review of Biochemistry* 2006. 75:137-163

Alexander A, Walker CL. The role of LKB1 and AMPK in cellular responses to stress and damage. *FEBS Letters* 2011. 585(7):952-957

Amin RMS, Hiroshima K, Miyagi Y, Kokubo T, Hoshi K, Fujisawa T, Nakatani Y. Role of the PI3K/Akt, mTOR, and STK11/LKB1 pathways in the tumorigenesis of sclerosing hemangioma of the lung. *Pathology International* 2008. 58:38-44

Amin RMS, Hiroshima K, Iyoda, Hoshi K, Honma K, Kuroki M, Kokubo T, Fujisawa T, Miyagi Y, Nakatani Y. LKB1 protein expression in neuroendocrine tumors of the lung. *Pathology International* 2008. 58:84-88

Ampofo E, Kietzmann T, Zimmer A, Jakupovic M, Montenarh M, Gotz C. Phosphorylation of the von Hippel-Lindau protein (VHL) by protein kinase CK2 reduces its protein stability and affects p53 and HIF-1α mediated transcription. *The International Journal of Biochemistry & Cell Biology* 2010. 42(10):1729-1735

Arita Y, Kihara S, Ouchi N, Takahashi M, Maeda K, Miyagawa J, Hotta K, Shimomura I, Nakamura T, Miyaoka K, Kuriyama H, Nishida M, Yamashita S, Okubo K, Matsubara K, Muraguchi M, Ohmoto Y, Funahashi T, Matsuzawa Y. Paradoxical decrease of an adipose-specific protein, adiponectin, in obesity. *Biochemical and Biophysical Research Communications* 1999. 257(1):79-83

Bjursell M, Ahnmark A, Bohlooly-Y M, William-Olsson L, Rhedin M, Peng X, Ploj K, Gerdin A, Arnerup G, Elmgren A, Berg A, Oscarsson J, Linden D. Opposing Effects of Adiponectin Receptors 1 and 2 on Energy Metabolism. *Diabetes* 2007. 56:583-593

Bonnard C, Durand A, Vidal H, Rieusset J. Changes in adiponectin, its receptors and AMPK activity in tissues of diet-induced diabetic mice. *Diabetes & Metabolism* 2008. 34:52-61

Boudeau J, Deak M, Lawlor MA, Morrice NA, Alessi DR. Heat-shock protein 90 and Cc37 interact with LKB1 and regulate its stability. *Biochemistry Journal* 2003. 370:849-857

Boudeau J, Sapkota G, Alessi DR. LKBI, a protein kinase regulating cell proliferation and polarity. *FEBS Letters* 2003. 546:159-165

Boudeau J, Baas AF, Deak M, Morrice NA, Kielock A, Schutkowski M, Prescott AR, Clevers HC, Alessi DR. MO25α/β interact with STRADα/β enhancing their ability to bind, activate and localize LKB1 in the cytoplasm. *The European Molecular Biology Organization Journal* 2003. 22(19):5102-5114

Bub JD, Miyazaki T, Iwamoto Y. Adiponectin as a growth inhibitor in prostate cancer cells. *Biochemical and Biophysical Research Communications* 2006. 340:1158-1166

Buechler C, Wanninger J, Neumeier M. Adiponectin receptor binding proteins – recent advances in elucidating adiponectin signalling pathways. *FEBS Letters* 2010. 584(20):4280-4286

Bui MHT, Seligson D, Han K, Pantuck AJ, Dorey FJ, Huang Y, Horvath S, Leibovich BC, Chopra S, Lio S, Stanbridge E, Lerman MI, Palotie A, Figlin RA, Belldegryn AS. Carbonic anhydrase IX is an independent predictor of survival in advanced renal clear cell carcinoma: implications for prognosis and therapy. *Clinical Caner Research* 2003. 9:802-811

Calle EE, Rodriguez C, Walker-Thurmond K, Thun MJ. Overweight, obesity, and mortality from cancer in a prospectively studied cohort of U.S. adults. *New England Journal of Medicine* 2003. 348(17):1625-1638

Cammisotto PG, Bendayan M. Adiponectin stimulates phosphorylation of AMP-activated protein kinase α in renal glomeruli. *Journal of Molecular Histology* 2008. 39:579-584

Chandran M, Phillips SA, Ciaraldi T, Henry RR. Adiponectin: more than just another fat cell hormone? *Diabetes Care* 2003. 26(8):2442-2450

Charlton HK, Webster J, Kruger S, Simpson F, Richards AA, Whitehead JP. ERp46 binds to AdipoR1, but not AdipoR2, and modulates adiponectin signalling. *Biochemistry and Biophysical Research Communications* 2010. 392(2):234-239

Chou SH, Tseleni-Balafouta S, Moon HS, Chamberland JP, Liu X, Kavantzas N, Mantzoros CS. Adiponectin receptor expression in human malignant tissues. *Hormones and Cancer* 2010. 1:136-145

Chow WH, Gridley G, Fraumeni JF, Jr., Jarvholm B. Obesity, hypertension, and the risk of kidney cancer in men. *New England Journal of Medicine* 2000. 343(18):1305-1311

Chow WH, Devesa SS, Warren JL, Fraumeni JF, Jr. Rising incidence of renal cell cancer in the United States. *The Journal of the American Medical Association* 1999. 281(17):1628-1631

Conde E, Suarez-Gauthier A, Farcia-Garcia E, Lopez-Riios F, Lopez-Encuentra A, Garcia-Lujan R, Morente M, Sanchez-Verde L, Sanchez-Cespedes M. Specific pattern of LKB1 and phosphor-acetyl-CoA carboxylase protein immunostaining in human normal tissues and lung carcinomas. *Human Pathology* 2007. 38:1351-1360

Corradetti MN, Inoki K, Bardeesy N. Regulation of the TSC pathway by LKB1: evidence of a molecular link between tuberous sclerosis complex and Peutz-Jeghers syndrome. *Genes & Development* 2010. 18:1533-1538

Crimmins NA, Dolan LM, Martin LJ, Bean JA,Daniels SR, Lawson ML, Goodman E, Woo JG. Stability of adolescent body mass index during three years of follow-up. *Journal of Pediatrics* 2007. 151:383-387

David R. LKB1 maintains the balance. *Nature Reviews Molecular Cell Biology* 2010. 468(1):4

Deckert C, Heiker J, Beck-Sickinger A. Localization of Novel Adiponectin Receptor Constructs. *Journal of Receptors and Signal Transduction* 2006. 26:647-657

Deepa SS, Dong LQ. APPL1: role in adiponectin signaling and beyond. *American Journal of Physiology, Endocrinology and Metabolism* 2009. 296:E22-E36

Dieudonne M, Bussiere M, Santos ED, Leneveu M, Giudicelli Y, Pecquery R. Adiponectin mediates antiproliferative and apoptotic responses in human MCF7 breast cancer cells. *Biochemical and Biophysical Research Communications* 2006. 345:271-279

Diez JJ, Iglesias P. The role of the novel adipocyte-derived hormone adiponectin in human disease. *European Journal of Endocrinology* 2003. 148(3):293-300

Ding ST, Liu CH, Ko YH. Cloning and expression of porcine adiponectin and adiponectin receptor 1 and 2 genes in pigs. *Journal of American Science* 2004. 82(31):3162-3174

Furukawa S, Fujita T, Shimabukuro M, Iwaki M, Yamada Y, Nakajima Y, Nakayama O, Makishima M, Matsuda M, Shimomura I. Increased oxidative stress in obesity and its impact on metabolic syndrome. *Journal of Clinical Investigation* 2004. 114(12):1752-1761

Fruebis J, Tsao T, Javirschi S, Ebbets-Reed D, Erickson MR, Yen FT, Bihain BE, Lodish HF. Proteolytic cleavage product of 30-kDa adipocyte complement-related protein increases fatty acid oxidation in muscle and causes weight loss in mice. *Proceedings of the National Academy of Sciences USA* 2001. 98(4):2005-2010

Gavrila A, Chan JL, Yiannakouris N, Kontogianni M, Miller LC, Orlova C, Mantzoros CS. Serum adiponectin levels are inversely associated with overall and central fat distribution but are not directly regulated by acute fasting or leptin administration in humans: cross-sectional and interventional studies. *The Journal of Clinical Endocrinology and Metabolism* 2003. 88(10):4823-4831

Ghaffar H, Sahin F, Sanchez-Cepedes M, Su GH, Zahurak M, Sidransky D, Westra WH. LKB1 protein expression in the evolution of glandular neoplasia of the lung. *Clinical Cancer Research* 2003. 9:2998-3003

Gormand A, Henriksson E, Strom K, Jensen TE, Sakamoto K, Goransson O. Regulation of AMP-activated protein kinase by LKB1 and CaMKK in adipocytes. *Journal of Cellular Biochemistry* 2011. 112(5):1364-1375

Grossmann ME, NkhataKJ, Mizuno NK, Ray A, Cleary MP. Effects of adiponectin on breast cancer cell growth and signalling. *British Journal of Cancer* 2008. 98:370-379

Hada Y, Yamauchi T, Waki H, Tsuchide A, Hara K, Yago H, Miyazaki O, Ebinuma H, Kadowaki T. Selective purification and characterization of adiponectin multimer species from human plasma. *Biochemical and Biophysical Research Communications* 2007. 356:487-493

Hanif IM, Hanif IM, Shazib MA, Ahmad KA, Pervaiz S. Casein kinase II: an attractive target for anti-cancer drug design. *The International Journal of Biochemistry & Cell Biology* 2010. 42(10):1602-1605

Hawley SA, Boudeau J, Reid JL, Mustard KJ, Udd L, Makela TP, Alessi DR, Hardie DG. Complexes between the LKB1 tumour suppressor, STRAD alpha/beta and MO25 alpha/beta are upstream kinases in the AMP-activated protein kinase cascade. *Journal of Biology* 2003. 2(4):28.1-28.16

Hawley SA, Davison M, Woods A, Dacies SP, Beri RK, Carling D, Hardie DG. Characterization of the AMP-activated protein kinase kinase from rat liver and identification of threonine 172 as the major site at which it phosphorylates AMP-activated protein kinase. *The Journal of Biological Chemistry* 1996. 271(44):27879-27887

He L, Ingram A, Rybak AP, Tang D. Shank-interacting protein-like 1 promotes tumorigenesis via PTEN inhibition in human tumor cells. *The Journal of Clinical Investigation* 2010. 120(6):2094-2108

Hebbard LW, Garlatti M, Young LJT, Cardiff RD, Oshima RG, Ranscht B. T-cadherin supports angiogenesis and adiponectin association with the vasculature in a mouse mammary tumor model. *Cancer Research* 2008. 685):1407-1416

Heiker JT, Wottawah CM, Juhl C, Kosel D, Morl K, Beck-Sickinger AG. Protein kinase CK2 interacts with adiponectin receptor 1 and participates in adiponectin signalling. *Cell Signalling* 2009. 21(6):936-942

Hemminki A, Markie D, Tomlinson I, Avizienyte E, Roth S, Loukola A, Bignell G, Warren W, Aminoff M, Hoglund P, Jarvinen H, Kristo P, Pelin K, Ridanpaa M, Salovaara R, Toro T, Bodmer W, Olschwang S, Olsen AS, Stratton MR, de la Chapelle A, Aaltonen LA. A serine/threonine kinase gene defective in Peutz-Jeghers syndrome. *Nature* 1998. 391:185-187

Herrmann JL, Byekova Y, Elmets CS, Athar M. Liver Kinase B1 (LKB1) in the pathogenesis of epithelial cancers. *Cancer Letters* 2011. 306(1):1-9

Horiguchi A, Ito K, Sumitomo M, Kimura F, Asano T, Hayakawa M. Decreased serum adiponectin levels in patients with metastatic renal cell carcinoma. Japanese Journal of Clinical *Oncology* 2008. 38(2):106-111

Hug C, Wang J, Ahmad NS, Bgan JS, Tsao T, Lodish HF. T-cadherin is a receptor for hexameric and high-molecular-weight forms of Acrp30/adiponectin. *Proceedings of the National Academy of Sciences USA* 2004. 101(28):10308-10313

Ishikawa M, Kitayama J, Yamauchi T, Kadowaki T, Maki T, Miyato H, Yamashita H, Nagawa H. Adiponectin inhibits the growth and pereitoneal metastasis of gastric cancer through its specific membrane receptors AdipoR1 and AdipoR2. *Cancer Science* 2007. 98(7):1120-1127

Isobe K, Fu L, Tatsuno I, Takahashi H, Nissato S, Hara H, Yashiro T, Suzukawa K, Takekoshi K, Shimano H, Kawakami Y. Adiponectin and adiponectin receptors in human pheochromocytoma. *Journal of Atherosclerosis and Thrombosis* 2009. 16(4):442-447

Iwashima Y, Horio T, Kumada M, Suzuki Y, Kihara S, Rakugi H, Kawano Y, Funahashi T, Ogihara T. Adiponectin and renal function, and implication as a risk of cardiovascular disease. *The American Journal of Cardiology* 2006. 98:1603-1608

Iwata H, Kobayashi S, Iwase H, Massoka A, Fujimoto N, Okada Y. Production of matrix metalloproteinases and tissue inhibitors of metalloproteinases in human breast carcinomas. *Japanese Journal of Clinical Research* 1996. 87:602-611

Just W. Focus on ... LKB1/AMPK signalling. *FEBS Letters* 2011. 585(7):943

Kadowaki T, Yamauchi T. Adiponectin and adiponectin receptors. *Endocrine Reviews* 2005. 26(3):439-451

Kadowaki T, Yamauchi T. Adiponectin receptor signalling: a new layer to the current model. *Cell Metabolism* 2011. 13(2):123-124

Kaklamani VG, Sadim M, Hsi A, Offit K, Oddoux C, Ostrer H, Ahsan H, Pasche B, Mantzoros C. Variants of the adiponectin and adiponectin receptor 1 genes and breast cancer risk. *Cancer Research* 2008. 68(9:3178-3184

Karuman P, Gozani OO, Odze RD, Zhou XC, Zhu H, Shaw R, Brien TP, Bozzuto CD, Ooi D, Cantley LC, Yuan J. The peutz-jegher gene product LKB1 is a mediator of p53-dependent cell death. *Molecular Cell* 2001. 7:1307-1319

Kelesidia I, Kelesidis T, Mantzoros CS. Adiponectin and cancer: a systematic review. *British Journal of Cancer* 2006. 94:1221-1225

Kim AY, Lee YS, Kim KH, Lee JH, Lee HK, Jang SH, Kim SE, Lee GY, Lee JW, Jung SA, Chung HE, Jeong S, Kim JB. Adiponectin represses colon cancer cell proliferation via AdipoR1- and –R2-mediated AMPK activation. *Molecular Endocrinology* 2010. 24(7):1441-1452

Kishida K, Nagaretani H, Kondo H, Kobayashi H, Tanaka S, Maeda N, Nagasawa A, Hibuse T, Ohashi K, Kumada M, Nishizawa H, Okamoto Y, Ouchi N, Maeda K, Kihara S, Funahashi T, Matsuzawa Y. Disturbed secretion of mutant adiponectin associated with the metabolic syndrome. *Biochemical and Biophysical Research Communications* 2003. 306:286-292

Kline ER, Muller S, Pan L, Tighiouart M, Chen Z, Marcus AI. Localization-specific LKB1 loss in head and neck squamous cell carcinoma metastasis. *Head & Neck* 2010. DOI: 10.1002/hed.21638

Kobayashi H, Ouchi N, Kihara S, Walsh K, Kumada M, Abe Y, Funahashi T, Matsuzawa Y. Selective suppression of endothelial cell apoptosis by the high molecular weight form of adiponectin. *Circulation Research* 2004. 94:e27-e31

Koenig M, Beggs AH, Moyer M, Scherpf S, Heindrich QK, Bettecken T, Meng G, Mullerj CR, Lindlof M, Kaariainent H, Chapellet A, Kiuru A, Savontaus ML, Gilgenkrantz H, Rkan D, Chelly J, Kaplanll JC, Covone AE, Archidiacono N, Romeo G, Liechti-Gailati S, Schneider V, Braga S, Moser H, Darras BT, Murphytt R, Francke U, Chen JD, Morgan G, Denton M, Greenberg CR, Wrogemann K, Blonden LA, Paassen HMB, van Ommen GJB, Kunkel LM. The molecular basis for duchenne versus becker muscular dystrophy: correlation of severity with type of deletion. *American Journal of Human Genetics* 1989. 45:498-506

Korner A, Pazaitou-Panayiotou K, Kelesidis T, Kelesidis I, Williams CJ, Kaprara A, Bullen J, Neuwirth A, Tseleni S, Mitsiades N, Kiess W, Mantzoros CS. Total and high-molecular weight adiponectin in breast cancer: in vitro and in vivo studies. *The Journal of Clinical Endocrinology & Metabolism* 2007. 92(3):1041-1048

Kourelis TV, Siegel RD. Metformin and cancer: new applications for an old drug. *Medical Oncology* 2011. DOI: 10.1007/s12032-011-9846-7

Laramas M, Pasquier D, Filhol O, Ringeisen F, Descotes J, Cochet C. Nuclear localization of protein kinase CK2 catalytic subunit (CK2α) is associated with poor prognostic factors in human prostate cancer. *European Journal of Cancer* 2007. 43:928-934

Li Y, Xu S, Mihaylova MM, Zheng B, Hou X, Jiang B, Park O, Luo ZZ, Lefai E, Shyy JYJ, Gao B, Wierzbicki M, Verbeuren TJ, Shaw RJ, Cohen RA, Zang M. AMPK Phosphorylates and Inhibits SREBP Activity to Attenuate Hepatic Steatosis and Atherosclerosis in Diet-Induced Insulin-Resistnat Mice. *Cell Metabolism* 2011. 13:376-388

Linehan WM, Srinivasan R, Schmidt LS. The genetic basis of kidney cancer: a metabolic disease. *Nature Reviews Urology* 2010. 7:277-285

Liu J, Mao Z, Gallick GE, Yung WKA. AMPK/TSC2/MTOR-signaling intermediates are not necessary for LKB1-mediated nuclear retention of PTEN tumor suppressor. *Neuro-Oncology* 2011. 13(2):184-194

Maeda K, Okubo K, Shimomura I, Funahashi T, Matsuzawa Y, Matsubara K. cDNA cloning and expression of a novel adipose specific collagen-like factor, apM1 (adipose most abundant gene transcript 1). *Biochemical and Biophysical Research Communications* 1996. 221:286-289

Mao X, Kikani CK, Riojas RA, Langlais P, Wang L, Ramos FJ, Fang Q, Christ-Roberts CY, Hong JY, Kim RY, Liu F, Dong LQ. APPL1 binds to adiponectin receptors and mediates adiponectin signalling and function. *Nature Cell Biology* 2006. 8(5):516-523

Mao X, Hong JY, Dong LQ. The adiponectin signaling pathway as a novel pharmacological target. *Mini-reviews in Medicinal Chemistry* 2006. 6:1331-1340

Marcus AI, Zhou W. LKB1 regulated pathways in lung cancer invasion and metastasis. *Journal of Thoracic Oncology* 2010. 5:1883-1886.

Marignani PA. LKB1, the multitasking tumour suppressor kinase. *Journal of Clinical Pathology* 2005. 58:15-19.

Martinez-Agustin O, Hernandez-Morante J, Matrinez-Plata E, Sanchez de Medina F, Garaulet M. Differences in AMPK expression between subcutaneous and visceral adipose tissue in morbid obesity. *Regulatory Peptides* 2010. 163(1):31-36

Matsuzawa Y. Establishment of a concept of visceral fat syndrome and discovery of adiponectin. *Proceedings of the Japan Academy, Physical and Biological Sciences* 2010. 86(2):131-141

McAinch AJ, Steinberg GR, Mollica J, O'Brien PE, Dixon JB, Macaulay SL, Kemp BE, Cameron-Smith D. Differential regulation of adiponectin receptor gene expression by adiponectin and leptin in mytotubes derived from obese and diabetic individuals. *Obesity* 2006. 14(11):1898-1904

Michalakis K, Williams CJ, Mitsiades N, Blakeman J, Balafouta-Tselenis S, Giannopoulos A, Mantzoros CS. Serum adiponectin concentrations and tissue expression of adiponectin receptors are reduced in patients with prostate cancer: a case control study. *Cancer epidemiology, biomarkers & prevention* 2007. 16(2):308-313

Michell BJ, Stapleton D, Mitchelhill KI, House CM, Katsis F, Witters LA, Kemp BE. Isoform-specific purification and substrate specificity of the 5'-AMP-activated protein kinase. *Journal of Biological Chemistry* 1996. 271(45):28445-28450

Mirouse V, Billaud M. The LKB1/AMPK polarity pathway. *FEBS Letters* 2011. 585(7):981-985

Mistry T, Digby JE, Chen J, Desai KM, Randeva HS. The regulation of adiponectin receptors in human prostate cancer cell lines. *Biochemical and Biophysical Research Communications* 2006. 348:832-838

Miyata Y, Yahara I. The 90-kda heat shock protein, HSP90, binds and protects casein kinase II from self-aggregation and enhances its kinase activity. *The Journal of Biological Chemistry* 1992. 267(10):7042-7047

Miyata Y, Chambraud B, Radanyi C, Leclerc J, Lebeau M, Renoir J, Shirai R, Catelli M, Yahara I, Baulieu E. Phosphorylation of the immunosuppressant FK506-binding protein FKBP52 by casein kinase II: regulation of HSP90-binding activity of FKBP52. *Proceedings of the National Academy of Science USA* 1997. 94:14500-14505

Miyata Y, Nishida E. CK2 controls multiple protein kinases by phosphorylating a kinase-targeting molecule chaperone, Cdc37. *Molecular Cell Biology* 2004. 24(9):4065-4074

Miyata Y, Nishida E. Evaluating CK2 activity with the antibody specific for CK2-phoshorylated form of a kinase-targeting cochaperone Cdc37. *Molecular Cell Biochemistry* 2008. 316(12):127-134.

Miyata Y. CK2: the kinase controlling the HSP90 chaperone machinery. *Cellular and Molecular Life Sciences* 2009. 66:1840-1849

Montenarh M. Cellular regulators of protein kinase CK2. *Cell and Tissue Research* 2010. 342(2):139-146

Morton JP, Jamieson NB, Karim SA, Athineos D, Ridgway RA, Nixon C, McKay CJ, Carter R, Brunton VG, Frame MC, Ashworth A, Oien KA, Evan TRJ, Sansom OJ. LKB1 haploinsufficiency cooperates with KRAS to promote pancreatic cancer via suppression of p21 dependent growth arrest. *Gastroenterology* 2010. 139(2):586-597

Nedvidkova J, Smitka K, Kopsky V, Hainer V. Adiponectin, an adipocyte-derived protein. *Physiological Research* 2005. 54:133-140

Nony P, Gaude H, Rossel M, Fournier L, Rouault JP, Billaud M. Stability of the Peutz-Jeghers syndrome kinase LKB1 requires its binding to the molecular chaperones Hsp90/Cdc37. *Oncogene* 2003. 22(57)9165-9175

Olsen BB, Guerra B. Ability of CK2β to selectively regulate cellular protein kinases. *Molecular and Cellular Biochemistry* 2008. 316:115-126

Otani K, Kitayama J, Kamei T, Soma D, Miyato H, Yamauchi T, Kadowaki T, Nagawa H. Adiponectin receptors are downregulated in human gastric cancer. *Journal of Gastroenterology* 2010. 45(9):918-927

Pajvani UB, Du X, Combs TP, Berg AH, Rajala MW, Schulthess T, Engel J, Brownlee M, Scherer PE. Structure-function studies of the adipocyte-secreted hormone acrp30/adiponectin. *The Journal of Biological Chemistry* 2003. 278(11):9073-9085

Pfeiler G, Hudelist G, Wulfing P, Mattsson B, Konigsberg R, Kubista E, Singer CF. Impact of AdipoR1 expression on breast cancer development. *Gynecologic Oncology* 2010. 117:134-138

Pierre P, Froment P, Negre D, Rame C, Barateau V, Chabrolle C, Lecomta P, Dupont J. Role of adiponectin receptors, AdipoR1 and AdipoR2, in the steriodogenesis of the human granulose tumor cell line, KGN. *Human Reproduction* 2009. 24(11):2890-2901

Pinthus JH, Kleinmann N, Tisdale B, Chatterjee S, Lu JP, Gillis A, Hamlet T, Singh G, Farrokhyar F, Kapoor A. Lower plasma adiponectin levels are associated with larger tumor size and metastasis in clear-cell carcinoma of the kidney. *European Urology* 2008. 54(4):866-873

Pinthus JH, Whelan KF, Gallino D, Lu JP, Rothschild N. Metabolic features of clear-cell renal cell carcinoma: mechanisms and clinical implications. *Canadian Urological Association Journal* 2011. 5(4): 274-282

Pressey JG, Wright JM, Geller JI, Joseph DB, Pressey CS, Kelley DR. Sirolimus therapy for fibromatosis and multifocal renal cell carcinoma in a child with tuberous sclerosis complex. *Pediatric blood & cancer* 2010. 54:1035-1037

Renehan AG, Tyson M, Egger M, Heller RF, Zwahlen M. Body-mass index and incidence of cancer: a systematic review and meta-analysis of prospective observational studies. *The Lancet* 2008. 371(9612):569-578

Robb VA, Karbowniczek M, Klein-Szanto A, Henske EP. Activation of the mTOR signaling pathway in renal cell carcinoma. *The Journal of Urology* 2007. 177:346-352

Rojas J, Arraiz N, Aguirre M, Velasco M, Bermudez V. AMPK as target for intervention in childhood and adolescent obesity. *Journal of Obesity* 2011. 2011:1-19

Rowan A, Churchman M, Jeffrey R, Hanby A, Poulsom R, Tomlinson I. In situ analysis of LKB1/STK11 mRNA expression in human normal tissues and tumours. *Journal of Pathology* 2000. 192:203-206

Ruzzene M, Pinna LA. Addiction to protein kinase CK2: a common denominator of diverse cancer cells? *Biochemical and Biophysical Acta* 2010:499-504

Sanchez-Cespedes M, Parrella P, Esteller M, Nomoto S, Trink B, Engles JM, Westra WH, Herman JG, Sidransk D. Inactivation of LKB1/STK11 is a common event in adenocarcinomas of the lung. *Cancer Research* 2002. 62:3659-3662

Sanchez-Cespedes M. A role for LKB1 gene in human cancer beyond the peutz-jeghers syndrome. *Oncogene* 2007. 26:7825-7832

Sanchez-Cespedes M. The role of LKB1 in lung cancer. *Familial Cancer* 2011. DOI: 10.1007/s10689-011-9443-0

Sahra IB, marchand-Brustel YL, Tanti JF, Bost F. Metformin in cancer therapy: a new perspective for an old antidiabetic drug. *Molecular Cancer Therapeutics* 2010. 9(5):1092-1099

Sapkota GP, Boudeau J, Deak M, Kieloch A, Morrice N, Alessi DR. Identification and characterization of four novel phosphorylation sites (Ser31, Ser325, Thr336 and Thr366) on LKB1/STK11, the protein kinase mutated in peutz-jeghers cancer syndrome. *Biochemical Journal* 2002. 362:481-490

Schalkwijk CG, Chaturvedi N, Schram MT, Fuller JH, Stehouwer CDA. Adiponectin is inversely associated with renal function in type 1 diabetic patients. *The Journal of Clinical Endocrinology & Metabolism* 2006. 91(1):129-135

Sebbagh M, Olschwang S, Santoni MJ, Borg JP. The LKB1 complex-AMPK pathway: the tree that hides the forest. *Familial Cancer* 2011. DOI: 10.1007/s10689-011-9457-7

Setiawan VW, Stram DO, Nomura AM, Kolonel LN, Henderson BE. Risk factors for renal cell cancer: the multiethnic cohort. *American Journal of Epidemiology* 2007. 166(8):932-940

Shackelford DB, Shaw RJ. The LKB1-AMPK pathway: metabolism and growth control in tumour suppression. *Nature Reviews* 2009. 9:563-575

Shen YY, Peake PW, Charlesworth JA. Review article: adiponectin: its role in kidney disease. *Nephrology* 2008. 13:528-534

Shen YY, Charlesworth JA, Kelly JJ, Loi KW, Peake PW. Up-regulation of adiponectin, its isoforms and receptors in end-stage kidney disease. *Nephrology Dialysis and Transplant* 2007. 22:171-178

Sherr CJ. Principles of Tumor Suppression. *Cell* 2004. 116:235-246

Shorning B, Clarke A. LKB1 loss of function studied *in vivo*. *FEBS Letters* 2011. 585(7):958-966

Sloan KA, Marquez HA,Li J, Cao Y, Hinds A, O'Hara CJ, Kathuria S, Ramirez MI, Williams MC, Kathuria H. Increase PEA3/E1AF and decreased Net/Elk-3, both ETS proteins, characterize human NSCLC progression and regulate caveolin-1 transcription in Calu-1 and NCI-H23 NSCLC cell lines. *Carcinogenesis* 2009. 30(8):1433-1442

Spyridopoulos TN, Petridou ET, Skalkidou A, Dessypris N, Chrousos GP, Mantzoros CS. Low adiponectin levels are associated with renal cell carcinoma: a case-control study. *International Journal of Cancer* 2007. 120:1573-1578

Steinberg GR, Kemp BE. AMPK in health and disease. *Physiology Reviews* 2009. 89:1025-1078

Steinberg GR, Kemp BE. Adiponectin: starving for attention. *Cell Metabolism* 2007. 6:3-4

Sun Y, Connors KE, Yang DQ. AICAR induces phosphorylation of AMPK in an AMT-dependent, LKB1-independent manner. *Molecular and Cellular Biochemistry* 2007. 306:239-245

Takahata C, Miyoshi Y, Irahara N, Taguchi T, Tamaki Y, Noguchi S. Demonstration of adiponectin receptors 1 and 2 mRNA expression in human breast cancer cells. *Cancer Letters* 2007. 250:229-236

Thijssen VLJL, Brandwijk RJMGE, Dings RPM, Griffioen AW. Angiogenesis gene expression profiling in xenograft models to study cellular interactions. *Experimental Cell Research* 2004. 299:286-293

Tiainen M, Vaahtomeri K, Ylikorkala A, Makela TP. Growth arrest by the LKB1 tumor suppressor: induction of p21WAF1/CIP1. *Human Molecular Genetics* 2002. 11(13):1497-1504

Tomayko MM, Reynolds CP. Determination of subcutaneous tumor size in athymic (nude) mice. *Cancer Chemotherapy and Pharmacology* 1989. 24:148-154

Treeck O, Lattrich C, Juhasz-Boess I, Buchholz S, Pfreiler G, Ortmann O. Adiponectin differentially affects genes expression in human mammary epithelial and breast cancer cells. *British Journal of Cancer* 2008. 99:1246-1250

Trembley JH, Wang G, Unger G, Slaton J, Ahmed K. CK2: a key player in cancer biology. *Cellular and Molecular Life Sciences* 2009. 66:1858-1867

Trujillo ME, Scherer PE. Adipose tissue-derived factors: impact on health and disease. *Endocrine Reviews* 2006. 27(7):762-778

Ukkola O, Santaniemi M. Adiponectin: a link between excess adiposity and associated comorbidities? *Journal of Molecular Medicine* 2002. 80:696-702

Vaahtomeri K, Makela TP. Molecular mechanisms of tumor suppression by LKB1. *FEBS Letters* 2011. 585(7):944-951

Van Veelen W, Korsse SE, Van de Laar L, Peppelenbosch MP. The long and winding road to rational treatment of cancer associated with LKB1/AMPK/TSC/mTORC1 signaling. *Oncogene* 2011. 30(20):2289-2303

Vettor R, Milan G, Rossato M, Federspil G. Review article: adipocytokines and insulin resistance. *Alimentary Pharmacology & Therapeutics* 2005. 22:s3-s10

Viollet B, Horman S, Leclerc J, Lantier L, Foretz M, Billaud M, Giri S, Andreelli F. AMPK inhibition in health and disease. *Critical Reviews in Biochemistry and Molecular Biology* 2010. 45(4):276-295

Wade TE, Mathur A, Lu D, Swartz-Basile DA, Pitt HA, Zyromski NJ. Adiponectin receptor-1 expression is decreased in the pancreas of obese mice. *Journal of Surgical Research* 2009. 154:78-84

Wang Y, Xu LY, Lam KAL, Cooper GJS, Xu A. Proteomic characterization of human serum proteins associated with the fat-derived hormone adiponectin. *Proteomics* 2006. 6:3862-3870

Wei Y, Renard C, Labalette C, Wu Y, Levy L, Neuveut C, Prieur X, Flajolet M, Prigent S, Buendia M. Identification of the LIM protein FHL2 as a coactivator of β–catenin. *The Journal of Biological Chemistry* 2003. 278(7):5188-5194

Wei C, Amos CI, Rashid A, Sabripour M, Nations L, McGarrity TJ, Frazier ML. Correlation of staining for LKB1 and COX-2 in hamartomatous polyps and carcinomas from patients with peutz-jeghers syndrome. *The Journal of Histochemistry & Cytochemistry* 2003. 51(12):1665-1672

Williams CJ, Mitsiades N, Sozopoulos E, Hsi A, Wolk A, Nifli A, Tseleni-Balafouta S, Mantzoros CS. Adiponectin receptor expression is elevated in colorectal carcinomas but not in gastrointestinal stromal tumors. *Endocrine-Related Cancer* 2008. 15:289-299

Woodard J, Joshi A, Viollet B, Hay N, Platanias LC. AMPK as a therapeutic target in renal cell carcinoma. *Cancer Biology & Therapy* 2010. 11:1-10

Woods A, Johnstone SR, Dickerson K, Leiper FC, Fryer LGD, Neumann D, Schlattner U, Wallimann T, Carlson M, Carling D. LKB1 is the upstream kinase in the AMP-activated protein kinase cascade. *Current Biology* 2003. 13:2004-2008

Yamauchi T, Kamon J, Ito Y, Tsuchida A, Yokomizo T, Kita S, Sugiyama T, Miyagishi M, Hara K, Tsunoda M, Murakami K, Ohteki T, Uchida S, Takekawa S, Waki H, Tsuno NH, Shibata Y, Terauchi Y, Froguel P, Tobe K, Koyasu S, Taira K, Kitamura T, Shimizu T, Nagai R, Kadowaki T. Cloning of adiponectin receptors that mediate antidiabetic metabolic effects. *Nature* 2003. 423(6941):762-769

Yamauchi T, Nio Y, Maki T, Kobayashi M, Takazawa T, Iwabu M, Okada-Iwabu M, Kawamoto S, Kubota N, Kubota T, Ito Y, Kamon J, Tsuchida A, Kumagai K, Kozono H, Hada Y, Ogata H, Tokuyama K, Tsunoda M, Ide T, Murakami K, Awazawa M, Takamoto I, Froguel P, Hara K, Tobe K, Nagai R, Ueki K, Kadowaki T. Targeted disruption of AdipoR1 and AdipoR2 causes abrogation of adiponectin binding and metabolic actions. *Nature Medicine* 2007. 3(13):332-339

Ylikorkala A, Rossi DJ, Korsisaari N, Luukko K, Alitalo K, Henkemeyer M, Makela TP. Vascular abnormalities and deregulation of VEGF in LKB1-deficient mice. *Science* 2001. 293:1323-1326

Yoshida BA, Sokoloff MM, Welch DR, Rinker-Schaeffer CW. Metastasis-suppressor genes: a review and perspective on an emerging field. *Journal of the National Cancer Institute* 2000. 92(21):1717-1730